KINETIC STUDY OF THE DISSOLUTION OF CHALCOPYRITE IN THE PRESENCE OF A CATALYST UNDER ACIDIC SULFATE MEDIUM

by

Monserrat Rebolledo

B.Sc., University of Concepcion, 2013

A THESIS SUBMITTED IN PARTIAL FULFILLMENT OF THE REQUIREMENTS FOR THE DEGREE OF

MASTER OF APPLIED SCIENCE

in

THE FACULTY OF GRADUATE AND POSTDOCTORAL STUDIES

(Materials Engineering)

THE UNIVERSITY OF BRITISH COLUMBIA

(Vancouver)

July, 2017

Abstract

The main drawback of the atmospheric pressure hydrometallurgical process to recover copper from chalcopyrite is its slow dissolution rate. The aim of this study was to gain further insight of the kinetics of the leaching of chalcopyrite in the presence of thiourea (TU), as a catalyst, in acidic sulfate media. To do so, the influence of temperature, copper, acid and catalyst concentration on the leaching of chalcopyrite were measured and quantified.

Among the parameters tested, the tendency of TU to be oxidized was found to be very sensitive to the concentration of acid in solution. Besides, the rate of its oxidation was essentially dependent on the mineral surface available and only slightly dependent on the concentration of ferric ions in solution.

The data from the leaching test in this study demonstrated that in the presence of TU, it is possible to achieve ~98% of copper extraction from chalcopyrite in less than 216 hours at room temperature. Chemical reaction was determined to be the rate controlling step based on an apparent activation energy of 41 kJ/mol. The reaction order of chalcopyrite was found to be 1.7 and -0.9 with respect to TU and proton concentration (H^+), respectively.

The shrinking sphere model, assuming surface chemical reaction as the rate-controlling step, fitted very well the changing grain topology. The development of a single mathematical expression combining the thermal, chemical, and topological functions to predict the chalcopyrite conversion as a function of the known temperature, ferric and ferrous concentration, thiourea and proton concentration, particle size and time was also performed.

The present findings open a new direction of research oriented towards the development of a plausible alternative for a low-temperature processing route for chalcopyrite leaching.

Lay Summary

Nowadays, approximately 20% to 25% of primary world copper production is treated by hydrometallurgy. Chalcopyrite ($CuFeS_2$) is the most important copper sulfide mineral because it accounts for almost 70% of the world's known reserves of this metal. The main hindrance to the commercial application of hydrometallurgical processes for chalcopyrite is its low dissolution rate. One of the new alternatives that is currently under study, has shown a positive effect overcoming the slow dissolution rate of chalcopyrite.

The main goal of this research is to provide information for a better understanding of the key controls and rate-controlling factors for this patented technology, which comprises the use of a catalyst to enhance the dissolution of chalcopyrite at room temperature. The proposition of a mathematical expression to estimate the chalcopyrite extraction rates will be also attempted. Ultimately, the intention of the study is to provide useful guidance to industrial operations using the technology.

Preface

This thesis presents the research conducted by Monserrat Rebolledo in collaboration with Dr. David Dixon. Monserrat conducted all the testing and wrote the manuscripts regarding the kinetics study.

Chapter 2 section 5, subsection 5. Effect of temperature in the behaviour of thiourea in acidic and sulfate media is based on the work conducted by Pablo Zuñiga. A version of this work is in a manuscript in progress for a journal paper which will be published in the future.

Table of Contents

List of tables

List of figures

List of symbols and abbreviations

Symbols

atm	Standard atmosphere equal to 101,325 Pa
d	Particle size (µm)
E_0	Standard reduction potential
E	Reduction potential (V)
E_a	Activation energy (J/mol)
F	Faraday's constant (96,485 C/mol electron)
Fe^{3+}	Ferric ion
Fe^{2+}	Ferrous ion
ΔG_0	Standard Gibbs free energy
g	Grams
h	Hour
j	Rate of chalcopyrite dissolution per unit mineral surface area or mole flux (mol/m^2)
k	Rate constant (arbitrary units)
K	Kelvin
J	Joules
L	Liter
M	Molarity
m	Mass
mol	Mole
P_{80}	80% mass passing particle size
r	Rate(mol/h)

R Ideal gas constant (8.314 $Jmol^{-1}K^{-1}$)

s Second

T Absolute temperature (K)

t Time

w Weight factor for Gauss-Legendre integration conversion

X Particle conversion

z Root of a Legendre polynomial

Greek Letters

α Symmetry coefficient

τ Time required for the complete reaction

Subscripts

a Anode

c Cathode

ref Reference

0 Initial

Abbreviations

EDX Energy-Dispersive X-ray Spectroscopy

EW Electrowinning

FDS Formamidine disulfide

HPLC High-Performance Liquid Chromatography

ICP Inductively Coupled Plasma

ORP Oxidation Reduction Potential

PLS Pregnant Leach Solution

PPM Parts Per Million

PSD Particle Size Distribution

RPM Revolutions per Minute

SEM Scanning Electron Microscope

SHE Standard Hydrogen Electrode

SX Solvent Extraction

TU Thiourea

XRD X-ray Diffraction

Acknowledgements

First and foremost, I would like to express my sincere gratitude to my supervisor Dr. David Dixon for his continuous guidance and support, and his immense knowledge that helped me throughout my journey as a graduate student.

I would like to thank my thesis committee, Dr. Edouard Asselin and Dr. Wenying Liu, for their insightful comments, and their questions that inspired me to widen my research from various perspectives.

I gratefully acknowledge the generous financial support provided by Jetti Resources who made possible this entire project and Mitacs, through the Mitacs Accelerate Initiative.

I am truly indebted to Dr. Zihe Ren and Mr. Jacob Kabel for their infinite patience, helpful suggestions, and comments that enriched my work by enlarging my vision of science.

I would like to extend my appreciation to my colleagues in the Materials Department, especially the Hydrometallurgy group. It has been a great privilege to spend all these years working alongside these amazing people. Particularly, I thank my fellow labmates: Mr. Pablo Zuñiga, Mr. Prashanth Krishnamoorthy, and Mr. Kush Shah, for all the stimulating discussions, for the sleepless nights we were working together, and mostly for all the fun we had in the last two years.

Last but definitely not least, I must express my very profound gratitude to my family and friends. Their endless patience, love, support and understanding has guided me through good and bad times. This accomplishment would not have been possible without them, and it is to them that I dedicate this work.

Chapter 1 Introduction

1.1 Background

Chalcopyrite ($CuFeS_2$) is the most important copper sulfide mineral, mainly because it is one of the most abundant copper minerals in the world (Fuentes et al., 2008) accounting for almost 70% of the world's known reserves of this metal (Rivadeneira, 2006).

Copper can be extracted from chalcopyrite by conventional pyrometallurgical or hydrometallurgical processes. Nowadays, approximately 20% to 25% of primary world copper production is treated by hydrometallurgy, where the dominant process is heap and dump leaching and SX-EW (Munoz et al., 2007). In fact, in Chile, the largest copper-producing country in the world, hydrometallurgical processing accounted for 34% in 2014 (Brininstool & Wallace, 2014).

Pyrometallurgy, which involves mineral processing, smelting and electro refining, has been the predominant process for copper recovery from cuprous mineral resources for more than a century. In fact, it still remains as the preferential process for the copper industry due to its simplicity and economy. However, there are a number of disadvantages besides the environmental issues when it comes to treating low-grade ores. In order to overcome these disadvantages, considerable efforts have been made to find alternatives to this process in the past thirty years.

The increasing demand for copper and the continuous exploitation of high-grade ores have resulted in a decrease in the quality of the remaining natural sources, with an additional increase in ore complexity as well as higher impurity concentrations. As a result of this, the development of hydrometallurgical alternatives for the treatment of chalcopyrite has been encouraged. Hydrometallurgical processes can treat low-grade ores (increasingly more abundant in the case of copper), complex sulfides and chalcopyrite concentrates with impurities, at comparatively lower capital cost and without SO_2 production and/or emission.

The hydrometallurgical processes can be categorized according to the leaching media used, with the most common media being chloride, nitrogen, ammonia and sulfate. The sulfate-based processes have some advantages over the others due to the fact that the leaching chemistry is generally simpler and better understood, and copper recovery from sulfate media (by SX-EW) is straightforward (Hackl, 1995).

Hence, hydrometallurgical processes have received considerable attention over recent years. Ferric ions, cupric ions, oxygen, and other oxidants have been used as leaching agents for chalcopyrite in sulfate and chloride media under atmospheric or pressure leaching conditions.

The main reason why a substantial amount of research has been undertaken and all these alternative leaching agents have been tested is because of the well-known hindrance that hydrometallurgical processes presents: the slow copper dissolution rate from chalcopyrite.

This drawback has been attributed to the formation of a passivating layer on the mineral surface (Li et al., 2010). It is noteworthy to mention that the composition of the passivating layer and the mechanism by which it forms are still the subject of considerable dispute. Although, in order to be able to increase the leaching rates of chalcopyrite to extract copper and overcome this problem, the formation of this passive layer must be prevented.

Several solutions have been proposed to solve this problem. Among them, the use of microorganisms to oxidize the passive layer (Brierley & Brierley, 2001) and increasing the temperature to decompose the passive layer (Cordoba et al., 2009). Also, several catalysts and/or promoters have been proposed, such as the addition of silver, which changes the electrochemical behavior of chalcopyrite (Munoz et al., 2007); the addition of pyrite to favor the galvanic interaction between the minerals (Tshilombo & Dixon, 2003); the addition of activated carbon (Nakazawa et al., 1998); and the addition of ions like Sn(II), Co(II), Hg(II), Bi(III) and Mn(II), which in certain conditions have been shown to enhance the leaching kinetics of chalcopyrite (Barriga et al., 1987). Also, Solis-Macial & Lapidus (2013) showed that the use of polar organic solvents, as part of the acid leaching solution, offered a solution to the formation of the protective layer and an improvement of the kinetics of chalcopyrite leaching at ambient temperature.

1.2 Problem Definition

The main hindrance to the commercial application of hydrometallurgical processes for chalcopyrite is the low dissolution rate. Several studies have shown that even in high acidic solutions, surface passivity of chalcopyrite at solution potential above certain level is the most important problem (Hiroyoshi et al., 2001; Pinches et al., 2001; Cordoba et al., 2008). So far, the oxidative leaching of chalcopyrite in the presence of ferric media is a good and viable alternative, chiefly because of the consumption of ferric sulfate as the oxidant, which presents a big economic advantage and because ferric is available *in situ* in most acidic leaching systems.

During the past decades, several alternatives have been presented to overcome the low dissolution rate of chalcopyrite. However, the key controls of the aqueous oxidation process under both environmental and industrially relevant conditions are poorly understood. Improving the understanding of chalcopyrite dissolution and the factors that maximize the amount of copper released during hydrometallurgical treatment are therefore matters of huge economic importance.

One of the new alternatives that is currently under study, has some preliminary results that indicate a positive effect in overcoming the slow copper dissolution rate from chalcopyrite. This patented technology uses thiourea, an organic reagent, which serves as the catalyst for low-temperature chalcopyrite leaching in acidic media, using ferric ions (Fe^{3+}) as an oxidant. Relevant work has been reported by many researchers in regards to copper interactions with thiourea, although some ambiguities still remain.

It is that specific line of investigation that provides the impetus for the present study.

1.3 Objective of the Research

The aim of this study is to gain further insight into the interactions of the catalyst in acidic sulfate media. To do so, the influence of temperature, acid, ferric, and catalyst concentration on the leaching of chalcopyrite will be measured and quantified. Furthermore, the development of a global rate law for chalcopyrite leaching, incorporating all of those factors, and the topology of the leaching solids will be attempted.

Chapter 2 Literature Review

2.1 General properties of chalcopyrite

2.1.1 Nature of chalcopyrite

Chalcopyrite is one of the most abundant and widespread copper bearing minerals, accounting for approximately 70% of the earth's copper (Cordoba et al., 2008). Its name is derived from the Greek *chalkos* which means copper, and *pyros*, which means fire. The chemical formula is $CuFeS_2$, and the theoretical mass composition is 34.6% Cu, 30.5% Fe and 34.9% S.

Chalcopyrite is predominantly found in porphyry copper deposits associated with pyrite (FeS_2), bornite (Cu_5FeS_4), sphalerite (ZnS), chalcocite (Cu_2S), covellite (CuS), enargite (Cu_3AsS_4) or molybdenite (MoS_2), frequently in a quartz (SiO_2) matrix (Velazquez, 2009).

2.1.2 Structure

The crystal structure of $CuFeS_2$ was initially determined by Burdick & Ellis (1917). The structure is derived from the zinc blende (ZnS) group, in which four zinc atoms are replaced by one iron and two copper atoms. Thus, the chalcopyrite unit cell is twice the volume of the unit cell of sphalerite with c = 525 pm and a = 1032 pm. Figure 1 shows the crystal structure of the chalcopyrite.

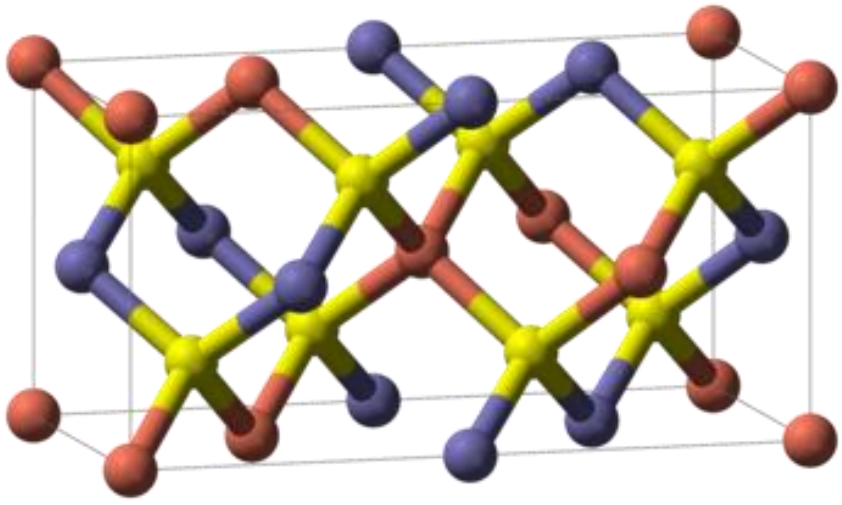

Figure 1. Unit cell model of chalcopyrite. Copper is shown in red, iron in blue and sulfur in yellow.

Each metal atom is coordinated by a tetrahedron of sulfur atoms and each sulfur atom by a tetrahedron of metal atoms (two copper and one iron). Sulfur atoms are displaced slightly from the center of the metal tetrahedron towards the iron-iron axis, with inter-atomic distances d_{Cu-S} = 2.30 Å, d_{Fe-S} = 2.26 Å and $d_{Cu-Fe} = d_{Cu-Cu} = d_{Fe-Fe}$ = 3.71 Å (Edelbro et al., 2003).

The bonding in chalcopyrite is essentially covalent where each atom is bonded to its four nearest neighbours. The valence states in the chalcopyrite are most often considered to be Cu^{+} Fe^{3+} $(S^{2-})_2$ rather than Cu^{2+} Fe^{3+} $(S^{2-})_2$ (De Filippo et al., 1988; Mikhlin, et al., 2004; Boekema, et al., 2004).

2.1.3 Physical properties

Chalcopyrite has a deep brass yellow color. The average density is 4.1 to 4.3 kgm^{-3}. It is moderately hard, being 3.5 to 4.0 on the Mohs scale. Iron occupies a regular tetrahedral arrangement with all Fe-S bond angles equal to 109.47º, whereas the coordination for both Cu and S is not a regular tetrahedron, with angles varying from 108.67º to 111.06º (Habashi, 1978).

2.1.4 Electronic properties

Chalcopyrite behaves likes an n-type semiconductor (electron donation to the conduction band) with a resistivity in a range of 2 x 10^{-4} to 3 x 10^{-1} Ωm at room temperature. An n-type semiconductor should favor chemisorption of cations and p-type favor (electron acceptor to the conduction band) sorption chalcopyrite of anions. The energy band gap of chalcopyrite is in the order of 0.53 to 0.6 eV (Tributsch & Bennett, 1981), hence it is likely that both holes and electrons can contribute to the dissolution.

According to the literature (Habashi, 1978) chalcopyrite undergoes a two-phase transformation at 550 and 657ºC, the Néel temperature, above which thermal energy causes the loss of magnetic ordering so that an antiferromagnetic material becomes paramagnetic. The first transformation is: $\alpha - CuFeS_2$ (tetragonal) $\rightarrow \beta - CuFeS_2$ (cubic), and the second is an antiferromagnetic transition. These transformations, lead to an irreversible increase in conductivity due to the loss of sulfur (Li et al., 2013).

2.2 Hydrometallurgical processes for copper sulfides

The leaching of copper from sulfide ore bodies occurs naturally, releasing copper and iron. The first reference to the application of ferric acid sulfate solution for the leaching of copper minerals is dated to 1752 at the Rio Tinto mine in Huelva, Spain.

Prior to late 1960's, the copper was recovered by cementation with metal iron, and the iron then was recovered by evaporation of the solution in the form of ferrous sulfate. By late March in 1968, The Bluebird plant of Ranchers Exploration and Development Corp. started the first copper SX plant in Miami, Arizona. The results of this plant proved that L/SX/EW technology could produce large quantities of good quality cathode copper. Copper SX-EW became the modern standard by which hydrometallurgical copper was produced, and greatly expanded the potential for the business (Kordosky, 2002).

During the past decades, many studies have been conducted to find and develop an efficient process for extracting copper from chalcopyrite. As a result, there are many different hydrometallurgical processes for copper recovery from chalcopyrite. These processes can be grouped according to the leaching media used: sulfate, chloride, sulfate/chloride, ammonia, and nitrogen. Moreover, within the sulfate grouping, processes can be sub-grouped as either atmospheric or super-atmospheric in pressure and chemical or biological in the leaching process. This chapter presents a brief description of the processes based on sulfate as a leaching medium.

2.2.1 Sulfate processes

Processes based on the sulfate medium are today the most established technology for chalcopyrite leaching. Among all the alternatives, ferric sulfate leaching has several advantages, such as simplicity of the leaching reaction and low operational and capital costs.

In general, ferric sulfate leaching of chalcopyrite can be represented by the following reactions (Dutrizac & MacDonald, 1974):

$$CuFeS_2 + 2\ Fe_2(SO_4)_3 \rightarrow CuSO_4 + 5\ FeSO_4 + 2\ S^0 \qquad \text{Eq. 1}$$

$$CuFeS_2 + 8\ Fe_2(SO_4)_3 + 8\ H_2O \rightarrow CuSO_4 + 17\ FeSO_4 + 8\ H_2SO_4 \qquad \text{Eq. 2}$$

Ferric ions are regenerated via oxidation of ferrous to ferric according to the following reaction:

$$4\ FeSO_4 + O_2 + H_2SO_4 \rightarrow 2\ Fe_2(SO_4)_3 + 2\ H_2O \qquad \text{Eq. 3}$$

Oxygen consumption is substantially higher when sulfate is a reaction product rather than elemental sulfur. Each mole of sulfur consumes 1.5 moles of oxygen when oxidized to sulfate, according to the following reaction:

$$S + 1.5\ O_2 + H_2O \rightarrow H_2SO_4 \qquad \text{Eq. 4}$$

Three additional moles of oxygen are required for each mole of chalcopyrite when sulfate is a reaction product. Therefore, high yields of elemental sulfur are desirable to reduce the oxygen consumption.

The Galvanox™ Process

The Galvanox™ process is a technology developed at the University of British Columbia (UBC) for leaching copper from primary copper concentrates (Dixon & Tshilombo, 2005). This process takes advantage of the galvanic couple between pyrite and chalcopyrite to ensure rapid and complete oxidation of chalcopyrite in acidic iron sulfate solution, without the need for microbes, ultrafine grinding or chemical additives such as chloride, nitrate or surfactants.

Furthermore, since the operating temperature is low (80ºC) and the chemical conditions are mild, the near-quantitative yield of elemental sulfur is observed. This decreases both oxygen consumption and the need to neutralize large quantities of sulfuric acid. Copper recoveries of 98% or greater can be achieved at 80°C under atmospheric conditions in as little as 4 hours of residence time (Dixon et al., 2008).

The Albion Process (Nenatech)

The Albion process (Hourn & Halbe, 1999) is a sulfate-based technology that employs fine grinding (P_{80} = 10 to 15 µm). This process operates at 85 to 90°C and atmospheric pressure. One of the drawbacks of this process is that the elemental sulfur formed in the leaching remains in the residue, leading to difficulties in recovering precious metals.

On the other hand, some of the advantages of the Albion process are relatively low process risk and lower operating cost. This process has been successfully used by Xstrata at their Mt. Isa plant located in Australia to leach arsenic-containing smelter dusts, and has full scale application in gold and zinc processing.

The Activox Process

The Activox process was developed for the treatment of a wide variety of sulfide mineral concentrates (Corrans & Angove, 1993). This process operates at 90 to 110°C and oxygen pressures of 10 to 12 atm (Dreisinger, 2006). Leaching temperature in this process is lower than the melting point of sulfur (119°C), so the addition of a surfactant is not required.

This technology consists of the activation of the mineral surfaces by fine grinding (P_{80} = 5 to 10 µm). The total surface area increases by decreasing the initial mineral particle size, which leads to increasing copper extraction (Nazari, 2011).

The Anglo American - University of British Columbia Process (AAC-UBC)

Anglo American Copper Corporation and the University of British Columbia have developed a process for chalcopyrite leaching under moderate oxygen pressure (10 to 12 atm) at 150°C. As the operating temperature is higher than the melting point of sulfur, surfactants are required to prevent coating of unreacted chalcopyrite by liquid sulfur (Dreisinger et al., 2003).

The concentrate is reground very fine (P_{80} = 5 to 20 µm) and leached in an acid–sulfate system. In this process, surfactants such as calcium lignosulfonate and orthophenylenediamine (OPD) are used to disperse the molten sulfur. The viscosity of sulfur decreases from 115 to 159°C but increases dramatically at temperatures higher than 159°C. Hence, the operating temperature for this process must be lower than 159°C. The AAC-UBC process is distinguished by high copper extractions, hematite or jarosite formation, and elemental sulfur as the dominant reaction product (Dreisinger, 2006).

The Total Pressure Oxidation Process

The total pressure oxidation (TPOX) process operates under high temperature (220 to 230°C) and high pressure (30 to 40 atm) conditions to achieve high copper extractions. Conveniently, total pressure oxidation also results in iron precipitation as hematite. This process was initially developed for the treatment of gold ores (King & Dreisinger, 1995).

The advantages of this process are rapid and complete chalcopyrite leaching, and a high degree of iron hydrolysis, mainly as hematite (Glen et al., 2003). TPOX has been commercially demonstrated at a large scale and could easily be scaled up to larger size if required. However, the oxygen consumption is high due to the total conversion of sulfur to sulfate.

The Dynatec Process

The Dynatec process was first developed for the treatment of zinc concentrates and refractory gold ores (Collins & Kofluk, 1998). The leach operates at 150ºC and the feed is ground to 30 to 40 µm. The Dynatec process was also used to dissolve copper from chalcopyrite under 10 to 12 atm pressure (Peacey et al., 2003).

Similar to the AAC-UBC process, the addition of surfactant is required to avoid coating of unleached mineral by molten sulfur.

A high extraction of copper, about 98%, is achieved by either recycling the unreacted sulfide to the leach after flotation and removing elemental sulfur, or pre-treating the concentrates with fine grinding.

The Mt. Gordon Copper Process

The Mt. Gordon Copper Process was develop to treat chalcocite ores. Using low temperature pressure oxidation, the leaching of the copper from the ore is achieved, and is followed by SX/EW of copper from the resulting leach solution.

In this process, chalcocite first leaches to form a covellite reaction product and then the covellite product leaches to form soluble copper and elemental sulfur. Ferric ion is regenerated by oxygen *in situ* in the autoclave. Other copper minerals will also leach with oxygen in the presence of a ferric/ferrous solution. In addition to the reactions involving the copper minerals, pyrite in the ore will also oxidize to a limited extent (2 to 3%). This minor oxidation is beneficial in regenerating soluble iron and acid for the leach system.

The Mt. Gordon Copper Process was one of the few technologies to achieve implementation in a commercial facility, but the plant was shut down in 2004 due to a change of the ore type and a corporate change in the ownership of the company (Dreisinger, 2006).

The FLSMIDTH® Rapid Oxidative Leach (rol) Process

A new leaching process for chalcopyrite discovered by FLSmidth enables manipulation of the 2-D semi-conductor properties of chalcopyrite surfaces to the benefit of higher electrochemical reactivity (Chaiko et al., 2015).

The FLSmidth® ROL process uses a Stirred Media Reactor (SMRt reactor) to achieve copper recoveries of 98% in 6 hours or less at 80°C. Prior to oxidative leaching, the chalcopyrite concentrate is reductively activated to obtain a partial conversion of chalcopyrite to a binary, copper sulfide thereby activating the chalcopyrite for rapid oxidative leaching.

The chalcopyrite was activated at 80 °C at pH 1.8. The degree of conversion was typically 2% to 6%. The pre-activation process takes only minutes to complete at temperatures of 80°C. The total atmospheric leaching process, incorporating the pre-activation and Stirred Media Reactor is compatible with existing SX/EW processes (Chaiko, et al., 2015).

The Sepon Copper Process

The Sepon Copper Process can be considered as a “hybrid” of a copper leach and pyrite oxidation process. This process was developed for the recovery of copper from the Sepon copper deposit in Laos. The mineralogy of this deposit is complex. Copper is present mainly as chalcocite with pyrite and a large component of clay mineralization.

The autoclave process of the flotation concentrate produces a basic ferric sulfate product (as opposed to the usual hematite product). The basic ferric sulfate product can then be re-leached to produce a strong ferric sulfate solution for application to atmospheric leaching.

One of the main advantages of the Sepon process is the possibility of scavenging any remaining copper minerals in the pyrite float concentrate that were not leached in the atmospheric leach (Dreisinger, 2006).

The Brisa Process

The BRISA process was developed by Carranza et al. (1997). In this process for copper recovery from chalcopyrite, the bioleaching is performed in two separate biological and chemical stages. In the chemical stage, chalcopyrite concentrates are leached with ferric sulfate in agitated reactors at 70ºC using silver as a catalyst. In the biological stage, biooxidation of ferrous to ferric uses mesophilic bacteria (Romero et al., 2003).

The BioCOP™ Process

The BioCOP™ process was developed by BHP Billiton to dissolve copper from chalcopyrite (Tunley, 1999). In this process, thermophiles leach chalcopyrite at 65 to 80°C. Pre-leaching ahead of oxidation leaching is helpful for copper recovery when treating secondary copper sulfides but it has a minor effect on chalcopyrite leaching (Peacey et al., 2003). Leaching of chalcopyrite concentrate is complete within 10 days.

Oxygen consumption is high due to the complete oxidation of sulfur to sulfate (Ramachandran et al., 2007). BHP Billiton and Codelco built a demonstration plant at Chuquicamata, in the north of Chile (Dresher, 2004).

The Bactech / Mintek Process

In the BacTech / Mintek process, moderate and extreme thermophilic cultures, in a range between 40 to 55°C and 70°C, respectively, are used for chalcopyrite concentrate leaching. In this process the feed is ground to a P_{80} of 10 µm, and leaching and ferrous biooxidation are carried out in separate tanks. Sulfide is converted to elemental sulfur and sulfate. Sulfate is precipitated as gypsum, and soluble iron is precipitated as hydronium jarosite.

BacTech and Mintek developed a bioleaching process for treatment of various copper concentrates (Staden, 1998). This technology was tested in a small demonstration plant at the Mt. Lyell mine in Tasmania over a period of 15 months (Potts, 2001). A large pilot plant of the process was also successfully operated at the research facilities of Peñoles in Monterrey, Mexico (Miller, 1999).

2.3 Thermodynamics of chalcopyrite dissolution

In order to establish the proper conditions for the dissolution of the chalcopyrite, it is imperative to study Eh-pH or Pourbaix diagrams, which consider both the reduction potential and the activity of the protons. These representations will help us to identify the predominant species in solution and any intermediate solid phases that are present at equilibrium.

However, Eh-pH diagrams represent only the equilibrium and do not indicate which leaching pathway will be the most appropriate nor show the kinetics of the reactions involved. The Pourbaix diagram for the $CuFeS_2$-H_2O system is in Figure 2. This diagram shows that the dissolution of chalcopyrite in an acid medium takes place through a solid transformation to different intermediate sulfides (Cu_5FeS_4, CuS, Cu_2S) that are increasingly richer in copper. According to this diagram, at a pH lower than 4, an oxidizing redox potential higher than +0.4 V is required to dissolve copper from chalcopyrite. These conditions are achieved using oxidizing agents such as ferric sulfate.

Ferric sulfate leaching of chalcopyrite can be represented by the following reactions (Dutrizac & MacDonald, 1974):

$$CuFeS_2 + 2\ Fe_2(SO_4)_3 \rightarrow CuSO_4 + 5\ FeSO_4 + 2\ S^0 \quad \text{Eq. 5}$$

$$CuFeS_2 + 8\ Fe_2(SO_4)_3 + 8\ H_2O \rightarrow CuSO_4 + 17\ FeSO_4 + 8\ H_2SO_4 \quad \text{Eq. 6}$$

Despite of all the information we can extract from the Pourbaix diagram, it should be noted that the kinetics of the reactions are not considered. For example, according to this diagram, covellite oxidizes to chalcocite and sulfate ions through the following reaction:

$$2\ CuS + 4\ H_2O \rightarrow Cu_2S + SO_4^{-2} + 8\ H^+ + 6\ e^- \quad \text{Eq. 7}$$

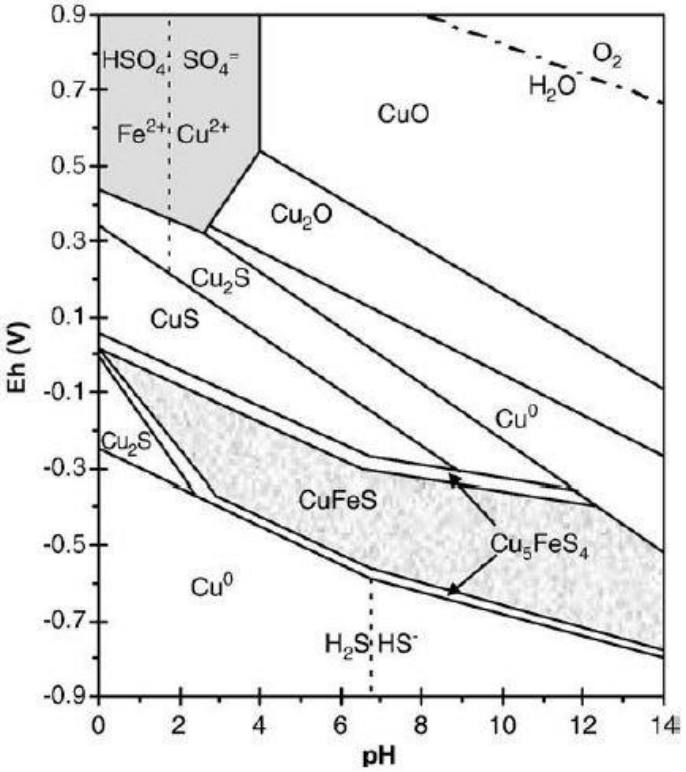

Figure 2. Pourbaix diagram for $CuFeS_2$-H_2O system at 25°C ©(Garrels & Christ, 1965) (Reproduced with permission from Elsevier).

However, this reaction only occurs over geological time (Peters, 1992). In addition, Figure 2 shows that elemental sulfur is thermodynamically stable over a narrow potential range at pH values lower than 9. However, sulfur has been shown to be far more stable with respect to oxidation in hydrometallurgical time frames of hours to days.

Figure 3 shows the extended sulfur stability region. This diagram more accurately reflects the sulfur behavior in hydrometallurgical processes. For instance, it is well known that sulfur is not oxidized by ferric ions at a significant rate. Previously, the oxidation of sulfur in the temperature range of 60 to 170°C and oxygen partial pressure of 0.10 to 0.69 MPa has been studied.

$$S + \tfrac{1}{2} O_2 + H_2O \rightarrow H_2SO_4 \qquad \text{Eq. 8}$$

This reaction has been observed to depend greatly on temperature and oxygen pressure (Habashi & Bauer , 1966). However, increasing the temperature moderately to the range of 120°C to 160°C is not useful, since molten sulfur wets and agglomerates the sulfide particles (Vizsolyi et al., 1967), unless surfactants are used to avoid agglomeration. Despite that, rapid and complete copper recovery can be obtained at higher temperatures.

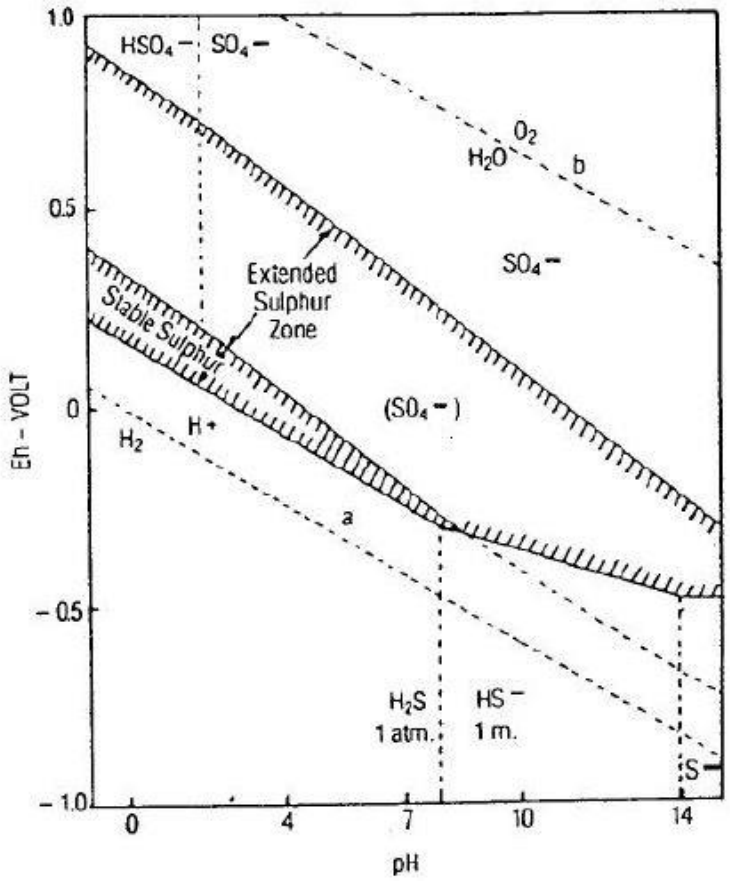

Figure 3. The potential-pH diagram for S-H_2O system showing the region of sulfur stability and the extended stability by a 300 kJ/mol barrier to the formation of sulfate (Peters, 1986).

According to previous studies, 98% copper extraction was achieved in ferric sulfate media at 200°C and 0.79 MPa oxygen pressure in only 30 min (Stanczyk, 1963). Other studies (King et al., 1993) showed results of the leaching of four different copper concentrates and obtained 98% copper extraction within 3 hours at 200°C and 0.69 MPa oxygen pressure. This rapid copper extraction at a high temperature is attributed to complete oxidation of elemental sulfur to sulfate.

2.4 Kinetics of chalcopyrite dissolution

Chalcopyrite is quite refractory to hydrometallurgical processing. Therefore, understanding the key controls of the aqueous oxidation and the rate controlling factors for chalcopyrite dissolution are imperative.

The kinetic information can only be derived from experimentation and observation, and is influenced by a number of factors, such as mineralogy, surface area, reactant concentrations, product layer formation and temperature. Although many studies have been conducted to establish the factors controlling chalcopyrite leaching, variable results and conclusions have been published because of the different conditions employed. This has made direct comparisons somewhat difficult.

Thus, despite the considerable literature on the kinetics of leaching in sulfate media, there is no agreement among the various authors about the rate-determining step, activation energy, form of the leaching curves and the dependence on the solution composition. This chapter summarizes some of the important conclusions relevant to the dissolution of chalcopyrite as reported in the literature.

2.4.1 Effect of temperature

High activation energy (greater than 40 kJ/ mol) generally indicates that the rate of reaction is controlled by the rate of a chemical or electrochemical reaction whilst a low activation energy (less than 40 kJ/mol) suggests a diffusion-controlled process.

The high values of activation energy determined by different authors shown in Table 1 demonstrate the need for high temperatures to break down bonds in the chalcopyrite crystal lattice. Results from the studies on chalcopyrite chemical leaching carried out by Cordoba et al. (2008), presented in Figure 4 showed that the effect of temperature is very pronounced in the range between 35 and 68°C. Chalcopyrite reaction rate is slow at low temperatures and increases at higher temperatures.

Furthermore, according to Dutrizac (1978) the leaching curves in the sulfate system are not linear. He looked at leaching synthetic chalcopyrite as a function of time at various temperatures in sulfate solutions. He claimed that the nonlinear kinetics observed in the sulfate system were caused by the blockage or partial blockage of the chalcopyrite surface by the elemental sulfur reaction product and/or precipitated iron compounds, which can form in fairly acidic solutions.

Table 1. Kinetics parameters for the leaching of chalcopyrite in sulfate media.

Initial $[Fe^{3+}]$	$[Fe^{2+}]$	$[Cu^{2+}]$	pH	Particle size	Leaching Kinetics	Leaching Time	Temp.	Activation Energy (kJ/mol)	Reference
-	-	-	-	-	Parabolic	~ 50 hours	95ºC	-	(Dutrizac, 1989)
No	No	No	No	Positive	Parabolic	~ 100 hours	60 - 80ºC	84	(Munoz et al., 1979)
Slightly	Negative	-	-	No	Linear	Over 55 days	90ºC	-	(Jones & Peters, 1976)
No	No	No	No	Positive	Parabolic	~ 3 hours	93ºC	-	(Beckstead, et al., 1976)
No	Negative	-	No	-	Parabolic	~ 60 hours	50 - 94ºC	71 ± 13	(Dutrizac et al., 1969)
Slightly	Negative	-	-	Positive	Linear – Parabolic	~ 300 hours	70ºC	83	(Hirato et al., 1987)
-	-	-	-	-	Parabolic	~ 50 hours	30 - 95ºC	38 - 63	(Dutrizac, 1978)
-	Negative	No	-	Positive	Parabolic	65 hours	90ºC	-	(Dutrizac, 1981)
No	-	-	No	Positive	Linear	~ 8 hours	32 - 50ºC	75	(Lowe, 1970)

The shape of the dissolution curves in sulfate media is one area of current controversy with some researchers (Dutrizac, 1989; Munoz et al., 1979; Beckstead, et al., 1976; Dutrizac, 1981) reporting "parabolic" kinetics while other workers (Jones & Peters, 1976; Lowe, 1970) observed linear kinetics.

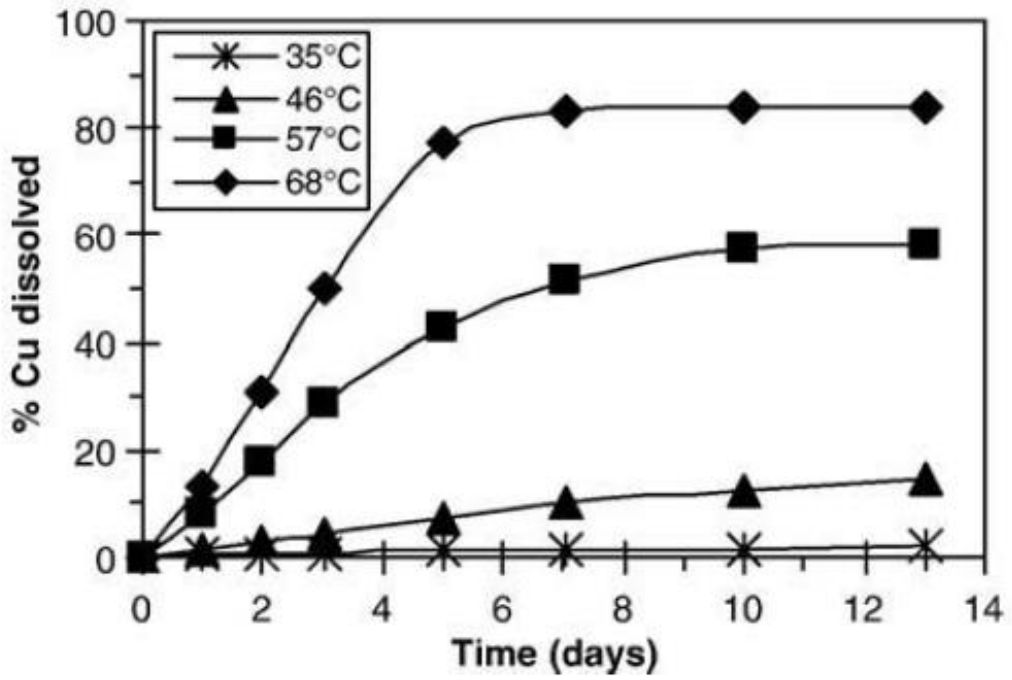

Figure 4. Effect of temperature in chalcopyrite leaching ©(Cordoba et al., 2008) (Reproduced with permission from Elsevier).

2.4.2 Effect of ferric ion concentrations

According to Hirato et al. (1987) the chalcopyrite dissolution rate improved when the concentration of ferric sulfate increased from 0.001 to 0.1 M. Later studies conducted by Dutrizac et al. (1969); and Lowe (1970) on pure chalcopyrite confirmed that the rate was nearly independent of the Fe^{3+} concentration above 0.01 M, but was sharply dependent on ferric concentration at lower levels.

These results were also confirmed by Dutrizac (1981), who suggested that the leaching rate in sulfate system was only marginally dependent, and varies as the 0.12 power of the Fe^{3+} concentration.

2.4.3 Effect of ferrous ion concentration

Controversial findings have been reported regarding the effect of ferrous ion concentrations on the chalcopyrite leaching rate. Several authors (Dutrizac et al., 1969; Dutrizac, 1981; Jones & Peters, 1976) have shown that the presence of ferrous ions decrease the leaching rate of chalcopyrite in sulfate solutions.

However, Hiroyoshi et al. (1987); Hiroyoshi et al. (2000); and Hiroyoshi (2001), have shown that chalcopyrite is more effectively leached in a ferrous sulfate solution than in a ferric sulfate solution. These authors explained the results on a model that involved the intermediate formation of chalcocite.

2.4.4 Effect of sulfuric acid concentration

As reported by Dutrizac et al. (1969), sulfuric acid prevents hydrolysis and precipitation of ferric salts, since proton attack is negligible. On the other hand, the results presented in Figure 5 by Cordoba et al. (2008) show that in a pH range of 0.5 to 2.0, dissolution of chalcopyrite with ferric sulfate diminishes with decreasing pH, although increased pH favours hydrolysis and precipitation of the oxidant.

Thus, a pH of less than 0.5 was observed to promote passivation due to the Fe-deficient surface resulting from the competition between Fe^{3+} and H^{+}. This effect becomes more obvious when the acid is very concentrated at 3 to 5 M (Antonijevic & Bogdanovic, 2004).

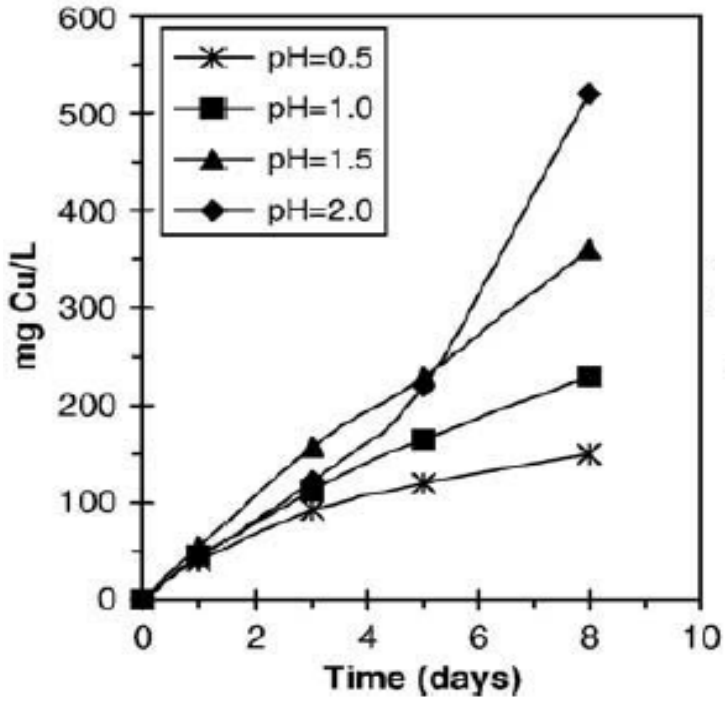

Figure 5. Influence of pH on chalcopyrite leaching at 68°C ©(Cordoba et al., 2008) (Reproduced with permission from Elsevier).

2.4.5 Effect of copper sulfate concentration

Considering the reaction for the dissolution of chalcopyrite in ferric sulfate media given by Eq. 1 it is a matter of interest to know what effect $CuSO_4$ has on the dissolution reaction.

Early work conducted by Dutrizac (1981) indicated that, at 90ºC, $CuSO_4$ slightly depresses the leaching rate. However, a different result was obtained by Hiroyoshi (2001) when he studied the effect of cupric ions in the presence of ferrous and ferric ions in sulfate media at 30ºC. He proposed a reaction model, which assumes that ferrous-promoted chalcopyrite leaching is due to the formation of intermediate Cu_2S, which is more amenable to oxidation than chalcopyrite. The Cu_2S formation occurs only when the redox potential of the solution is lower than a critical potential, which is a function of the ferrous and cupric ion concentrations. Therefore, he concluded that in the presence of high concentrations of cupric ions, chalcopyrite dissolution was enhanced by high concentrations of ferrous ions and that the copper extraction was mainly controlled by the ferrous to ferric ion concentration ratio.

2.4.6 Effect of particle size

Although it has been widely believed that fine grinding promoted more rapid dissolution of chalcopyrite, Jones & Peters (1976) reported that the leaching rate of chalcopyrite in 0.1 M ferric sulfate was independent of particle size below 149 µm at 90ºC. Later, Dutrizac (1981) showed that the reaction rate was directly proportional to sample surface area. Based on these results, presented in Figure 6, the author found that the rate increased as the mean particle size decreased below 149 µm. He stated that there is a direct correlation between the rate of dissolution and the surface area of the chalcopyrite. Hence, the role of fine grinding is to increase the surface area exposed, by decreasing the particle size.

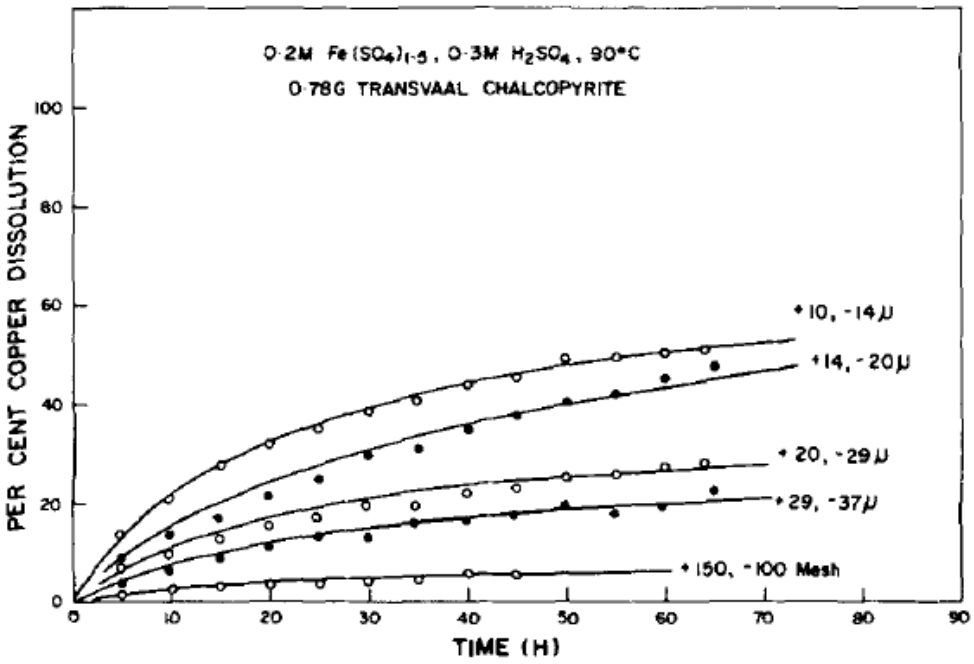

Figure 6. Effect of the particle size on the dissolution of chalcopyrite at 90ºC ©(Dutrizac, 1981).

2.4.7 Effect of agitation

According to Dutrizac & Macdonald (1974), there is a general agreement that agitation does not promote the leaching of chalcopyrite. In other words, the rate is not controlled by mass transfer across the liquid boundary layer. It is important to bear in mind that sufficient agitation must be provided to suspend the particles to prevent their caking, and to eliminate gross solution inhomogeneities.

2.4.8 Effect of redox potential

The redox potential determined by the concentration of Fe^{3+} to Fe^{2+} in solution is an important factor affecting metal sulfide minerals as noted by Hiroyoshi et al. (2002).

According to Hiroyoshi et al. (2001) and Petersen & Dixon (2006), the chalcopyrite leaching rate increases with increasing redox potential, reaches a maximum at an optimum redox ("active") potential, and then decreases at higher ("passive") potential. At very high ("transpassive") potential the rate increases again. Hence, controlling the solution potential is necessary to obtain rapid kinetics (Ahonen & Tuovinen, 1993).

2.4.9 Passivation of chalcopyrite

After almost a century of research into the mechanisms of chalcopyrite dissolution in ferric medium, there is finally a consensus on the formation of a passivating layer on the surface which slows down the oxidation reaction (Li et al., 2010). Despite that, the nature of this film, and the mechanism by which it forms, is still unknown and is a subject of considerable dispute.

Several theories and hypotheses have been proposed. One theory explained that two intermediate products of covellite and bornite, acting as a "solid electrolyte interphase" between the unreacted mineral and the solution, cause the passivation of the chalcopyrite (McMillan et al., 1982).

Another theory proposed that the elemental sulfur produced during the ferric leaching forms a compact and protective layer. This layer covers the ore particles and becomes increasingly denser as the reaction progresses. Therefore, it becomes a hindrance and impedes the transport of reactant and products to and from the surface of the chalcopyrite (Dutrizac, 1989; Munoz et al., 1979; Stott et al., 2000; Majima et al., 1985).

A third theory suggests that the passivating layer is a copper-rich polysulphide CuS_n ($n < 2$), which forms as a result of solid state changes that occur in the mineral during leaching (Mallikarjunar et al. 1984; Hackl et al., 1995).

The fourth theory was recently proposed by Stott et al. (2000). These authors postulated that the precipitation of iron-hydroxy compounds on the mineral surface during leaching coincided with a decrease in the dissolution rate. These compounds hinder the leaching by restricting mass transfer of ions to the surface. Thus, this layer can eventually cover the entire surface and prevent further leaching. A study by Parker et al. (2003) confirmed the formation of jarosite, which was suggested as causing the passivation.

The latest theory, based on the interpretation on the effect of visible light on the dissolution of chalcopyrite in sulfuric acid solution, states that the overall dissolution behavior is not limited by passive layer or films, but is an intrinsic property of the chalcopyrite determined by its semiconducting properties (Crundwell, et al., 2015).

2.5 Enhancing the kinetics of the dissolution of chalcopyrite in the presence of a catalyst

2.5.1 Thiourea

Thiourea (TU) is a sulfur-organic compound with the chemical formula CH_4N_2S; the chemical structure is presented in Figure 7. TU has a molecular weight of 76.12 g/mol and a density of 1.44 g/cm^3 (Sahu et al., 2011).

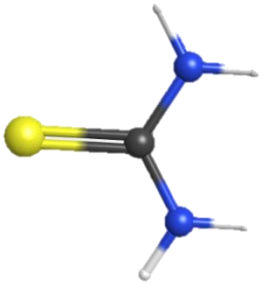

Figure 7. Scheme of thiourea chemical structure. Sulfur is shown in yellow, carbon in black, nitrogen in blue and hydrogen in white.

In the copper mining industry, the most important role of the TU is its ability to act as a copper cathode leveling and brightening agent, where TU is absorbed on the copper surface (Alodan & Smyrl, 1998). The adsorption of TU takes place in several stages: TU molecules are first adsorbed, and subsequently undergo a chemical transformation, leading to the appearance, on the cathode surface, of TU decomposition products. Some researchers (Bolzan et al., 2001) assume that TU forms complex compounds with monovalent copper in solution and that these compounds, on becoming adsorbed on the cathode, influence the electrodeposition of Cu^{2+}.

On the other hand, investigations on copper in dilute acidic solutions have shown conflicting results. Some indicated that TU acts as an accelerator to enhance the dissolution rate of copper. Others demonstrated that TU acts as an inhibitor to depress the dissolution rate of copper (Zheng, 2001).

In the gold industry, given the environmental concerns associated with the leaching of gold with cyanide, considerable efforts have been made to search for alternatives to cyanidation. The dissolution of gold and silver in acidic TU solution was initially reported by Plaskin in 1941 (Plaskin & Kozhukeva, 1960). TU was found to dissolve gold effectively and could be a potential substitute for cyanide leaching solution. Leaching with TU, has several advantages over the cyanidation process, including leaching rates that are up to 10 times higher (Orgul & Atalay, 2002).

2.5.2 Thermodynamics of thiourea

The thermodynamic data for the formation of Fe(III) - TU complexes was taken from Li & Miller (2007):

$Fe^{3+} + SO_4^{2-} + Tu \rightarrow [FeSO_4(Tu)]^+$ $\log\beta = 6.6$ Eq. 9

$Fe^{3+} + Tu \rightarrow Fe(Tu)^+$ $\log\beta = 2.2$ Eq. 10

$Fe^{3+} + 2\ Tu \rightarrow Fe(Tu)_2^{3+}$ $\log\beta = 8.4$ Eq. 11

As for the complex formation equilibrium data for the Cu- U system, Krewska et al. (1980) reported the following data for the Cu(I)-TU and Cu(II)-TU systems:

$Cu^+ + Tu \rightarrow Cu(Tu)^+$ $\log\beta = 11.0$ Eq.12

$Cu^+ + 2\ Tu \rightarrow Cu(Tu)_2^+$ $\log\beta = 12.8$ Eq.13

$Cu^+ + 3\ Tu \rightarrow Cu(Tu)_3^+$ $\log\beta = 14.0$ Eq.14

$Cu^+ + 4\ Tu \rightarrow Cu(Tu)_4^+$ $\log\beta = 15.4$ Eq.15

$Cu^{2+} + 2\ Tu \rightarrow Cu(Tu)^+ + ½\ FDS^{2+}$ $\log K = 5.7$ Eq.16

$Cu^{2+} + 3\ Tu \rightarrow Cu(Tu)_2^+ + ½\ FDS^{2+}$ $\log K = 8.5$ Eq.17

$Cu^{2+} + 3\ Tu \rightarrow Cu(Tu)_3^+ + ½\ FDS^{2+}$ $\log K = 11.3$ Eq.18

$Cu^{2+} + 4\ Tu \rightarrow Cu(Tu)_4^+ + ½\ FDS^{2+}$ $\log K = 13.6$ Eq.19

2.5.3 Behavior of thiourea in ferric sulfate-sulfuric acid solutions

According to the literature, in the presence of oxidants such as hydrogen peroxide or ferric ions, TU is oxidized in successive stages to give a number of products, including hydrogen sulfide, sulfur and sulfate ion. If these species are formed, there is an irreversible consumption of TU (Cheng & Lawson, 1987).

Figure 8 presents some of the results of the degree of TU decomposition and $Fe_2(SO_4)_3$ consumption after successive reactions between TU and $Fe_2(SO_4)_3$.

Based on these results, the authors found that there was a significant amount of decomposition of TU in the first few hours of the reaction, while no more decomposition of TU occurred after 6 h in the presence of initial 5, 10 and 15 g/L of TU.

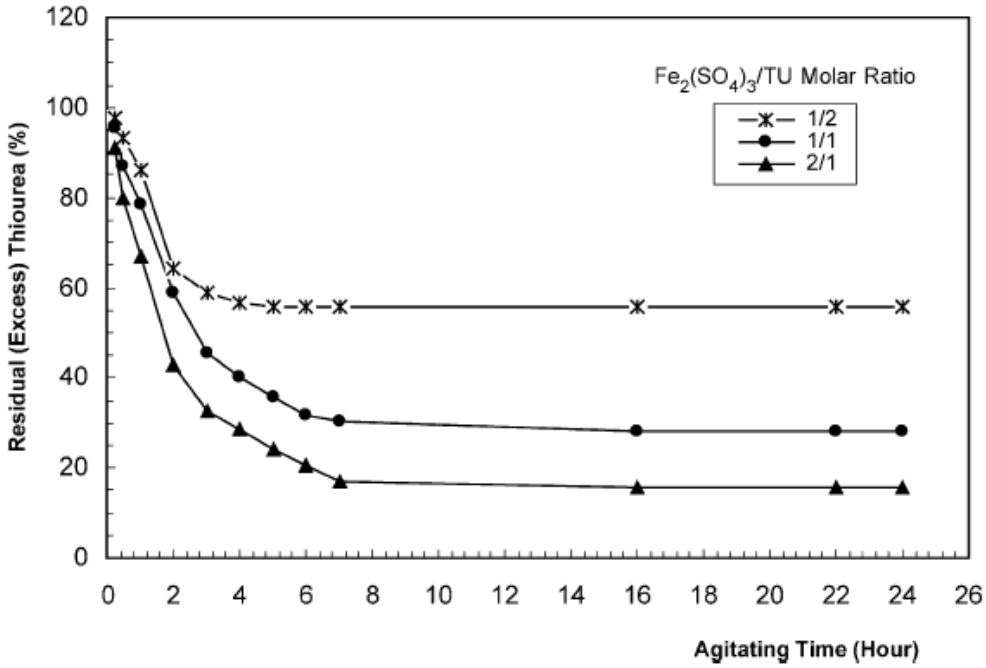

Figure 8. Degree of thiourea decomposition and $Fe_2(SO_4)_3$ consumption over time ©(Orgul & Atalay, 2002) (Reproduced with permission from Elsevier).

2.5.4 Behavior of thiourea in copper sulfate-sulfuric acid solutions

In a concentrated acidic solution ($CuSO_4$, H_2SO_4), Javet et al. (1967) and Javet & Hintermann (1969) reported that TU slowly forms a complex with Cu^+, which decomposes slowly,

$$Cu^+ + Tu \rightarrow^{k_1} (CuTu)^+ \rightarrow^{k_2} \text{degradation products} \qquad \text{Eq. 20}$$

where k_1 and k_2 are kinetic constants whose values decrease when the TU concentration decreases (at 100 mg/L TU, $k_1 = 7.9 \times 10^{-4}$ sec^{-1} and $k_2 = 1.5 \times 10^{-5}$ sec^{-1}; while at 40 mg/L TU, $k_1 = 6.3 \times 10^{-4}$ sec^{-1} and $k_2 = 8.4 \times 10^{-6}$ sec^{-1}).

On the other hand, Baub & Schiffner (1971) observed the decomposition of TU in weakly acidic copper sulfate solutions (pH from 1.5 to 3.8, 0.5 M $CuSO_4$ at 20°C). When TU was added to the solution, the pH of the solution decreased as a function of time. The TU is oxidized by cupric ions, leading to release of protons and hence a decrease in pH.

According to Gupta (1963), TU may be oxidized in successive stages to form a number of products. The first product is formamidine disulfide (FDS), which is formed easily in acidic solution by the action of oxidants, such as hydrogen peroxide or ferric sulfate at room temperature. The reaction scheme is presented in Figure 9. This reaction is followed by slower reactions, in which products are formed with sulfur in higher oxidation states, such as in sulfates ions.

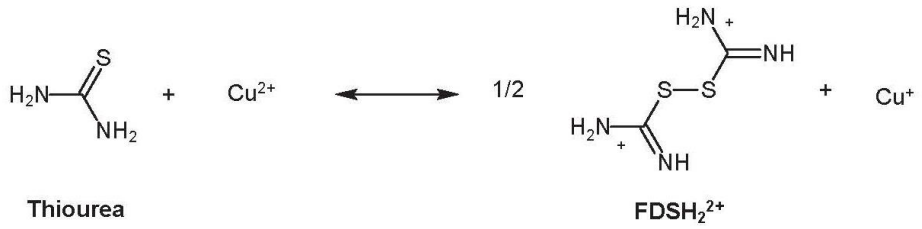

Figure 9. Scheme of the oxidation reaction of thiourea in the presence of Cu^{2+}.

2.5.5 Effect of temperature on the stability of thiourea

It is well established that the chalcopyrite leaching rate increases with a rise in temperature. Hence, a good control of TU concentration and a better knowledge of the effect of temperature on the stability of the catalyst is crucial for the leaching process.

The results of the work by Zuñiga & Ren (personal communication, 2017) are presented in the following sections to elucidate the stability of TU at different temperatures under the conditions of our system.

Effect of temperature in acidic water

Several studies have shown that TU undergoes slow hydrolysis in the presence of acids (Krewska et al., 1980; Fabricius et al., 1996). Therefore, the concentration of TU is constantly lowered in acidic solutions. Results obtained by Zuñiga & Ren (personal communication, 2017) for the test conducted at pH 1.8 with an initial 2 mM of TU in solution differs from the results reported by previous authors. Figure 10 shows that the free TU concentration remains fairly stable even after 10 days. In acidic water, increasing the temperature from 25ºC to 65ºC has no apparent effect on the stability of free TU concentration.

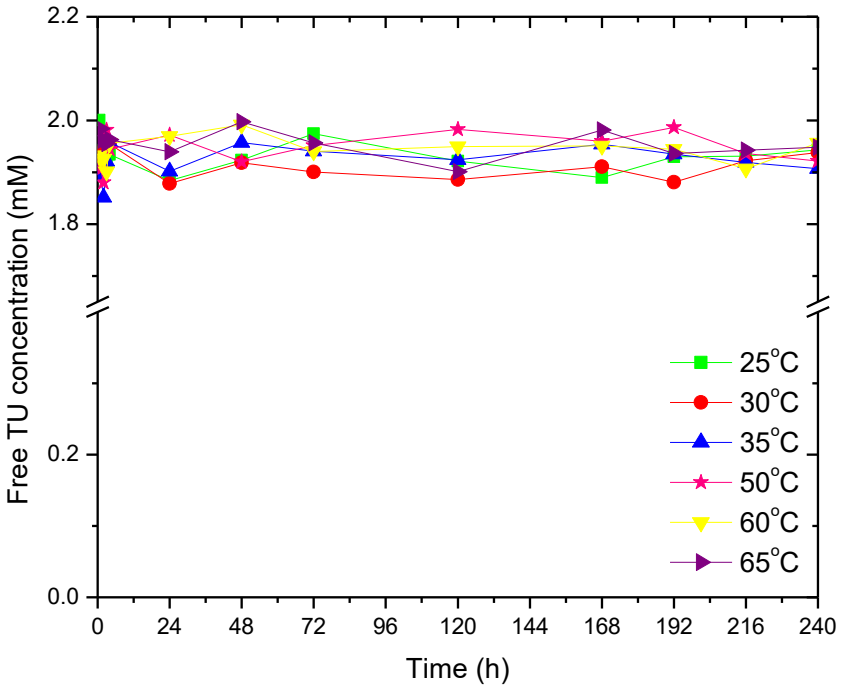

Figure 10. Effect of temperature on the stability of free thiourea in acidic water (Zuñiga & Ren, personal communication temperature, 2017).

Effect of temperature in ferric sulfate medium

In contrast to the effect of temperature in acidic water, ferric sulfate media has a strong effect on the oxidation of free TU. This marked difference increases as the temperature rises. As seen in Figure 11, once the temperature rises above 50ºC, the concentration of free TU in solution is roughly non-existent after 24 hours. This sudden drop could be attributed to the formation of a thin layer of precipitate on the walls of the reactors. This precipitate was found at the highest temperatures 60ºC and 65ºC and could be the result of the complete oxidation of the TU. It is noteworthy to mention that the amount of residue was insufficient to pursue further chemical analysis. Based on the excess of ferric ions in solution and the conditions present in this system, such as, temperature; and pH, the precipitate could be some iron compounds like jarosite. On the other hand, sulfur presents itself as a suitable candidate because it is the further oxidized form of TU, which could explain the drastic drop in free TU concentration in those experiments (Zuñiga & Ren, personal communication, 2017).

This significant loss of free TU due to the effect of temperature lead us to conclude that the experimental matrix of this study is impractical for temperatures above 50ºC. Increasing the temperature would be a major drawback while trying to maintain a constant free TU concentration for the leaching experiments, and could eventually alter the conditions of the system.

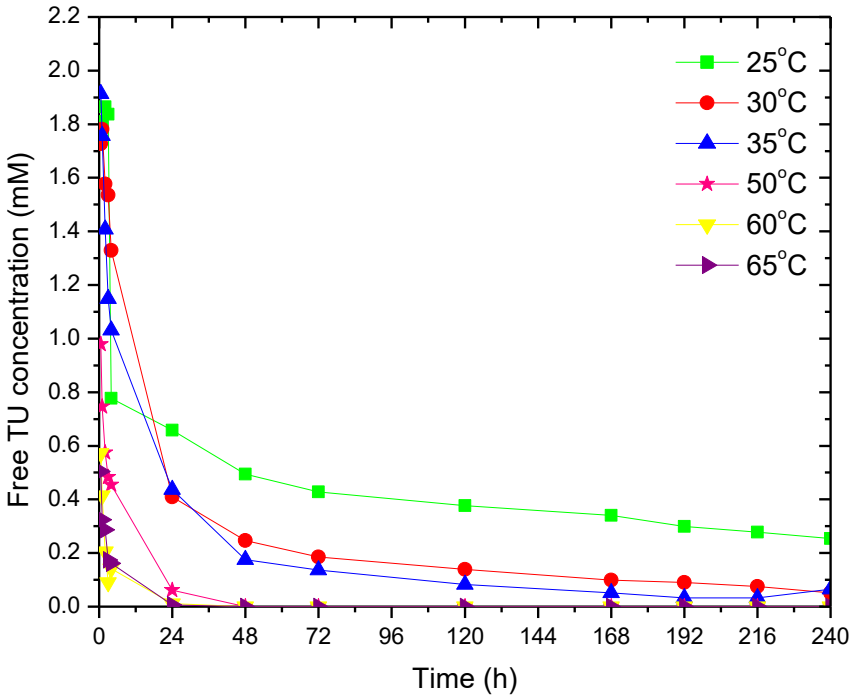

Figure 11. Effect of temperature on the stability of free thiourea in acidic ferric sulfate media at pH 1.8 (Zuñiga & Ren, personal communication, 2017).

Chapter 3 Experimental

A general description of the experimental considerations, materials, instrumentation, and analytical techniques employed during this study is presented in this chapter.

3.1 Experimental Considerations

The main objective of this study is to provide a better understanding of the effect of thiourea in the leaching kinetics of chalcopyrite. In order to apply the results in heap leaching technology, the following experimental considerations have been made:

- The temperature in the baseline in the experimental matrix was set at 20ºC (293 K).
- The pH value in the baseline was set at 1.8, to avoid iron precipitation.
- The solid sample used was pure chalcopyrite prepared using hydrothermal synthesis.
- All the tests were conducted under the assumption of unlimited lixiviant in order to simulate steady state conditions.
- The range of TU concentrations chosen was based on the fact that the technology is meant to be applied as a bioleaching process. According to the literature, TU and its possible complexes with Cu^{+} could act as an antibacterial (Arslan et al., 2009). Therefore, having an excessive amount of TU in solution would be detrimental and could eventually hinder bacteria activity.
- All the ORP measurements presented in this study are in terms of Ag/AgCl.

3.2 Materials

All the chemicals used for the preparation of the lixiviants were reagent grade: ferric sulfate pentahydrate, $Fe_2(SO_4)_3(H_2O)_5$ (Sigma-Aldrich, 97%); ferrous sulfate heptahydrate, $FeSO_4(H_2O)_7$ (Fisher Chemical, 100%); sulfuric acid, H_2SO_4 (Fisher Scientific, 95–98%); copper sulfate pentahydrate, $CuSO_4(H_2O)_5$ (Fisher Chemical, 100%); thiourea (Alfa Aesar, 99%); copper chloride, CuCl (Fisher Scientific, 93.99%); ferric chloride hexahydrate, $FeCl_3(H_2O)_6$ (Fisher Chemical, 99.1%); and tetrabutylammonium hydrogen sulfate, $C_{16}H_{37}NO_4S$ (Tokio Chemical Industry, 98%).

3.2.1 Lixiviant Preparation

The electrolyte of the baseline was mainly pH 1.8 sulfuric acid solution, except for specific cases, prepared with deionized water. TU was added in concentrations ranging from 0 to 2 mM, and ferric concentrations were varied from 0 to 120 mM.

3.2.2 Solid Preparation

In order to isolate the effects of impurities present in a mineral, this kinetic study was conducted using pure synthetic chalcopyrite.

The chalcopyrite synthesis was carried out in a Teflon lined reaction vessel. CuCl, $FeCl_3(H_2O)_6$ and CH_4N_2S aqueous solution were selected as the reactants. The chemical reaction is represented by Eq. 21.

$$CuCl + FeCl_3(H_2O)_6 + 2\ CH_4N_2S \rightarrow CuFeS_2 + 2\ CH_4Cl_2N_2 \qquad \text{Eq. 21}$$

For this procedure, appropriate amounts of CuCl, $FeCl_3(H_2O)_6$ and CH_4N_2S aqueous solution were put into a stainless steel autoclave of 250 mL capacity. The vessel was maintained at 225ºC for 24 h and allowed to cool to room temperature. The precipitate was separated by filtration and was then washed several times with acidic water to remove the $CH_4Cl_2N_2$ and any other impurities. After being dried at room temperature the samples were characterized by XRD.

3.3 Experimental Set-Up and Procedures

3.3.1 Instrumentation

All the tests were conducted in sealed Applikon Dependable Instruments 2-L jacketed glass reactors fitted with a single six-blade Rushton turbine impeller and three baffles made of 316 stainless steel. The stirring shaft was attached to an exterior motor and was set to around 500 rpm. Before adding the chalcopyrite, the solution was heated, when needed, to the desired temperature using a recirculating water bath.

A pH probe and a redox potential probe were connected to digital Applikon Dependable Instrument 1030 Bio Controller, and were inserted into the reactor. The data outputs from these probes were recorded to a computer from the controller using LabView software.

Before starting the leach test, the pH probe was calibrated using buffer solutions at pH 1 and pH 4. The redox potential probe was placed in a standard solution (470 mV *vs* Ag/AgCl at 25°C) to ensure that it was working properly. Figure 12 shows the set-up of the leaching experiments.

The hydrothermal synthesis of chalcopyrite described in section 3.2.2 was carried out in a Teflon-lined steel vessel shown in Figure 13.

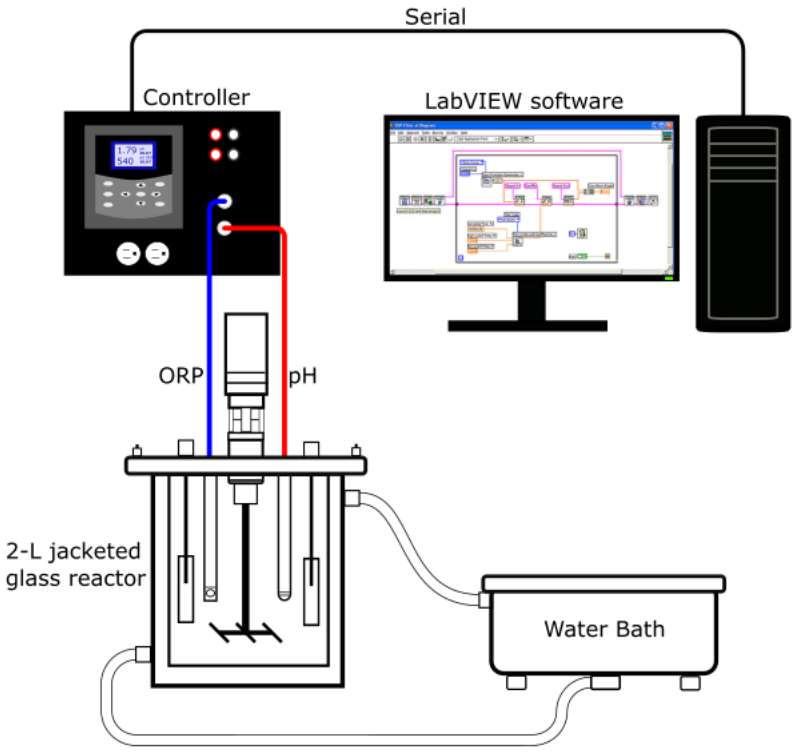

Figure 12. Schematic of the experimental set-up for the leaching experiments (not to scale).

Figure 13. Pressure vessel for hydrothermal synthesis.

3.3.2 Procedures

Leaching Test

All solutions used in the experiments were freshly prepared. Samples of 2.0 mL were taken at regular time intervals and assayed for copper and iron by inductively coupled plasma optical emission spectrometry (ICP-OES). ORP measurements were recorded every 5 minutes to evaluate changes over the course of the experiment. The volume used was 2 L, and the pulp density for all the test was 1 g/L. Hence, 2 g of synthetic chalcopyrite was added to each leaching test. Table 2 shows the experimental matrix of all the tests included in this study.

Table 2. Experimental matrix.

Exp	Effect	TU (mM)	Fe^{3+} (mM)	pH	Cu^{2+} (mM)	T (K)
1	Baseline	2	40	1.8	0	293
2	TU	**0.5**	40	1.8	0	293
3		**1**	40	1.8	0	293
4	Fe^{3+}	2	**20**	1.8	0	293
5		2	**80**	1.8	0	293
6		2	**120**	1.8	0	293
7	pH	2	40	**0.8**	0	293
8		2	40	**1.2**	0	293
9		2	40	**1.5**	0	293
10	Cu^{2+}	2	40	1.8	**2**	293
11		2	40	1.8	**4**	293
12		2	40	1.8	**10**	293
13	Temp	2	40	1.2	0	**308**
14		2	40	1.2	0	**323**
16	Control	**0**	**20**	1.8	0	293
17		**0**	**80**	1.8	0	293
18		**0**	**120**	1.8	0	293
19		**0**	40	**0.8**	0	293
20		**0**	40	**1.2**	0	293
21		**0**	40	**1.5**	0	293
22		**0**	40	1.8	**2**	293
23		**0**	40	1.8	**4**	293
24		**0**	40	1.8	**10**	293
25		**0**	40	1.8	0	**308**
26		**0**	40	1.8	0	**323**
27	PSD	0	40	1.8	0	293
28		0	40	1.8	0	293
29		2	40	1.8	0	293
30		2	40	1.8	0	293

Stability of thiourea test

In order to establish a baseline for the stability of the catalyst under the conditions of the system, the following experimental tests were carried out. For each test, the effect of each parameter on the concentration of free TU was determined using the same experimental set-up described for the leaching test.

- Effect of copper sulfate in solution

A solution of 2 L with 2 mM of TU, 40 mM Fe^{3+} and pH 1.8, was added into the stirred reactor. After 10 minutes, sample 0 was taken. After every 10 minutes interval, a stepwise addition of copper sulfate was performed and liquor samples were taken to be assayed by HPLC.

- Effect of mineral surface

A solution of 2 L with 2 mM of TU, 40 mM Fe^{3+} and pH 1.8, was added into the stirred reactor. After 10 minutes, sample 0 was taken. After every 10 minutes interval, a stepwise addition of synthetic chalcopyrite was performed and liquor samples were taken to be assayed by HPLC.

- Effect of pH

A solution of 2 L with 2 mM of TU, 40 mM Fe^{3+} and pH 1.8, was added into the stirred reactor. After 10 minutes, sample 0 was taken. After every 10 minutes interval, a stepwise addition of concentrated sulfuric acid was performed in order to decrease the pH. Every time acid was added, liquor samples were taken to be assayed by HPLC to study the change in the free TU concentration.

- Effect of different Fe^{3+}/Fe^{2+} ratios

A solution of 2 L with 2 mM of TU, a set total amount of 40 mM Fe, as different Fe^{3+}/Fe^{2+} ratios and pH 1.8 was added into the stirred reactor containing. Table 3 shows the tests conducted to study this parameter.

Once the TU was fully dissolved in solution, sample 0 was taken. Samples of 2.0 mL were taken at regular time intervals and assayed by HPLC to study the change in the free TU concentration over time.

Table 3. Experimental set to study the effect of different Fe^{3+}/Fe^{2+} in the stability of thiourea over time.

Exp	$[TU]_0$ (mM)	pH	$[Fe^{3+}]_0$ (mM)	$[Fe^{2+}]_0$ (mM)	$[Fe^{3+}/Fe^{2+}]_0$
1	2	1.8	0	40	-
2	2	1.8	10	30	0.33
3	2	1.8	20	20	1
4	2	1.8	30	10	3
5	2	1.8	35	5	7

3.4 Analytical Procedures

Once the samples were taken from the reactor, the aqueous leachates and the solid leaching residues were analyzed with the following techniques.

3.4.1 Liquid sample analysis

Inductively coupled plasma emission spectrometry (ICP-OES)

Copper and iron concentration in the leachates were assayed with a Varian 725 – ES ICP-OES. In order to analyze the samples, solutions were prepared in a solution of 2% nitric acid (HNO_3). The internal standard for the assays was 10 ppm europium (Eu) in 2% nitric acid. The standards range from 0 to 100 ppm for copper and 0 to 500 for iron. All the samples were diluted in a 1:20 ratio.

High-performance liquid chromatography (HPLC)

The concentration of the catalyst in the liquid samples was assayed using a Waters 600 E HPLC, which includes a Waters 717_{plus} auto sampler, an automatic eluent degassing device and a Waters 2487 dual λ absorbance detector.

The separation was performed on a Restek C18 column (5 μm, 250 × 4.6 mm i.d.). In order to achieve better separation, the mobile phase was prepared by mixing methanol and 1 mM of tetrabutylammonium hydrogen sulfate (TBA-HS) solution in a volumetric ratio of 5:95. Its pH was set to 1.7 and the flow rate was set to 1.2 mL/min.

3.4.2 Solid sample analysis

Particle Size Distribution

Particle size distribution was determined with a Malvern Mastersizer 2000 particle size analyzer. This equipment provides an accurate measurement of the size of a particle, and, more specifically, the distribution of different sizes within a sample.

Prior to the analysis, the sample was prepared in a 5% solid suspension in deionized water. In order to make sure that the measurement was accurate, each analysis was compared with a measurement after performing ultrasound, to disperse the particles. This process was repeated until the difference between the two measurements (before and after ultrasound) was less than 1%.

X-Ray Diffraction (XRD)

X-Ray diffraction was performed with a Rigaku Rotaflex D-Max diffractometer equipped with a rotation anode, a copper target X-ray tube (40 kV and 20 mA), a Cu Kα radiation source (= 1.5046 Å), and a diffracted beam monochromator composed of a graphite crystal and a scintillator detector.

Prior to the analysis, the solid samples were ground to a powder and spread on a slide. The scans were recorded between 0 and 90° (2θ), with a 0.01° step size and an acquisition time of 1 s/step. XRD simulations were done with the crystallographic software Match 3, version 4.1.

Scanning Electron Microscope (SEM)

The morphological characterization of the powders was conducted using a Hitachi S-3000, SEM-EDX. This technique provides images of the changes in morphology of the solid particle, such as cracks and pores that appear on the surface after leaching. Prior to the morphological analysis, the solid sample was mounted onto carbon double-sided tape and sputter-coated with a thin layer of Au-Pd.

Energy-dispersive X-ray spectroscopy (EDX)

The chemical characterization of the solid residues was conducted using a, FEI Quanta 650 SEM-EDX. This analytical technique was used to perform an elemental analysis of the sample.

Prior the analysis, the solid sample was embedded with an epoxy resin and inserted into a mold. The upper surface was ground and polished flat until 1 µm using monocrystalline diamond suspension water based. Finally, the polished surface was coated with carbon.

Chapter 4 Results and Discussions

4.1 Mineralogical characterization of the head ore

To avoid possible interactions with impurities, the chalcopyrite sample used in all experiments was 100% pure chalcopyrite prepared by hydrothermal synthesis. The sample was characterized by X-ray powder diffraction. The XRD pattern with the Rietveld refinement included is shown in Figure 14.

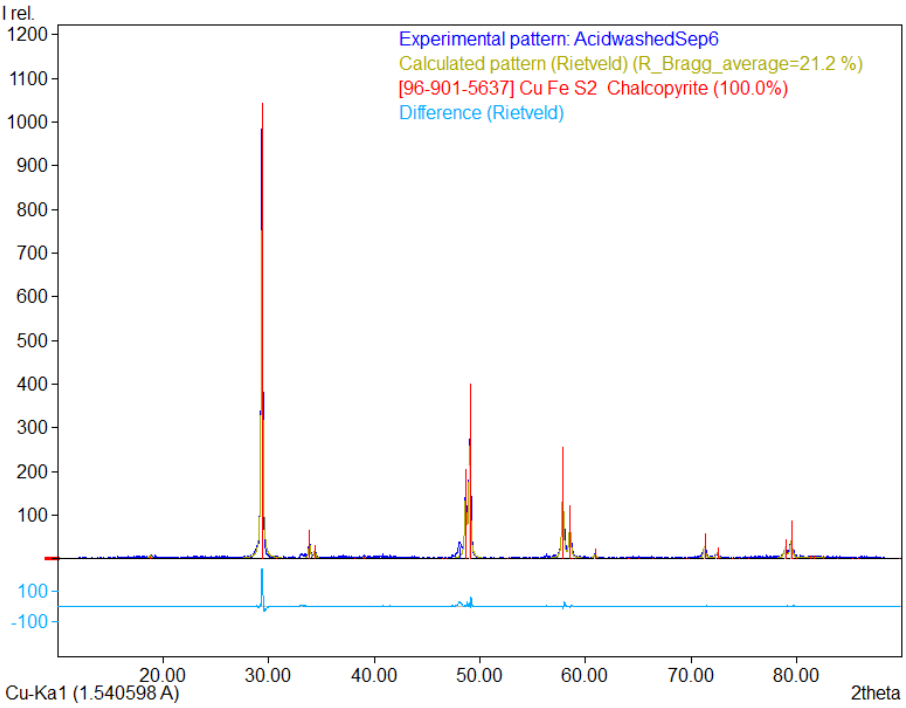

Figure 14. XRD pattern with Rietveld refinement analysis for the chalcopyrite sample used as head ore.

The XRD analysis and the Rietveld refinement were performed with the use of the software Match 3. The background, lattice parameters, background parameters, scale factor, sample displacement, atomic coordinates and isotropic displacement parameters were refined. All reflections are indexed to the chalcopyrite phase $CuFeS_2$.

After the refinement, the lattice constants were a = 5.2856 Å and c = 10.4192 Å, which are very similar to those reported in the literature (Burdick & Ellis, 1917; Hall & Stewart, 1973).

Moreover, no impurity phases, such as Cu_2S and FeS, were detected from this pattern. Although the R_{Bragg} is slightly higher (> 5%) to consider this as an ideal fit, some authors, e.g., (Toby, 2006), noted that R_{Bragg} is biased toward the model, since the information from the model is used to apportion intensity between overlapped reflections. Figure 15 shows a summary of the phase analysis report for the sample in the present study.

Match! Phase Analysis Report

Sample: AcidwashedSep6

Sample Data

File name	AcidwashedSep6.raw
Data range	10.061° - 90.062°
Number of points	8001
Step size	0.010
Rietveld refinement converged	Yes
Alpha2 subtracted	No
Background subtr.	Yes
Data smoothed	Yes
2theta correction	0.06582°
Specimen displacement correction (Bragg-Brentano geometry)	T = (-s/R) = 4.3477E-05
Radiation	X-rays
Wavelength	1.540598 Å

Matched Phases

Index	*Amount (%)*	*Name*	*Formula sum*
A	100.0	Chalcopyrite	Cu Fe S2
	30.6	*Unidentified peak area*	

A: Chalcopyrite (100.0 %)

Formula sum	Cu Fe S2
Entry number	96-900-7573
Figure-of-Merit (FoM)	0.968639
Total number of peaks	51
Peaks in range	51
Peaks matched	12
Intensity scale factor	1.05
Space group	I -4 2 d
Crystal system	tetragonal
Unit cell	a= 5.2890 Å c= 10.4230 Å
I/Ic	9.27
Calc. density	4.181 g/cm³
Reference	Hall S. R., Stewart J. M., "The crystal structure refinement of chalcopyrite, CuFeS2", Acta Crystallographica, Section B **29**, 579-585 (1973)

Figure 15. Summary phase analysis report for chalcopyrite sample.

The particle size of the synthetic chalcopyrite is d_{80} = 23.09 µm and the PSD results are presented in Figure 16.

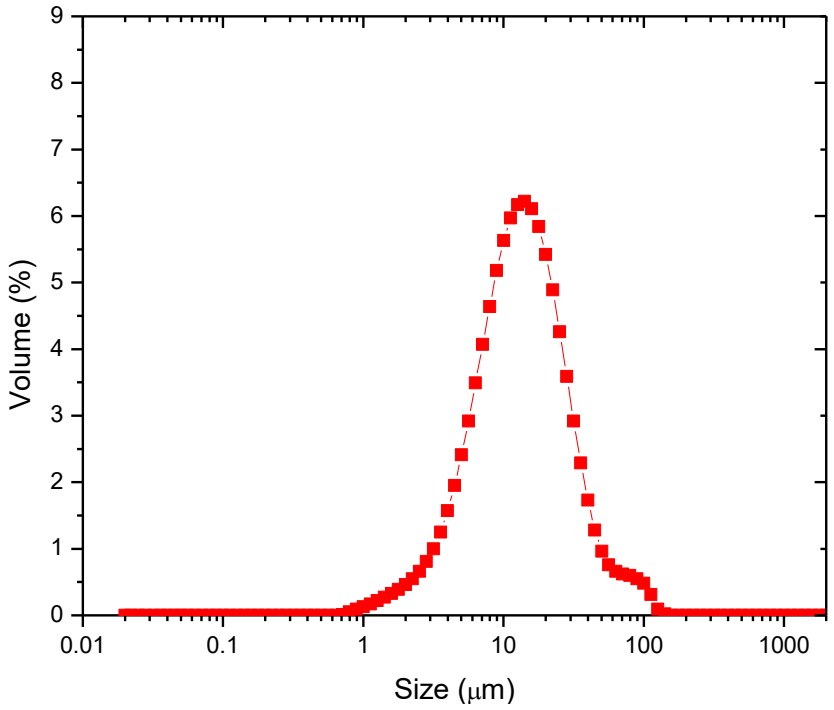

Figure 16. Particle size distribution of chalcopyrite sample used in the present study.

Based on these results, it can be concluded that the synthetic chalcopyrite has the same crystallographic properties as the natural mineral. In spite of this, if further analysis is required, the XRD pattern for each of the samples prepared by hydrothermal synthesis and used in the study are presented in Appendix A.

Furthermore, an XRD pattern of a sample of natural chalcopyrite is presented in Figure 17. From the figure, it can be observed, that even though, chalcopyrite is the only copper species present in the sample that is not the main phase. Among the impurities present in this sample, sphalerite could have some interactions with the catalyst. By using this sample as head the results could be misleading. Therefore, the need to isolate the effect of impurities and to study the chalcopyrite by itself, using 100% pure synthetic chalcopyrite is proven to be imperative.

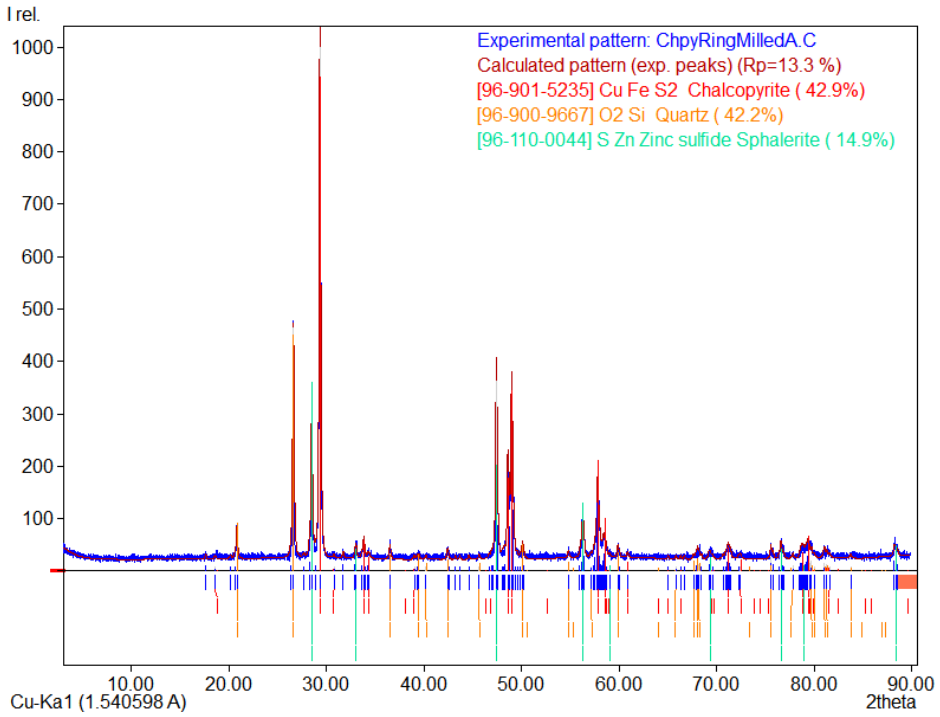

Figure 17. XRD pattern of natural chalcopyrite sample.

4.2 Determination of the baseline of thiourea concentration in the leaching test

The proposed mechanism for the leaching of chalcopyrite in the presence of TU clearly states that TU is responsible for the enhancement in leaching rates, not the oxidized forms such as FDS, nor the complexes that could be formed in the presence of ions like Cu^{+}/Cu^{2+} or Fe^{3+} (Ren, 2016). In light of this, it is crucial to maintain the "free TU" concentration as stable and high as possible. Therefore, to establish the role of important factors like copper concentration and mineral in solution on the behaviour of TU oxidation, additional experiments were carried out. The goal of these experiments was to determine which factor has an impact on the behaviour of the TU.

4.2.1 Effect of stepwise addition of copper sulfate on the free thiourea concentration

Figure 18 presents the results of the test conducted to study the behaviour of TU in the presence of increasing concentrations of copper sulfate in solution. After the addition of 136 ppm, which is ≈ 2 mM of Cu^{2+}, as copper sulfate, the change in free TU concentration was less than 0.7 mM. These results show that in the presence of copper, the free TU concentration available is not completely lost due to complexation. Moreover, copper is not the main factor that influences the TU oxidation under the conditions of our system.

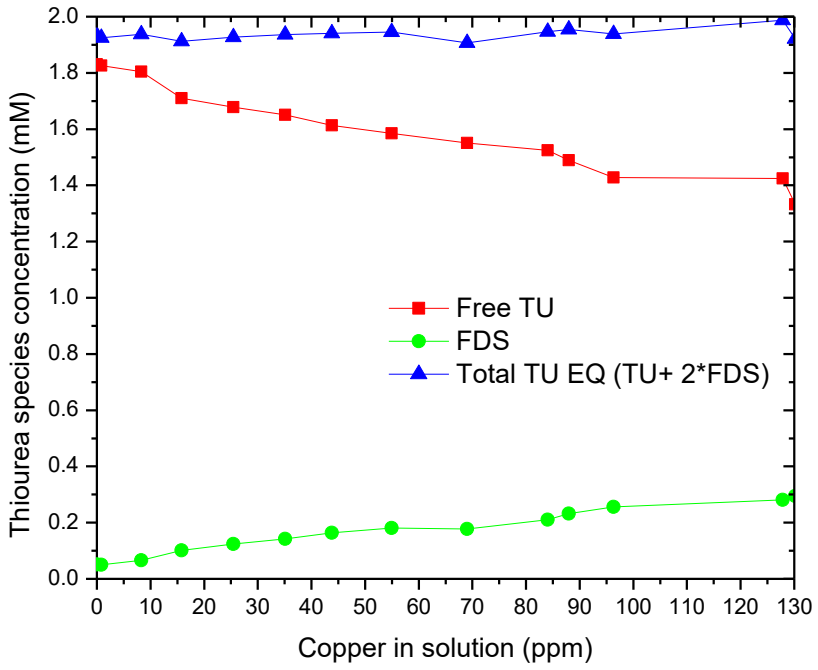

Figure 18. Behaviour of thiourea in the presence of increasing concentrations of copper sulfate in solution.

4.2.2 Effect of the stepwise addition of synthetic chalcopyrite on the free thiourea concentration

It is clear from Figure 19 that the rate of oxidation of TU to FDS is affected by the chalcopyrite surface area available in solution. In the presence of 0.25 g of chalcopyrite, 80 % of the TU was oxidized to FDS. Additions of even small quantities of mineral causes the free TU concentration to fall appreciably. These results indicate a direct correlation between the rate of oxidation and the surface area of the chalcopyrite available in solution to up to 0.19 m^2. Further additions after this point have no noticeable effect. The mineral surface available was determined using on the results given by the PSD analysis, which calculates the specific surface area assuming particles are spherical.

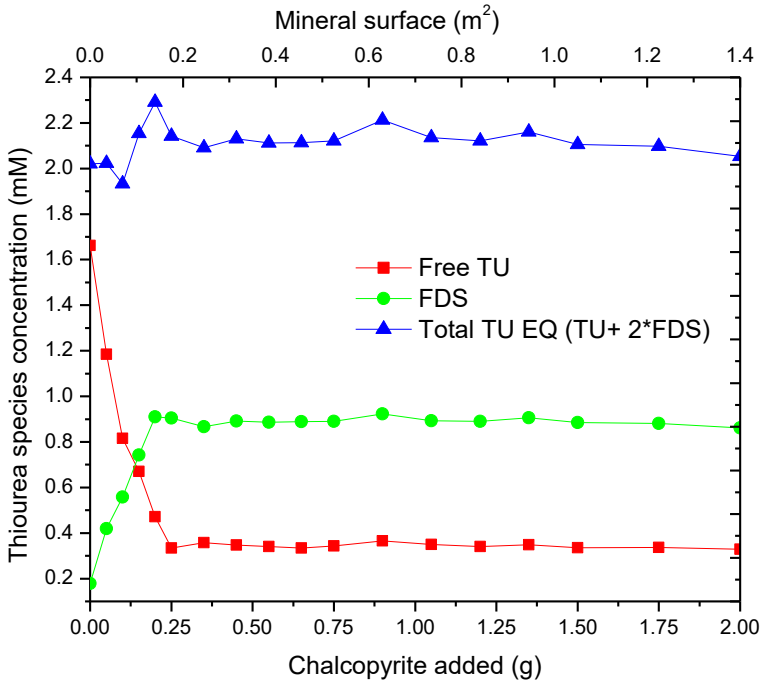

Figure 19. Behaviour of thiourea at stepwise addition of chalcopyrite.

4.2.3 Effect of pH on the stability of free thiourea concentration over time

The effect of increasing H^+ concentrations on the stability of free TU is shown in Figure 20. By comparing these four tests, it is observed that decreasing the pH has a direct influence on the stability of free TU in solution. After the first 24 h, the free TU concentration decreased to 0.45 mM; 0.32 mM; and 0.28 mM at pH 1.5; 1.2; and 0.8, respectively. It is believed that this abrupt decline in the free TU concentration is a direct result of the increase in proton concentration, which enhanced the rate of oxidation of TU to FDS, and at the same time helped to stabilize the latter compound in solution.

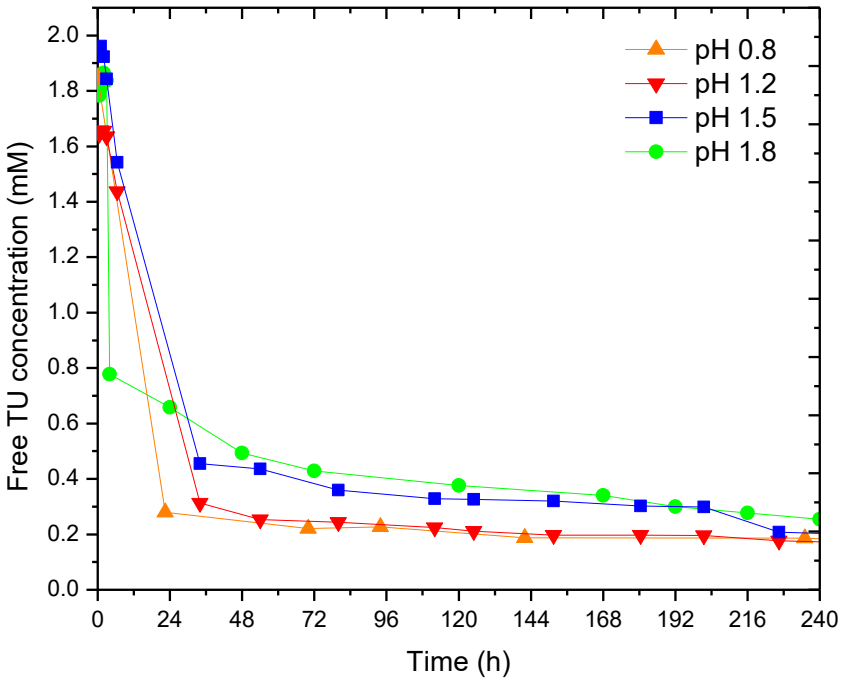

Figure 20. Effect of pH on the stability of free thiourea concentration over time.

4.2.4 Effect of different Fe^{3+}/Fe^{2+} ratios on the free thiourea concentration

In the absence of TU, the redox potential in solution is determined by the Fe^{3+}/Fe^{2+} concentration ratio. TU is particularly unstable in ferric media and undergoes a series of oxidation stages, where the resultant products depend very much on the pH and the conditions of the reaction medium (Arifoglu et al., 1992). Once TU is added to the leaching solution, there are several redox reactions taking place simultaneously and as a result of this, the ORP is no longer determined solely by the Fe^{3+}/Fe^{2+} concentration ratio.

Figure 21 shows the effect of different initial Fe^{3+}/Fe^{2+} concentration ratios in the free TU. As expected, in the presence of a higher concentration of ferric ions in solution, the free TU concentration reaches the minimum value compared with the other tests. On the other hand, based on the assumption that ORP is determined by the Fe^{3+}/Fe^{2+} ratios it should be expected that the test containing the highest concentration of ferric ions, 35:5, should have the highest ORP values. But, as is shown in Figure 22, in the presence of TU, ORP measurements are not strictly determined by the Fe^{3+}/Fe^{2+} ratio. Moreover, these results could imply that not only is the ORP not a reliable indicator of the Fe^{3+}/Fe^{2+} ratio, but also the ratio of TU : FDS or some other decomposition products could be the main reaction controlling the ORP values.

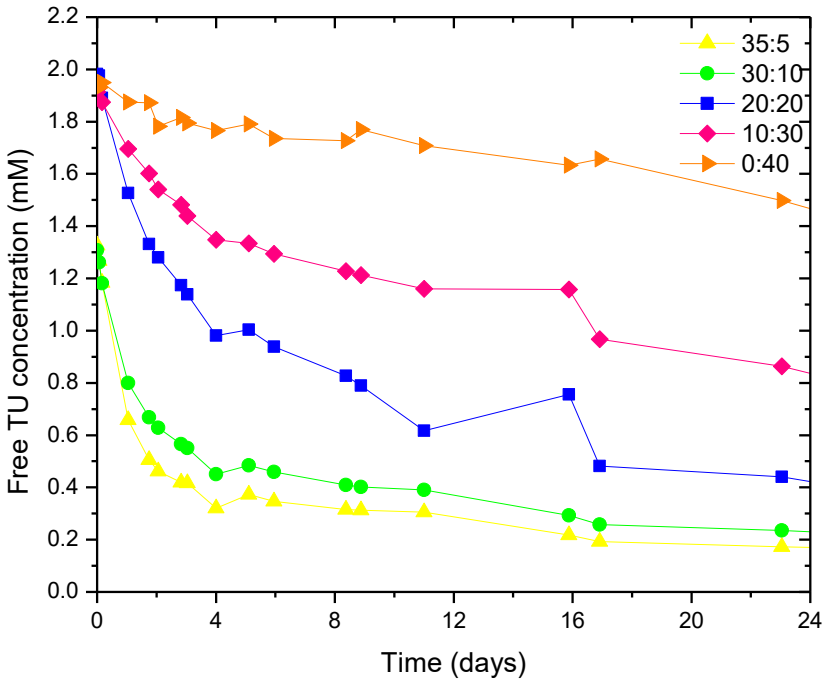

Figure 22. Effect of different initial Fe^{3+}/Fe^{2+} ratios on the free thiourea concentration over time for the tests with initial 2 mM TU, pH 1.8 at 20°C.

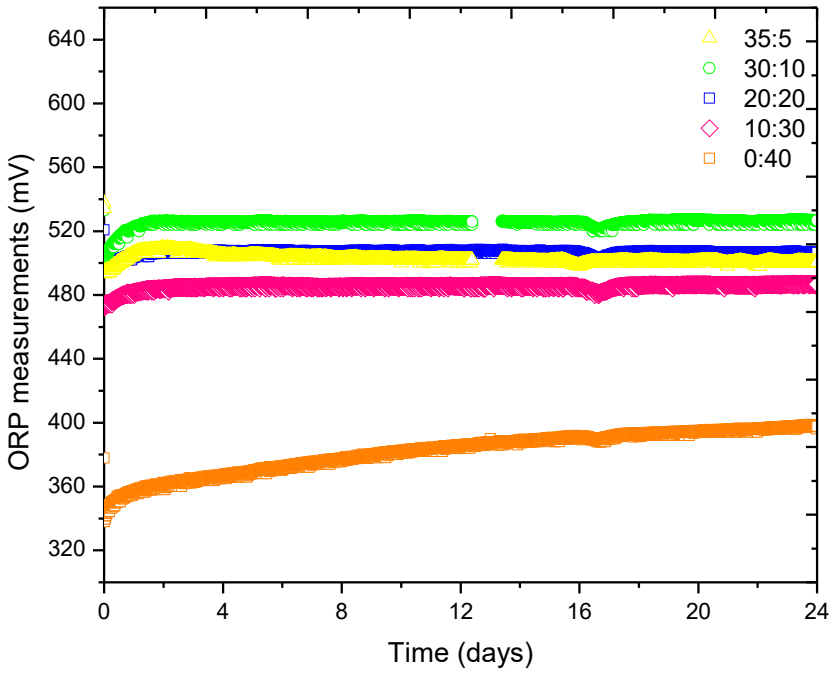

Figure 21. Effect of different initial Fe^{3+}/Fe^{2+} ratios on the free thiourea concentrations and its respective ORP values, for the tests with initial 2 mM TU, pH 1.8 at 20°C.

4.3 Effect of thiourea concentration

While it has been claimed that TU is an effective catalyst for enhancing the leaching rate of chalcopyrite, it has also been noted that 2 mM of TU is the maximum concentration that would not affect the feasibility of the bioleaching process. In light of this, the effect of the TU concentration below that threshold was evaluated. Figure 23 shows the effect of different TU concentrations in the copper extractions.

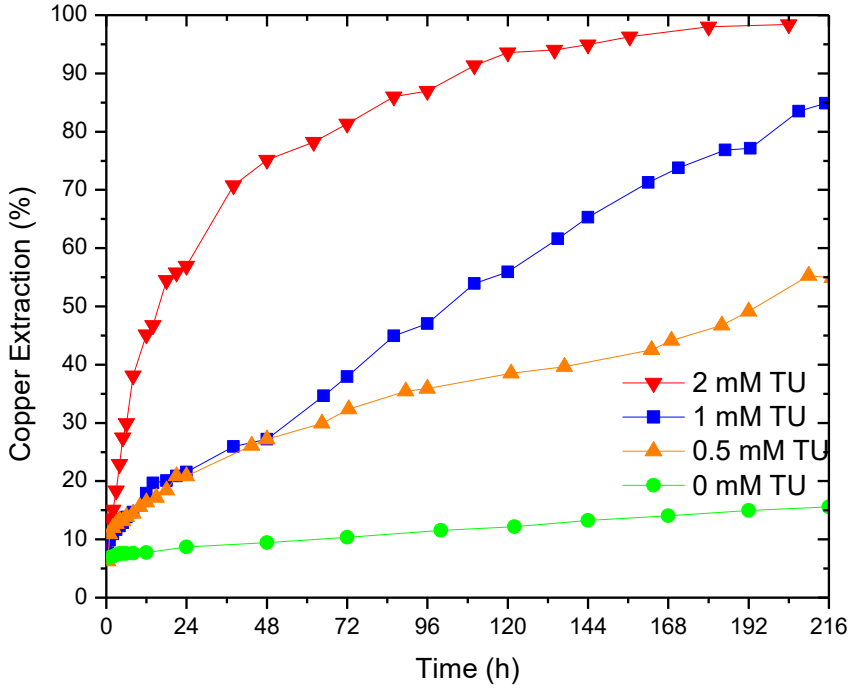

Figure 23. Effect of different thiourea concentrations at pH 1.8, with 40 mM Fe^{3+} and 20ºC.

For the experiments in the presence of the catalyst, a different experimental approach was followed. Since every addition of TU to the solution and caused a decrease in the ORP, ferric sulfate was also added to the solution until the desired ORP value (520 mV) was re-established. As observed from Figure 23, in the absence of TU the experiment showed signs of passivation, and the copper extraction achieved was only 16% after 216 h of leaching. However, when TU was added to the leaching reactor, a clear increase in the leaching rate was observed, with 88% and 98% of copper recovered after 216 h for 1 mM and 2 mM TU concentration, respectively. Moreover, the results presented in Figure 23 could indicate that TU can positively affect the dissolution of chalcopyrite in two different ways. First, it seems to catalyze the dissolution of the mineral, which could be observed by the increase in the leaching rate when compared with the test in the absence of TU. Second, it may also act as a depassivating agent. This is discussed in detail in the following sections.

Additionally, to observe the effect of leaching on the surface of the mineral, another set of tests, under the same conditions described above, were carried out and stopped after 24 h. SEM images of the synthetic chalcopyrite used as head ore are presented in Figure 24 (a) and (b). These images show that the mineral grains tend to form clusters of particles, and the surface prior to leaching is smooth and clear with well-defined edges.

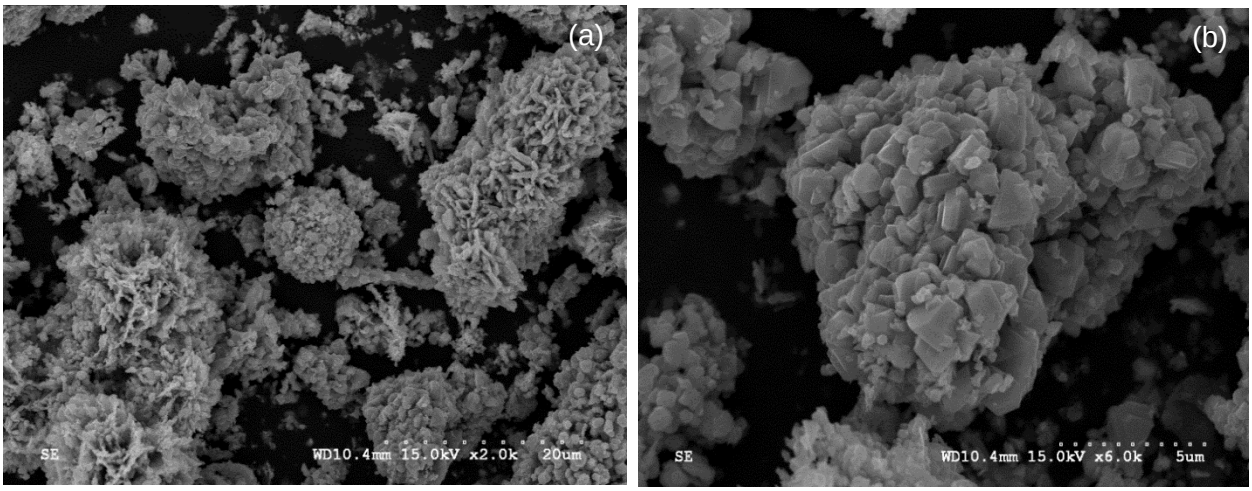

Figure 24. SEM images of synthetic chalcopyrite used as “head ore”.

Figure 25 (a) and (b) shows the effect of 0 and 1 mM of TU, respectively on the surface of the chalcopyrite particle after 24 h of leaching. At these concentrations, unlike in the head ore, the particles now have small cracks and porous surfaces. Figure 26 illustrates the strongest decrepitation of mineral particles leached after 24 h in the presence of 2 mM.

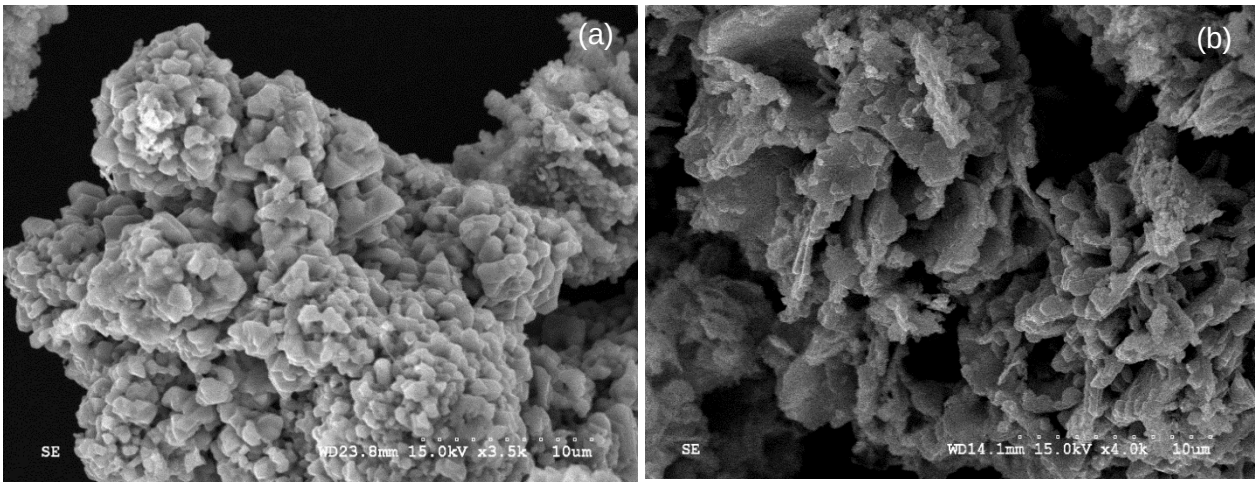

Figure 25. SEM images of the leaching residues at (a) 0 mM TU after 24 h and (b) 1 mM TU after 24 h.

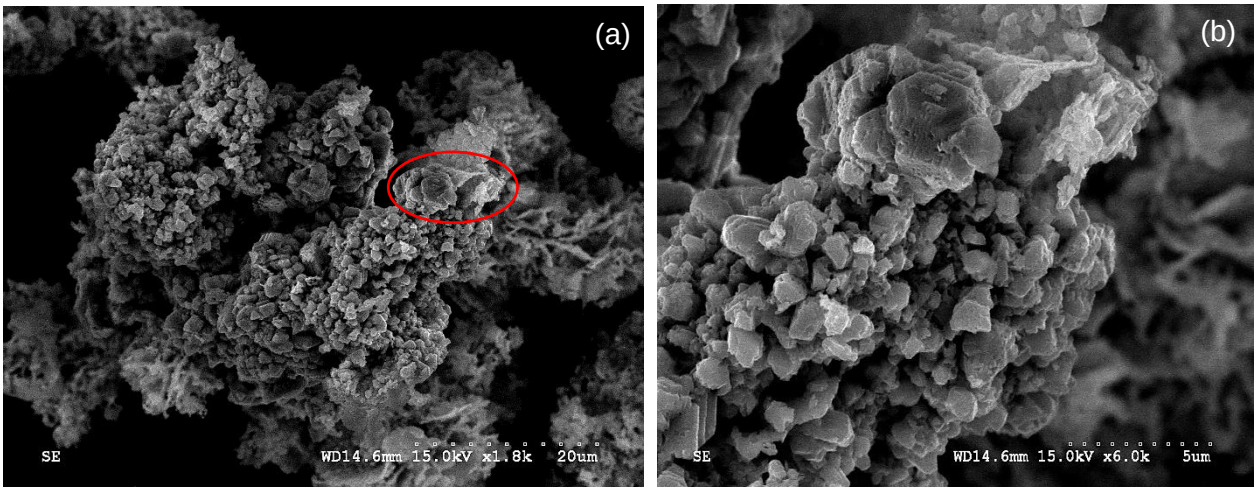

Figure 26. SEM images of the leaching residues at 2 mM TU after 24 h. Image (b) presents a close-up of the highlighted section on Figure (a).

4.4 Effect of initial ferric concentration

Figure 27 shows the copper extraction after 8 days of leaching for the test at different initial ferric ions concentration. The same experimental approach mentioned before was taken in the case of the experiments in the presence of the catalyst. Ferric sulfate was added to maintain an ORP set point of 520 mV.

As was expected, copper extraction increased dramatically from 16% to 98% in the presence of TU in the test containing 40 mM Fe^{3+}. On the other hand, when 20 mM Fe^{3+} was present in the solution, copper extraction was 82.1%. This decrease in the amount of copper extracted when ferric concentration was lowered was not expected but might be related to the considerable decrease in the free TU concentration at the beginning of the experiment. The drop in the free TU baseline for the test with initial 20 mM Fe^{3+}, could indicate some underlying relation between the Fe^{3+}/Fe^{2+} ratio with the stability of the catalyst and its tendency to be oxidized under certain conditions.

Opposite to this, in the absence TU, the results showed that increasing the initial ferric concentration from 20 to 120 mM has no apparent effect on the leaching kinetics of chalcopyrite. These results are consistent with previous studies by Dutrizac et al. (1969), which pointed out that the rate was nearly independent of the Fe^{3+} concentration above 0.01 M.

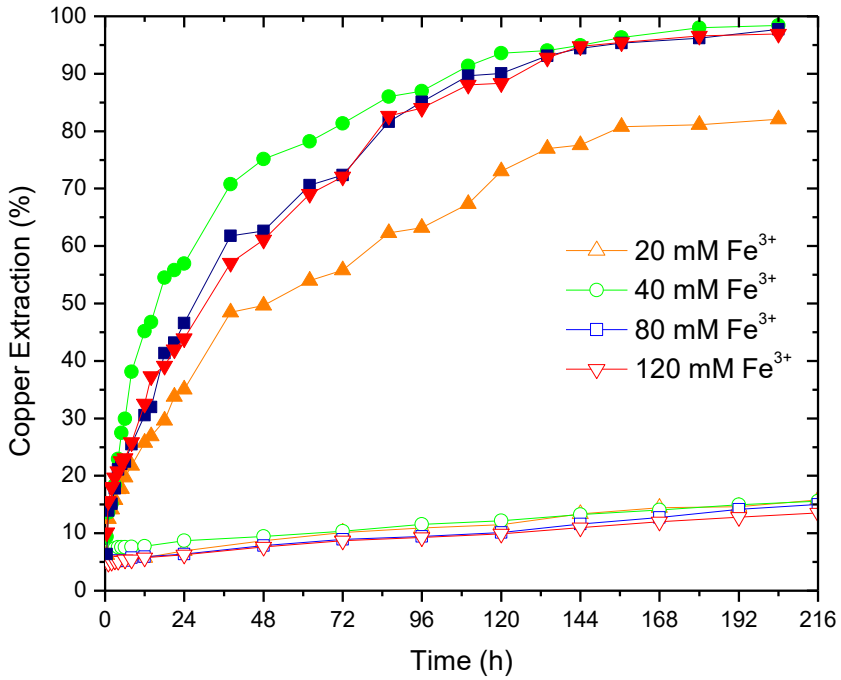

Figure 27. Effect of initial ferric concentration at pH 1.8 and 20ºC. Curves with filled (hollow) symbols represent the experiments carried out in the presence of 2 mM (0 mM) TU under the indicated ferric concentrations.

4.4.1 Solid residue characterization

To illustrate in further detail the effect of the TU in the leaching of chalcopyrite, the approach taken was twofold: 1) Perform an elemental mapping at the microstructural level by SEM with EDX, and 2) Conduct a XRD analysis on the leaching residues.

Elemental mapping by SEM-EDX

Figure 28 shows the particle chosen for the elemental mapping of the leaching residues at 0 mM TU. As observed from elemental compositional images (Figure 28 b-d) there is no indication of a change in the composition of the particle. This lack of change is somewhat expected, considering that only 16% of copper extraction was achieved under the conditions of this test.

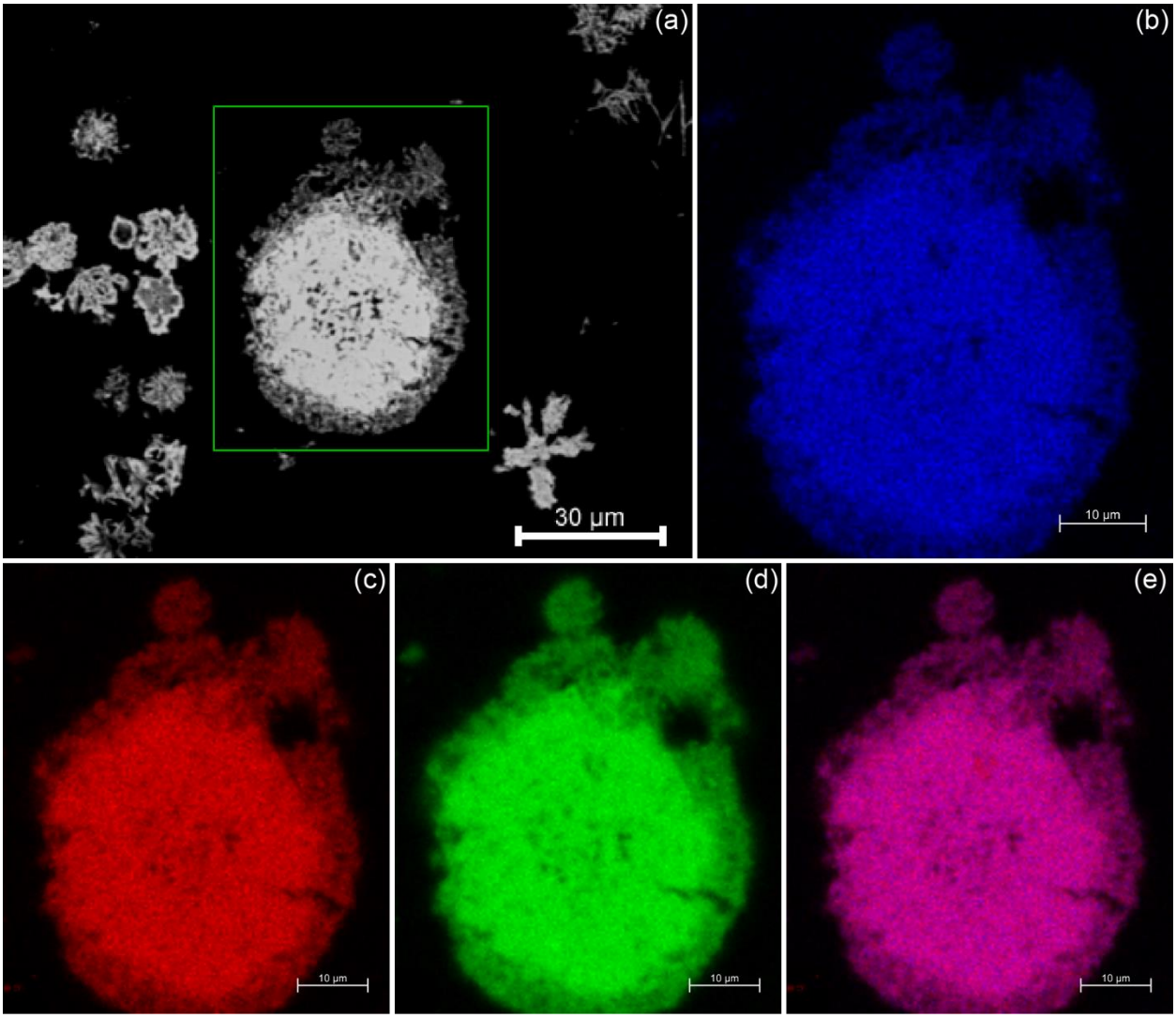

Figure 28. SEM-EDX compositional images of the leaching residues for the test carried out at 20ºC, with 0 mM TU, 40 mM Fe^{3+}, and pH 1.8. (a) Wide field of view. Green square indicates where magnified compositional images were taken in (b-e). Presence of (b) copper, (c) iron, (d) sulfur, and (e) copper-iron detected.

Adding TU to the system increases the dissolution rate of chalcopyrite. This increase was particularly noticeable at 2 mM TU. According to the one of the passivation theories, when chalcopyrite is leached, a porous sulfur layer is observed to cover the entire particle and the leaching proceeds at a centered shrinking core (Rivera, 2010). However, in the presence of TU, this layer does not represent a hindrance for the leaching process. As observed in the elemental compositional images in Figure 29 (b-d), the composition of the outside layer covering the core of the particle, is rich in both iron and sulfur. Based on these results, it could be concluded that in the presence of TU the porosity of the outside layer is high enough to allow ion transportation to and from the chalcopyrite surface.

XRD analysis

Figure 30 and 31 present the XRD patterns for the leaching residues for both the test conducted with 0 mM TU and 2 mM TU, respectively. As expected, the pattern in Figure 30 presents only phase, chalcopyrite, which confirms the results shown in the elemental compositional images. On the other hand, as observed in Figure 31, small quantities of sulfur were encountered in the leaching residues for the test at 2 mM TU.

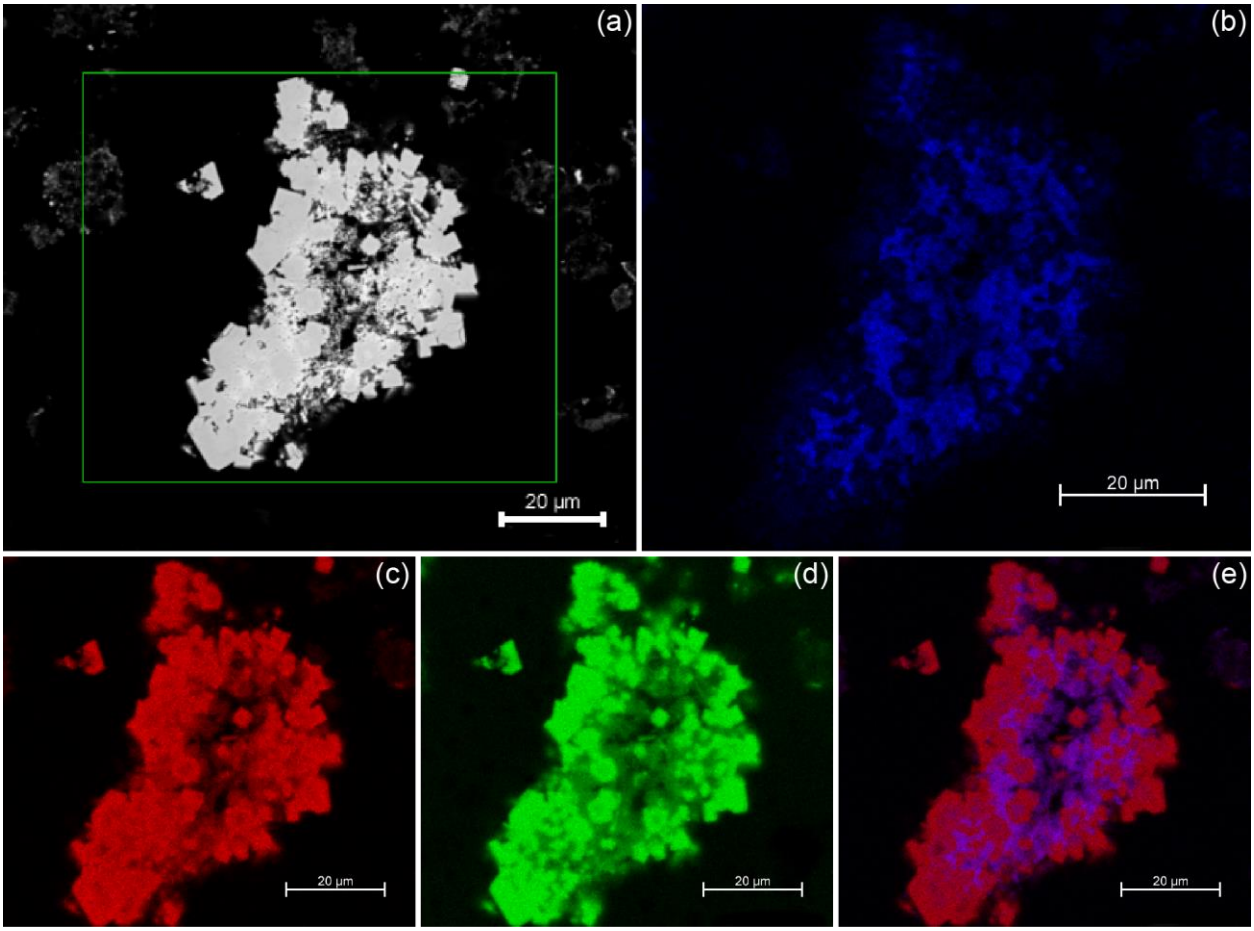

Figure 29. SEM-EDX compositional images of the leaching residues for the test carried out at 20ºC, with 2 mM TU, 40 mM Fe^{3+}, and pH 1.8. (a) Wide field of view. Green square indicates where magnified compositional images were taken in (b-e). Presence of (b) copper, (c) iron, (d) sulfur, (e) copper-iron detected.

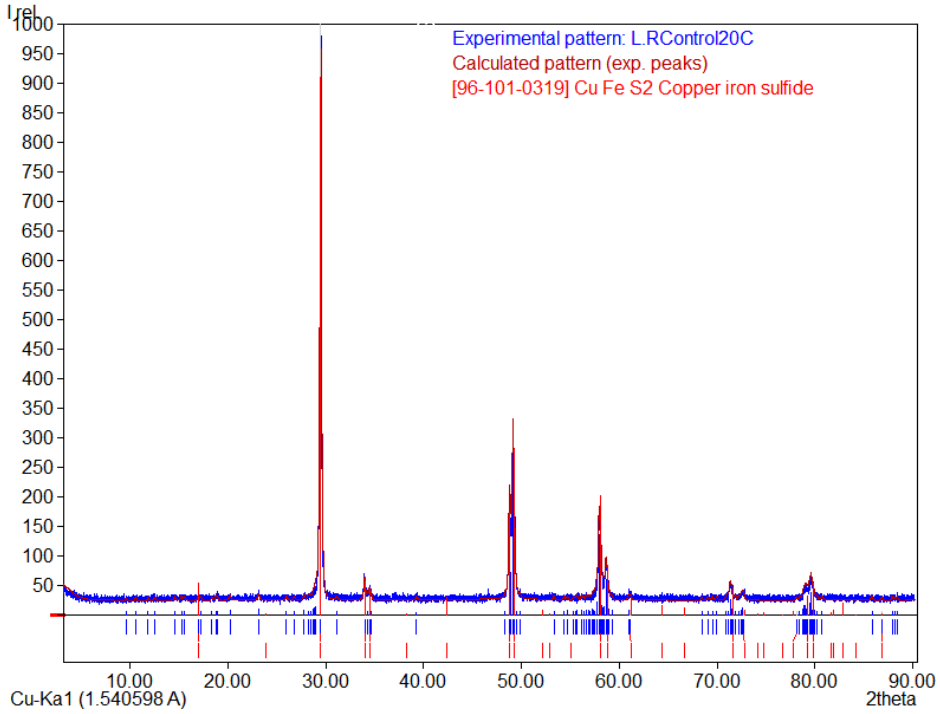

Figure 30. XRD pattern of the leaching residues for test conducted at 20ºC, with 0 mM TU, 40 mM Fe^{3+}, and pH 1.8.

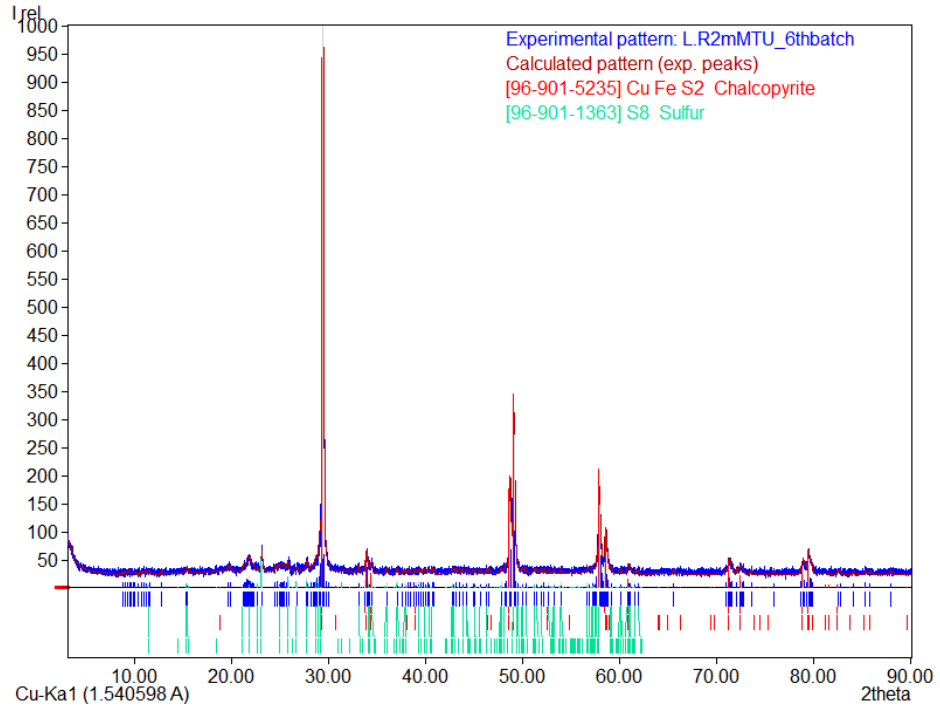

Figure 31. XRD pattern of the leaching residues for test conducted at 20ºC, with 2 mM TU, 40 mM Fe^{3+}, and pH 1.8.

4.5 Effect of initial pH

To evaluate the effect of sulfuric acid on the leaching of chalcopyrite, three experiments were performed with pH of 0.8, 1.2 and 1.5. The test run at pH 1.8 was considered as the baseline for the study of this variable and for the leaching variables studied subsequently. From Figure 32 it can be seen that in the presence of 2 mM TU, the concentration of acid had a significant effect on the dissolution kinetics, which corroborates the results presented by Cordoba et al. (2008). In the presence of the catalyst, increasing the acid concentration had a noticeable deleterious influence on the concentration of free TU available at the beginning of the experiment.

Based on these results, it is believed that the marked difference in the copper extractions could be attributed to the change of free TU available, which diminishes the effect of the catalyst in the leaching of chalcopyrite and the kinetics.

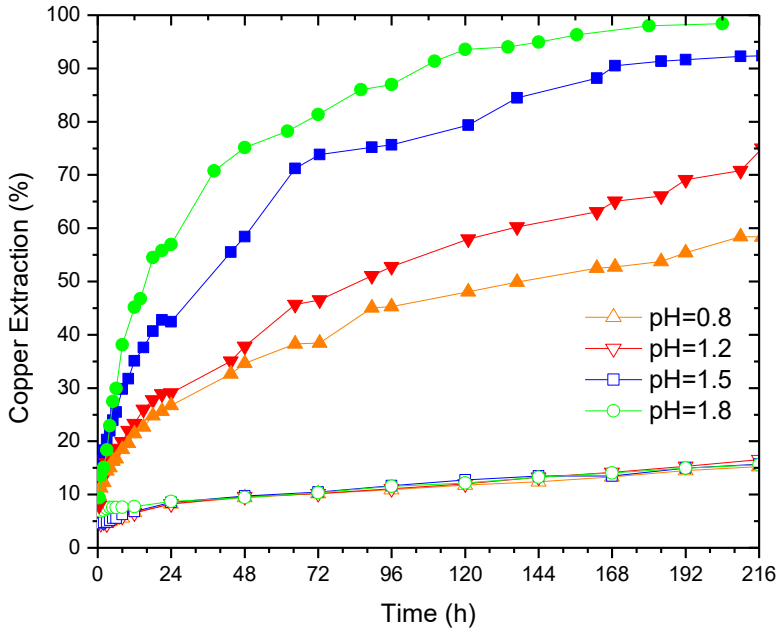

Figure 32. Effect of initial pH at 40 mM Fe^{3+} and 20ºC. Curves with filled (hollow) symbols represent the experiments carried out in the presence of 2 mM (0 mM) TU under the indicated pH values.

4.6 Effect of copper sulfate concentration

To examine the effect of initial copper concentration on the leaching rate, three experiments were carried out using 40 mM Fe^{3+} with various initial concentration of cupric ions. As observed from Figure 33, under control conditions, increasing copper sulfate concentration from 0 to 10 mM has a positive effect on the leaching kinetics of chalcopyrite. These results differ from the study of Dutrizac (1981), which indicated that the $CuSO_4$ slightly depresses the leaching rate. This discrepancy with Dutrizac's study could be attributed to the change in the temperature of the experiment from 90ºC to 20ºC.

Furthermore, in the presence of TU, the increase of cupric concentration has a clear effect on the kinetics compared to the test at 0 mM Cu^{2+}. Increasing the copper concentration, reduces the amount of free TU available at the beginning of the experiment, which compromises the kinetics of the leaching. Although, in the case of the test with initial 10 mM Cu^{2+}, the final copper extraction was not affected. Moreover, a slight decrease was observed for the test at 2 and 4 mM Cu^{2+}, reaching up to 90 and 86% after 216 h, respectively.

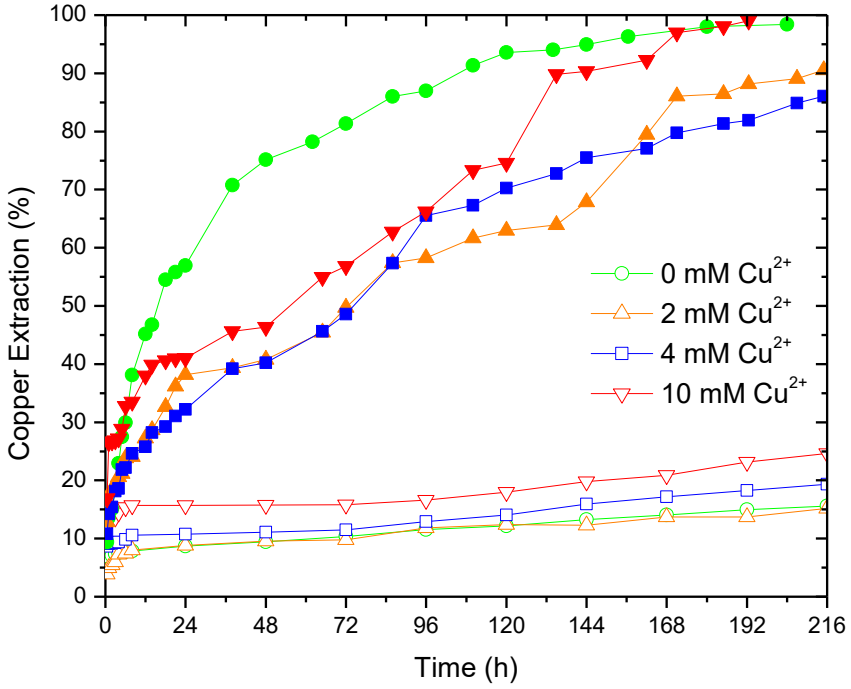

Figure 33. Effect of initial Cu^{2+} concentration at pH 1.8, with 40 mM Fe^{3+}, and 20ºC. Curves with filled (hollow) symbols represent the experiments carried out in the presence of 2 mM (0 mM) TU under the indicated cupric concentrations.

4.7 Effect of temperature

Three experiments were conducted to determine the effect of temperature on the rate of copper dissolution from chalcopyrite. The temperature was varied from 20 to 50ºC. The results of these tests are shown in Figure 34. Under control conditions of 0 mM TU, temperature had a strong effect on the leaching rate. About 16% of chalcopyrite was leached after 216 h at 20ºC while 43.2% was leached at 35ºC and 80.7% was leached at 50ºC. These results are in agreement with the study conducted by Cordoba et al. (2008), who stated that the chalcopyrite reaction rate is slow at low temperatures and increases at higher temperatures.

On the other hand, in the presence of TU, copper extraction of 100% was achieved after 120 h at 50ºC whilst 98% and 93% were extracted at 35ºC and 20ºC, respectively. Zuñiga & Ren (personal communication, 2017) reported that an increase in temperature significantly decreases the stability of TU in solution. Thus, increasing the temperature promotes the oxidation and further decomposition of TU into several species, with sulfur being one of the final products of the oxidation of TU. In the attempt to corroborate this assumption, the leaching residues of these tests were studied in more detail. The findings are discussed in the following section.

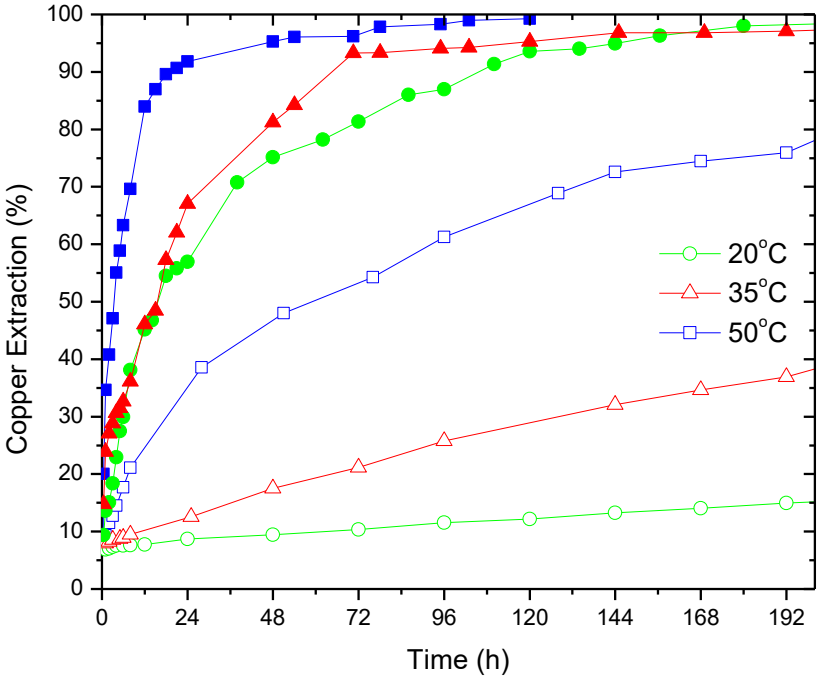

Figure 34. Effect of temperature at pH 1.2 and 40 mM Fe^{3+}. Curves with filled (hollow) symbols represent the experiments carried out in the presence of 2 mM (0 mM) TU under the indicated temperatures.

4.7.1 Solid residue characterization

Elemental mapping by SEM-EDX

In this section, the analysis performed on the leaching residues for the test conducted at 35 and 50ºC under control conditions, 0 mM TU, and at 2 mM TU are presented in Figures 35-36 and Figures 37-38, respectively.

Dutrizac (1978), pointed out that the nonlinear kinetics observed in the sulfate system at high temperatures were caused by the blockage or partial blockage of the chalcopyrite surface by the elemental sulfur reaction product and/or precipitated iron compounds, which can form in fairly acidic solutions. As observed in Figure 35, under control conditions of 0 mM TU, the chalcopyrite surface is blocked by a layer, which is particularly rich in iron and oxygen (Figure 35 c-e-g). It could be assumed that this layer is the one responsible of the passivation of the particle. The elemental mapping analysis for the leaching residues at 50ºC are shown in Figure 36. The results presented in Figure 36 (b-h), are in excellent agreement with the assumption given by Dutrizac (1978) to explain the nonlinear kinetic behaviour of chalcopyrite in the sulfate system at high temperatures. Under these conditions, the particle shown in Figure 36 is completely surrounded with an outside layer of what could be assumed to be some form of iron precipitate, given the presence of iron and oxygen (Figure 36 c-e-g). Although, research in more detail, with quantitative measurements of the elements compositions, is needed to reveal a more precise conclusion, the evidence of the formation of this iron-hydroxy rich layer provides a better understanding of the nonlinear kinetic behavior of chalcopyrite.

As observed in Figure 37, in the presence of 2 mM at 35ºC, the formation of the iron-hydroxy layer on the surface of the particle still occurs (Figure 37 e-f). As shown in Figure 37 b, there is a noticeable change in the composition of copper as compared with the test at 0 mM TU. Moreover, the results presented in Figure 38, showed that in the presence of 2 mM TU at 50ºC, although the particle surface is completely blocked by the iron-hydroxy layer. Further, as expected, based on the copper extraction achieved for this test, Figure 38 (b) shows that the copper amount in the particle is below the detection limit of the elemental mapping analysis. These results suggest that under the conditions of these test, TU does not act as a depassivation agent on the surface of the chalcopyrite. However, it is observed that in the presence of the catalyst, the passivation layer, is not as compact as observed under control conditions (0 mM TU), hence is more porous, which allows the dissolution of the chalcopyrite and does not present a barrier to leaching.

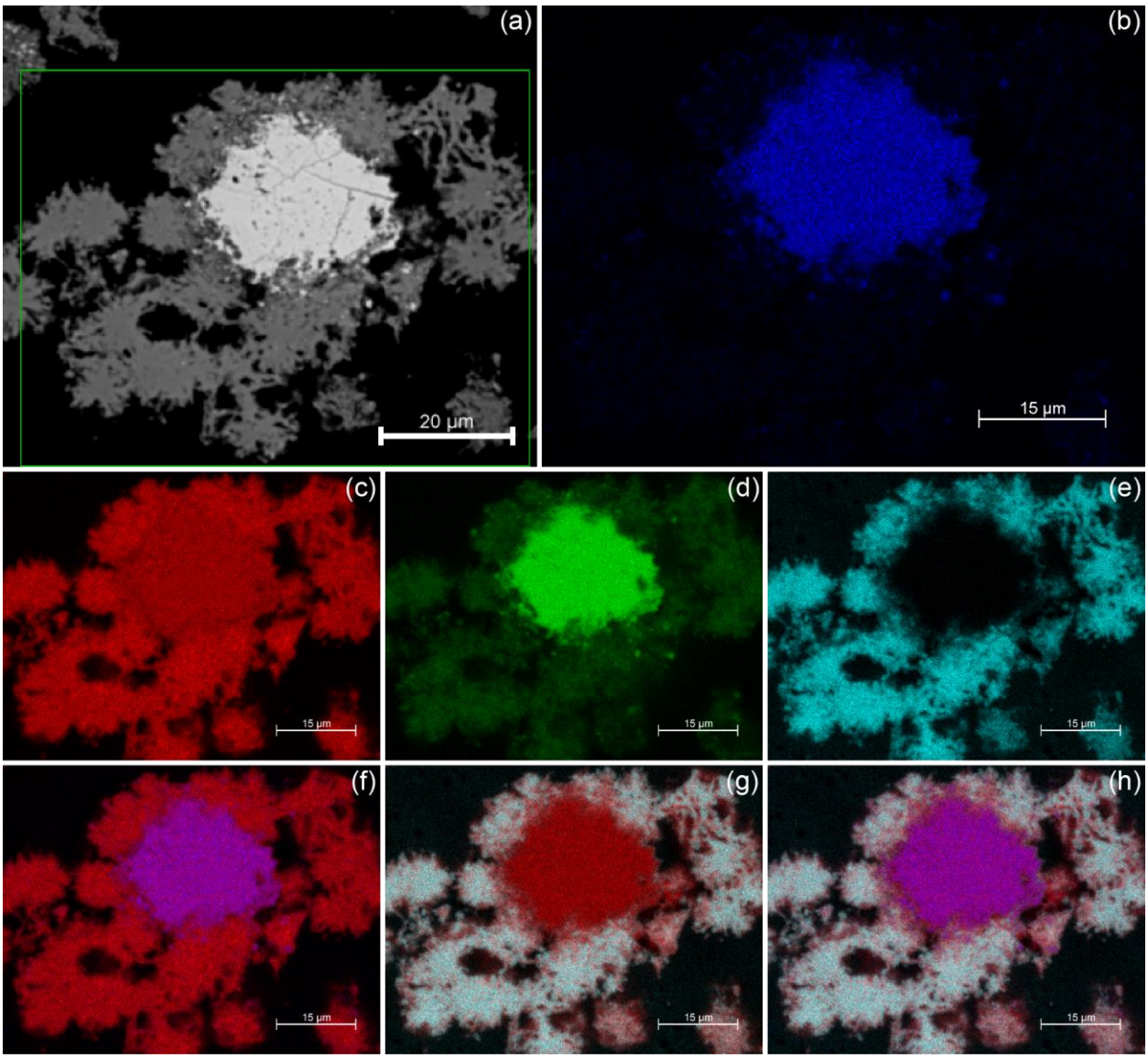

Figure 35. SEM-EDX compositional images of the leaching residues for the test carried out at 35ºC, with 0 mM TU, 40 mM Fe^{3+}, and pH 1.2. (a) Wide field of view. Green square indicates where magnified compositional images were taken in (b-h). Presence of (b) copper, (c) iron, (d) sulfur, (e) oxygen, (f) copper-iron, (g) oxygen-iron, and (h) copper-iron-oxygen detected.

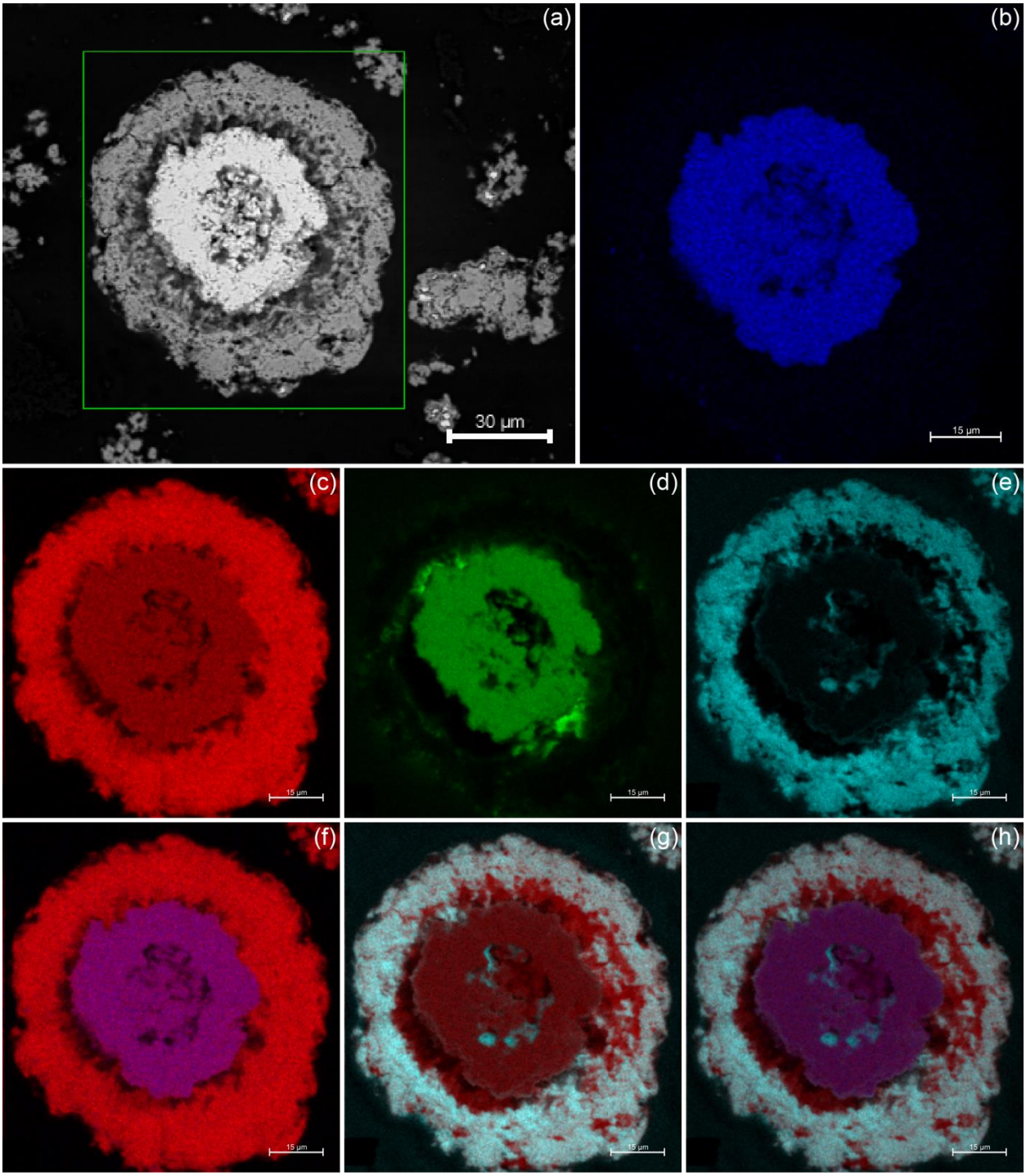

Figure 36. SEM-EDX compositional images of the leaching residues for the test carried out at 50ºC, with 0 mM TU, 40 mM Fe^{3+}, and pH 1.2. (a) Wide field of view. Green square indicates where magnified compositional images were taken in (b-h). Presence of (b) copper, (c) iron, (d) sulfur, (e) oxygen, (f) copper-iron, (g) iron-oxygen, and (h) copper-iron-sulfur-oxygen detected.

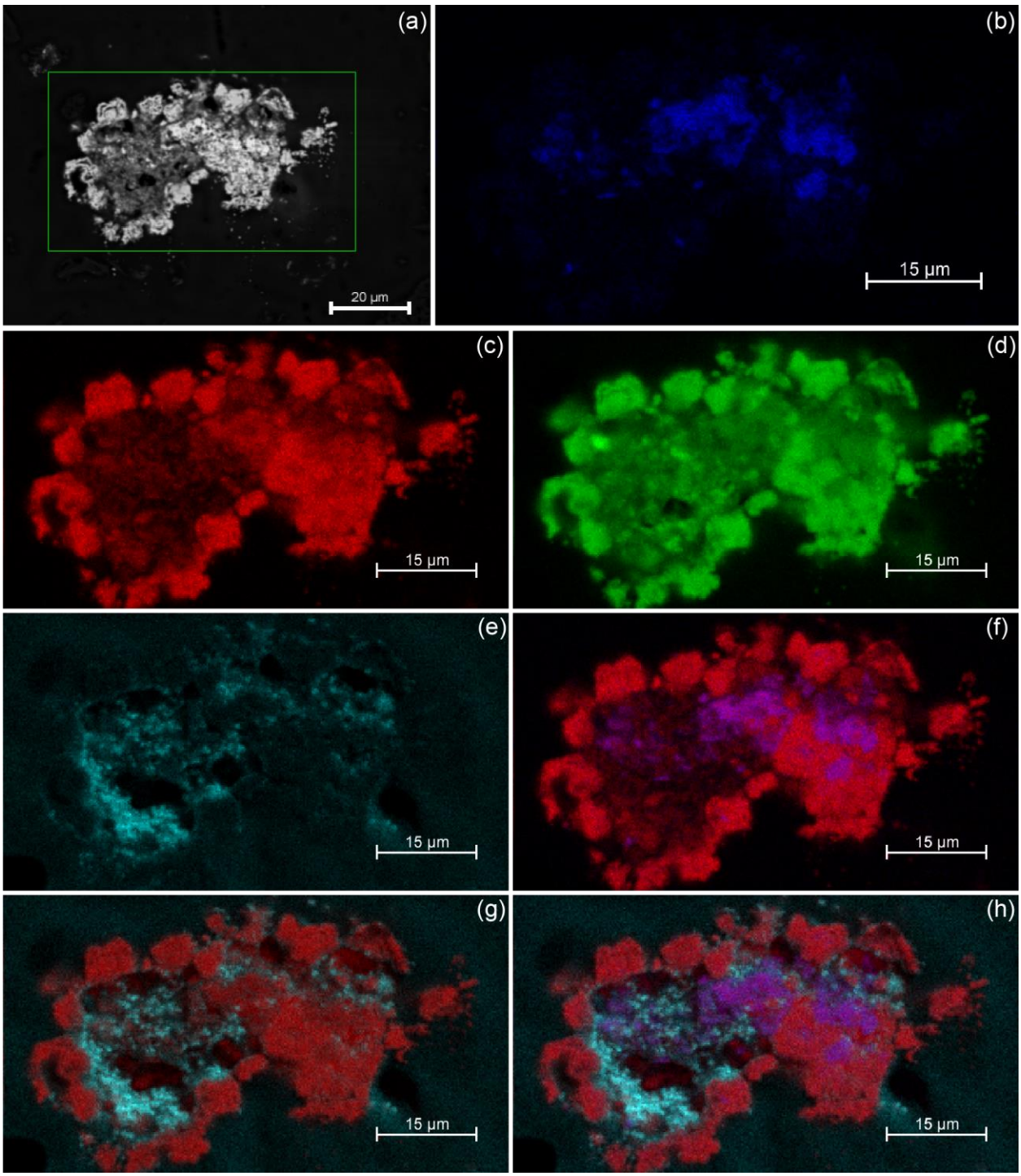

Figure 37. SEM-EDX compositional images of the leaching residues for the test carried out at 35ºC, with 2 mM TU, 40 mM Fe^{3+}, and pH 1.2. (a) Wide field of view. Green square indicates where magnified compositional images were taken in (b-h). Presence of (b) copper, (c) iron, (d) sulfur, (e) oxygen, (f) copper-iron, (g) iron-oxygen, and (h) copper-iron-oxygen detected.

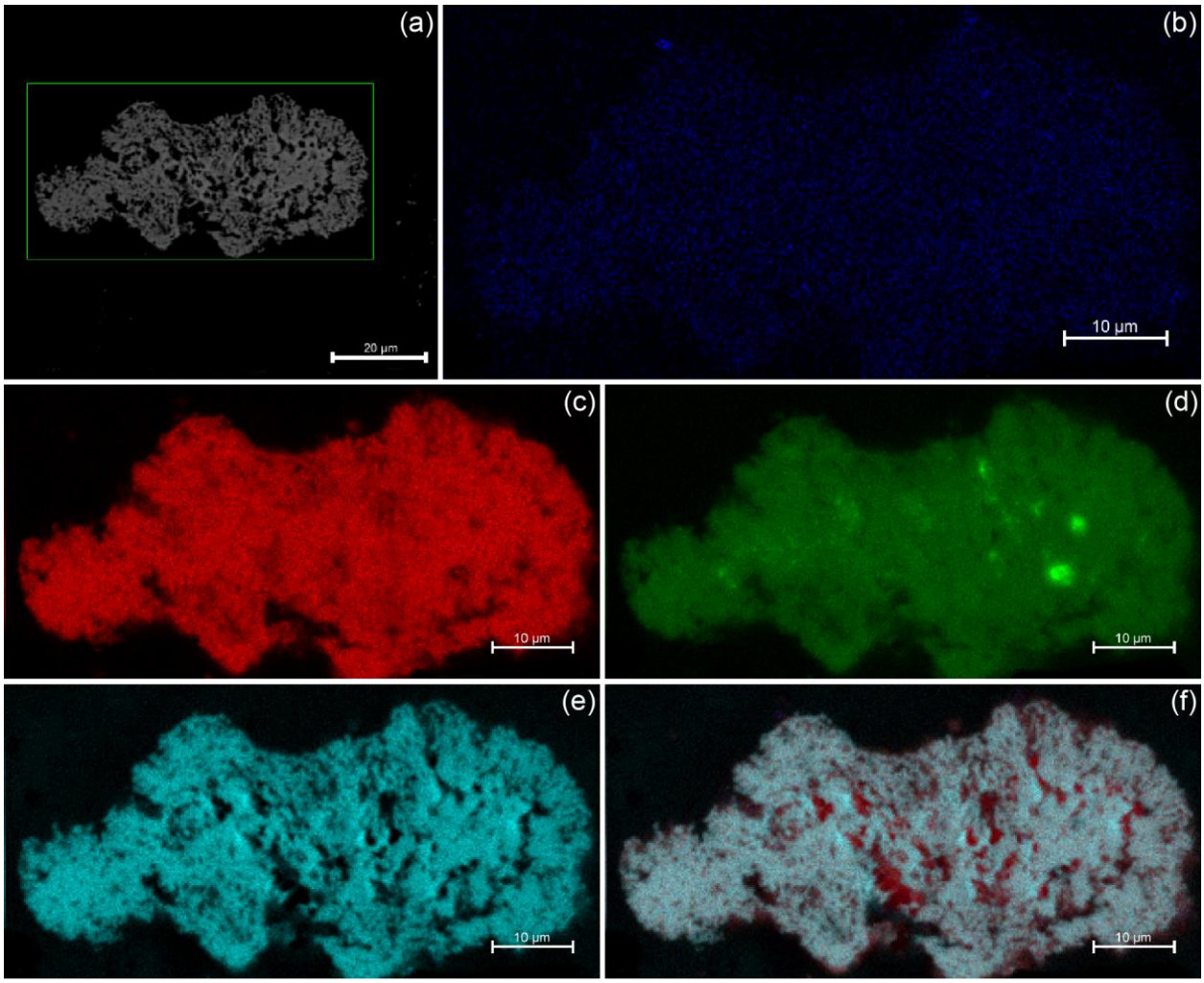

Figure 38. SEM-EDX compositional images of the leaching residues for the test carried out at 50ºC, with 2 mM TU, 40 mM Fe^{3+}, and pH 1.2. (a) Wide field of view. Green square indicates where magnified compositional images were taken in (b-f). Presence of (b) copper, (c) iron, (d) sulfur, (e) oxygen, and (f) iron-oxygen detected.

XRD analysis

Figure 39 and Figure 40 shows the XRD patterns for the leaching residues under control conditions (0 mM TU) at 35ºC and 50ºC, respectively. Is noteworthy to mention that the acquisition time for these samples was changed, aiming to reduce the noise present in the pattern. In spite of that, as observed on both figures, there is a significant amount of amorphous phases, hence the broader peaks. The amount of residue was insufficient to pursue further chemical analysis or to perform a sequential leach procedure to remove the amorphous phases. Based on these results, the presence of iron-hydroxy compounds forming the outside layer, observed on the elemental mapping analysis is confirmed, and according to the phase identification analysis the phases are hydronium jarosite and goethite for both temperatures.

On the other hand, in the presence of 2 mM TU, the iron-hydroxy compound found in the leaching residues was ammonium jarosite at both temperatures (35ºC and 50ºC). The presence of this phase is shown in Figure 41 and 42, and can be attributed to the decomposition of the catalyst. This is in perfect agreement with an assumption made by Zuñiga & Ren (personal communication, 2017) regarding the possible decomposition of TU at high temperatures.

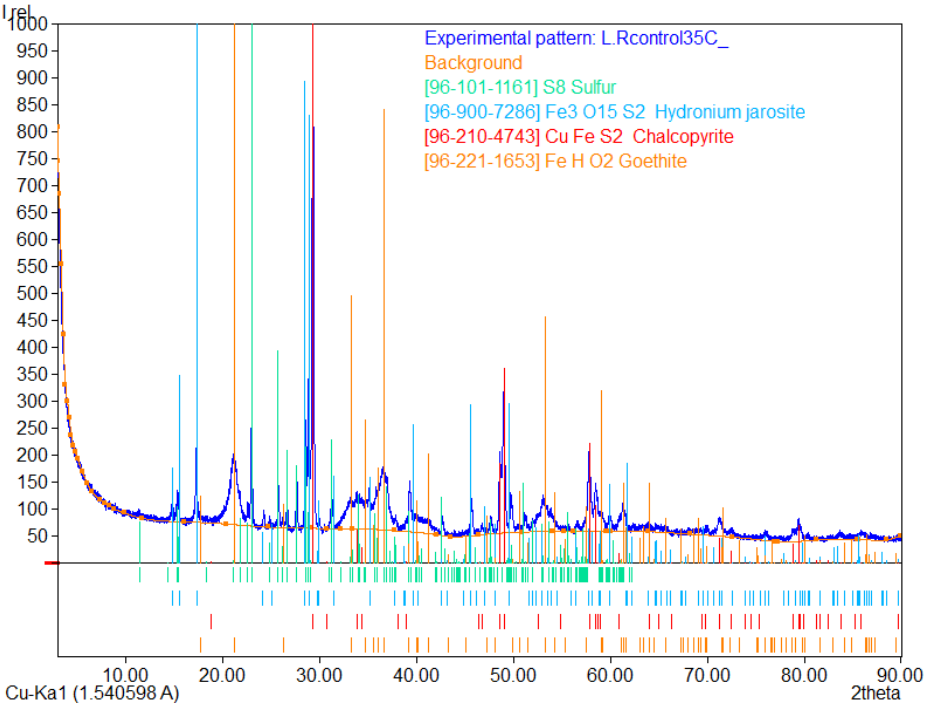

Figure 39. XRD pattern of the leaching residues for test conducted at 35ºC, with 0 mM TU, 40 mM Fe^{3+}, and pH 1.2.

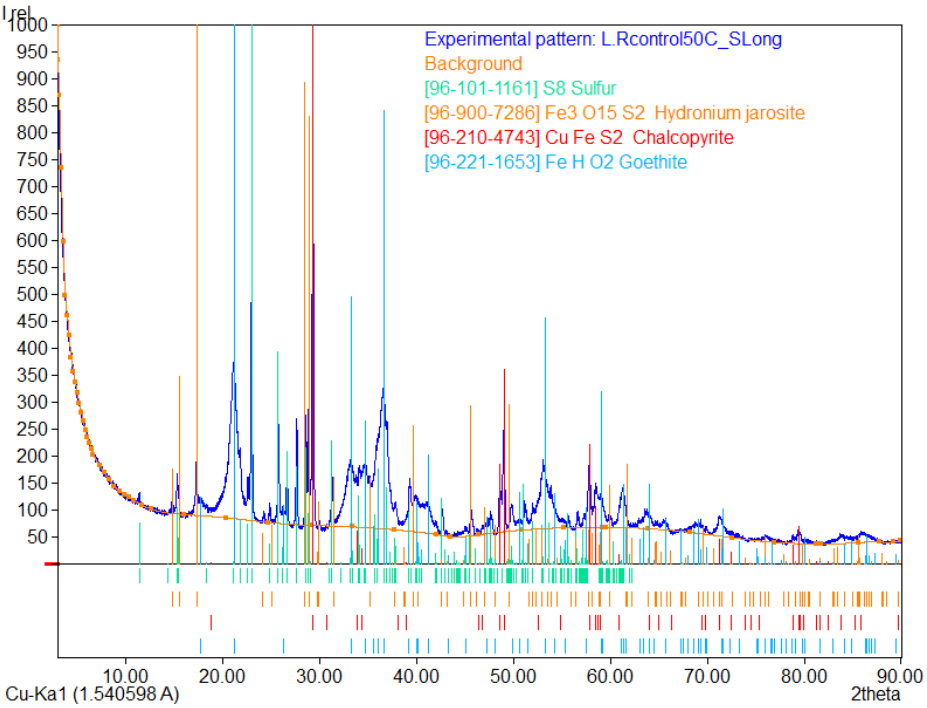

Figure 40. XRD pattern of the leaching residues for test conducted at 50ºC, with 0 mM TU, 40 mM Fe^{3+}, and pH 1.2.

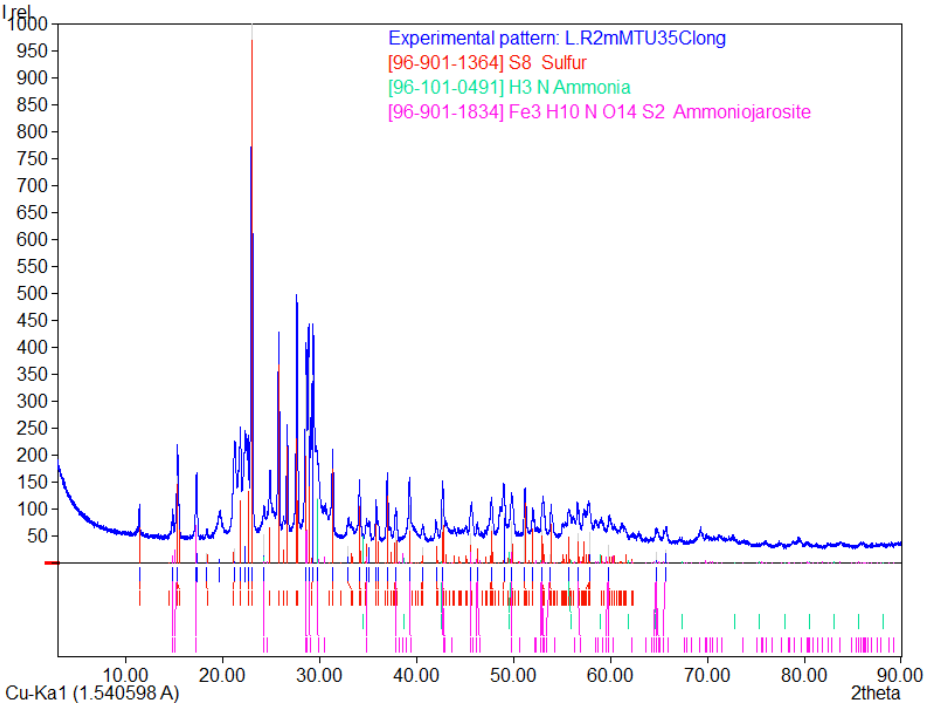

Figure 41. XRD pattern of the leaching residues for test conducted at 35ºC, with 2 mM TU, 40 mM Fe^{3+}, and pH 1.2.

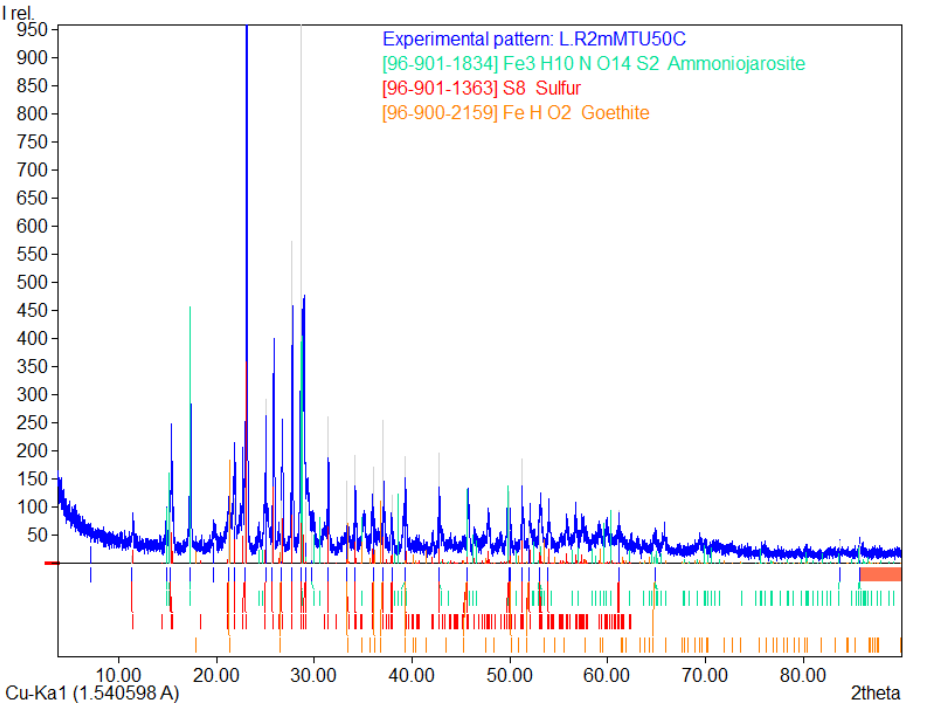

Figure 42. XRD pattern of the leaching residues for test conducted at 50ºC, with 2 mM TU, 40 mM Fe^{3+}, and pH 1.2.

4.8 Effect of particle size

The experimental conditions for the study of the effect of particle size in the dissolution of chalcopyrite tests were identical to those described before, with a solution potential controlled at 520 mV vs Ag/AgCl for the test in the presence of TU. In this case, however, the chalcopyrite sample was evaluated at two distributions of particle size. One test was carried out with the same particle size used in all previous tests with a P_{80} = 23.01 µm, to compare the results with the test conducted using finer particles.

Chalcopyrite samples with a P_{80} = 18.61 µm and P_{80} = 19.23 µm were prepared following the hydrothermal synthesis procedure but reducing the residence time of the vessel in the oven from 24 h to 2 and 6 h, respectively. Unfortunately, the experimental procedure for the hydrothermal synthesis of chalcopyrite was unable to yield a big range of particle sizes. Hence, the difference between the three samples tested is within a few microns, which is not is not considerably different in a statistical sense, notwithstanding, a noticeable effect was observed in the leaching test. The particle size distributions of the samples are shown in Figures 43 and 44.

The effect of particle size on the copper extraction from chalcopyrite is presented in Figure 45. As expected, in the absence of TU, the rate of chalcopyrite dissolution increased with increasing particle surface area. The reaction rate was observed to decrease with increasing particle size and a copper extraction of 50.9% was achieved after 200 h with the finer chalcopyrite sample, while only 16% of the copper was extracted from the coarser sample at room temperature.

However, in the presence of 2 mM TU, the decrease in particle size hindered the chalcopyrite leaching. As the particle size was decreased, the total mineral surface available at the beginning of the test was increased. Thus, by catalyzing the oxidation of free TU, the baseline of free TU for the experiment was considerable lower. This behaviour is consistent with the results presented in section 4.2.3 regarding the effect of the mineral surface in the stability of TU.

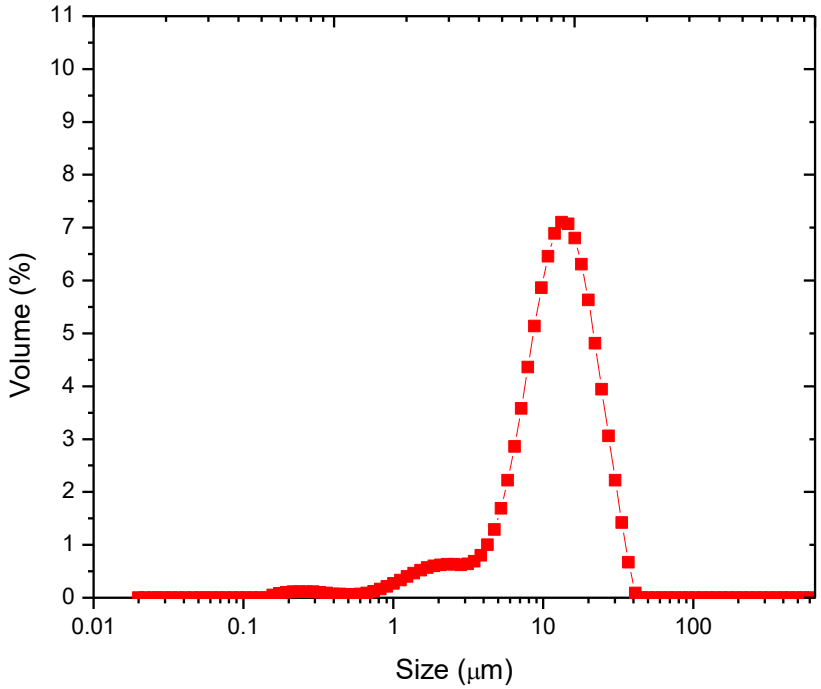

Figure 43. Particle size distribution chalcopyrite sample synthesized for 2 h.

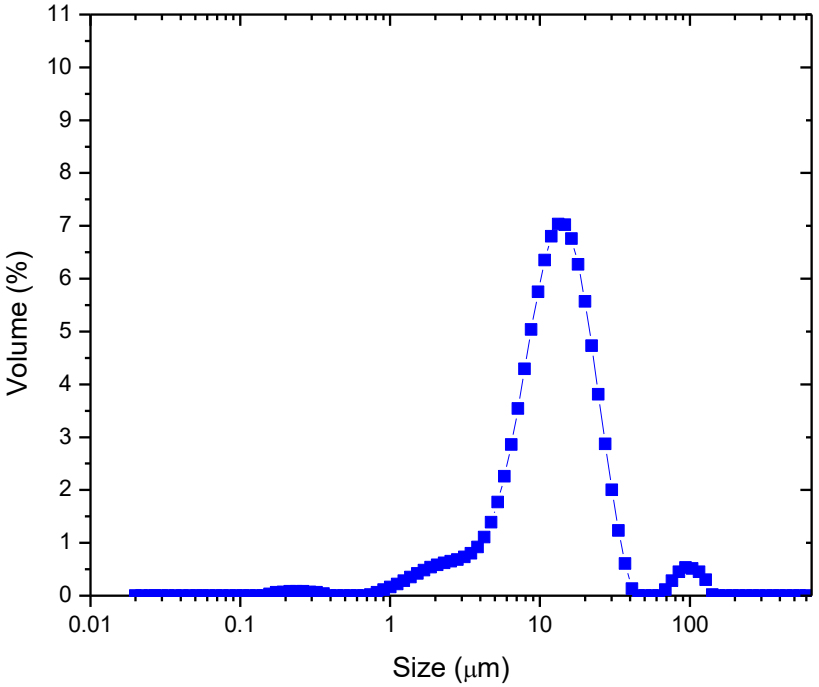

Figure 44. Particle size distribution chalcopyrite sample synthesized for 6 h.

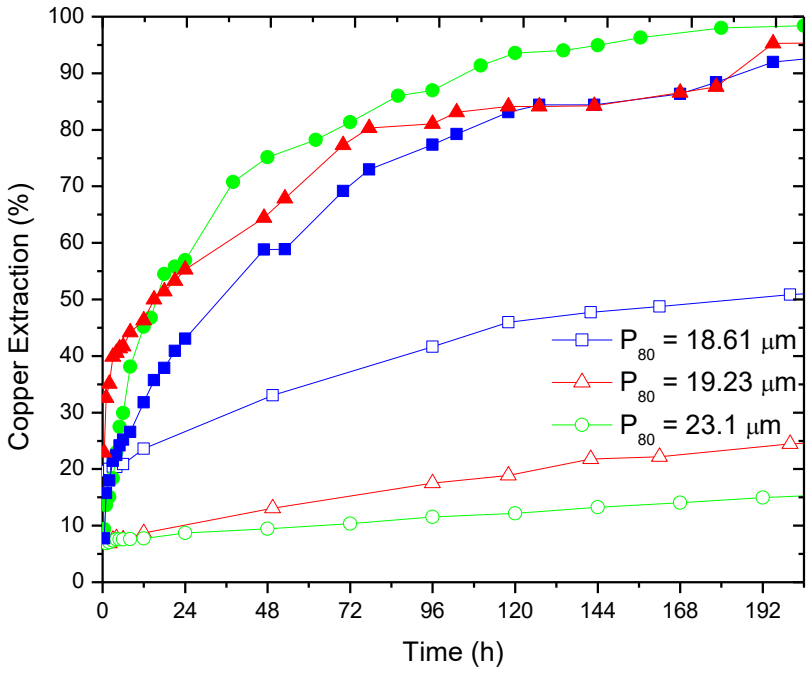

Figure 45. Effect of particle size distribution at 20ºC, with 40 mM Fe^{3+} and pH 1.8. Curves with filled (hollow) symbols represent the experiments carried out in the presence of 2 mM (0 mM) TU under the indicated particle size distributions.

4.9 Formulation of a kinetic model for the leaching of chalcopyrite in the presence of thiourea

In this section, a kinetic model that attempts to explain the leaching of chalcopyrite is developed using the leaching data obtained from the reactors leaching tests. The ultimate goal is to define a generalized topological leach model encompassing a thermal function k(T), a chemical function f(C), and a topological function g(1 – X) representing the changing chalcopyrite topology. The generalized expression can be written as:

$$r = \frac{dX}{dt} = k(T)\cdot f(C)\cdot g(1 - X) \qquad \text{Eq. 22}$$

where

r: Rate of dissolution for chalcopyrite

X: Chalcopyrite conversion

4.9.1 Thermal function

The thermal function k(T) is usually expressed as an Arrhenius function of temperature:

$$k(T) = k(T_{ref})\cdot \exp\left[-\frac{E_a}{R}\cdot\left(\frac{1}{T} - \frac{1}{T_{ref}}\right)\right] \qquad \text{Eq. 23}$$

where:

E_a: Activation energy (kJ/mol)

R: Universal gas constant ($Jmol^{-1}K^{-1}$)

T: Absolute temperature (K)

T_{ref}: Reference temperature (typically the baseline temperature) (K)

4.9.2 Chemical function

Generally, metallic sulfide minerals in ferric sulfate media are dissolved by the oxidative action of iron in solution as follows:

$$MS + 2\,Fe^{3+} \rightarrow M^{2+} + 2\,Fe^{2+} + S \qquad \text{Eq. 24}$$

where M is a divalent metal ion. The leaching reaction of metallic sulfide minerals is assumed to be electrochemical in nature and Eq. 24 is the result of two half-cell reactions (Eq. 25 and Eq. 26) which take place simultaneously on the surface of the mineral at mixed potential, E_m.

$$MS \rightarrow M^{2+} + S + 2e^{-} \qquad \text{Eq. 25}$$

$$Fe^{3+} + e^{-} \rightarrow Fe^{2+} \qquad \text{Eq. 26}$$

4.9.3 Topological function

Chemical controlled models

When chemical reactions control the rate of reaction, and this rate is unaffected by the presence of a product layer, then the conversion rate of the particle is proportional to the available surface area of the unreacted core. In this case, the fraction unreacted can be written:

$$1 - X = \left(1 - \left(\frac{\partial d}{\partial t}\right)\frac{t}{d_0}\right)^3 \qquad \text{Eq. 27}$$

Diffusion controlled models

When the reaction is controlled by the resistance to diffusion through a porous product layer, then the fraction unreacted can be written thus:

$$1 - X = \left\{\frac{1}{2} + \cos\left(\frac{\psi + 4\pi}{3}\right)\right\}^3 \qquad \text{Eq. 28}$$

where:

$$\psi = \cos^{-1}\left[1 - 2\left(1 - \frac{t}{\tau}\right)\right] \qquad \text{Eq. 29}$$

And τ represents the time required for a complete reaction. Furthermore, for a distribution of grain sizes Eq. 27 or Eq. 28 can be combined with a cumulative size distribution function $F(d_0)$ as follows:

$$1 - \overline{X}(t) = \int_0^1 [1 - X(d_0, t)]\, dF(d_0) \qquad \text{Eq. 30}$$

4.9.4 Topological model development

The synthetic chalcopyrite, used as head ore in the leaching tests, contained a distribution of grain sizes. Therefore, to use the equations presented in the previous section, the size distribution was fitted with a polynomial function, and from this fit, the 15 specific initial particle sizes d_0 were found, which gave cumulative distribution function values $F(d_0)$ corresponding to the 15 roots of a 14th-order Legendre polynomial (modified for limits of integrations between 0 and 1) (Bouffard et al., 2006). Figure 46 shows the Legendre root points corresponding to the F curve.

For the case of chemical controlled reaction, Eq. 30 could be written as:

$$1 - \overline{X}(t) = \int_0^1 \left[1 - \frac{t}{d_0}\left(\frac{\partial d}{\partial t}\right)\right]^3 dF(d_0) \qquad \text{Eq. 31}$$

$$1 - \overline{X}(t) = \frac{1}{2} \cdot \sum_{n=0}^{14} w_n \cdot \left[1 - \frac{t}{d_{0,n}}\left(\frac{\partial d}{\partial t}\right)\right]^3 \qquad \text{Eq. 32}$$

where

$$F(d_{0,n}) = \frac{z_n + 1}{2} \qquad \text{Eq. 33}$$

And where w_n and z_n are the weights and roots of a 14th-order Legendre polynomial, respectively.

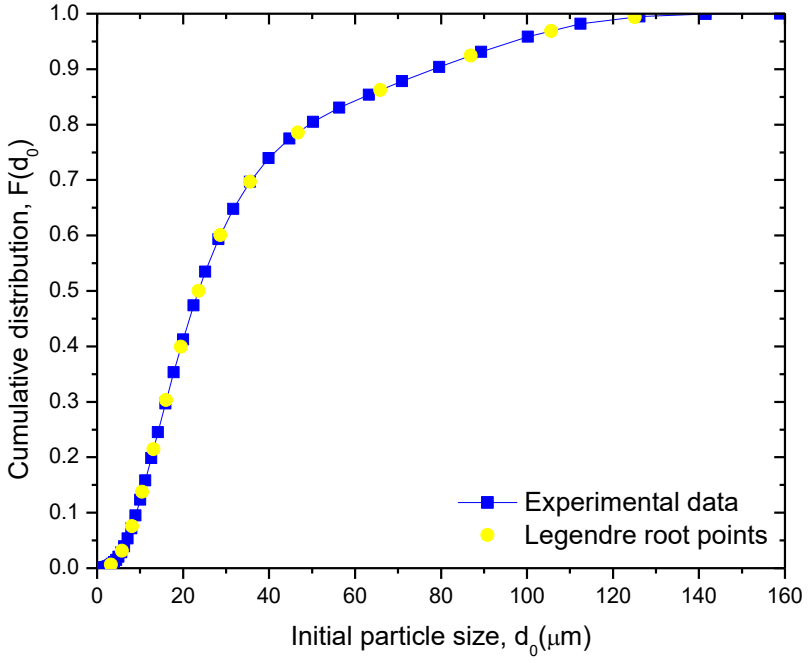

Figure 46. Particle size distribution for synthetic chalcopyrite sample.

A unique value of the shrinkage rate ∂d/∂t, presented in Table 4, constant throughout the duration of the test, was determined for each of the test conditions in this study, by minimizing the sum of the square error between the predicted conversions and the experimental chalcopyrite conversions. The resulting conversion plots are shown in Figures 47 to 51. The model that yielded the best fit was the shrinking sphere model, confirming the assumption made based on the results obtained from the SEM-EDX elemental compositional images, that the dissolution of chalcopyrite in the presence of TU is not affected by the formation of a product layer.

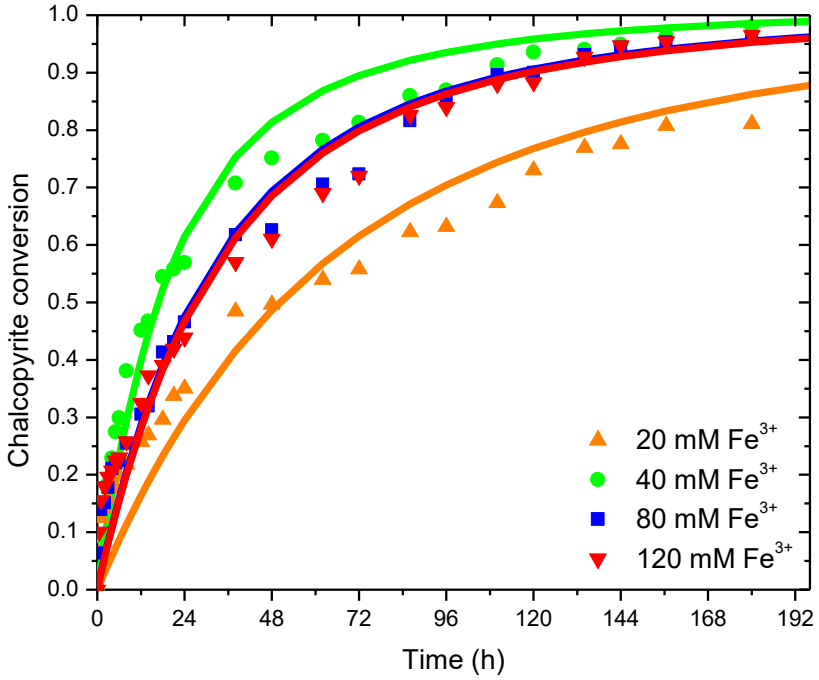

Figure 47. Model fitting for chalcopyrite conversion at different initial ferric concentrations.

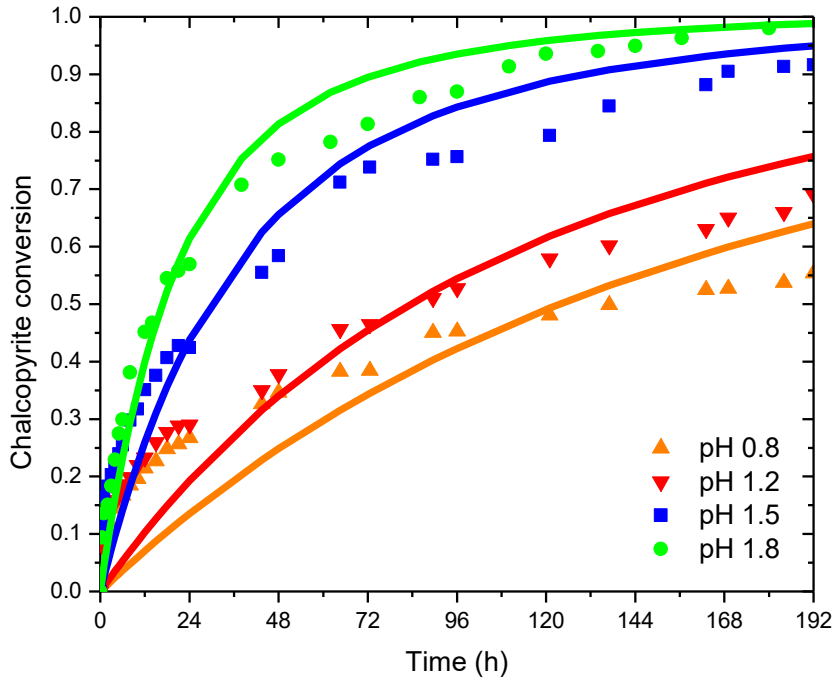

Figure 48. Model fitting for chalcopyrite conversion at different initial pH values.

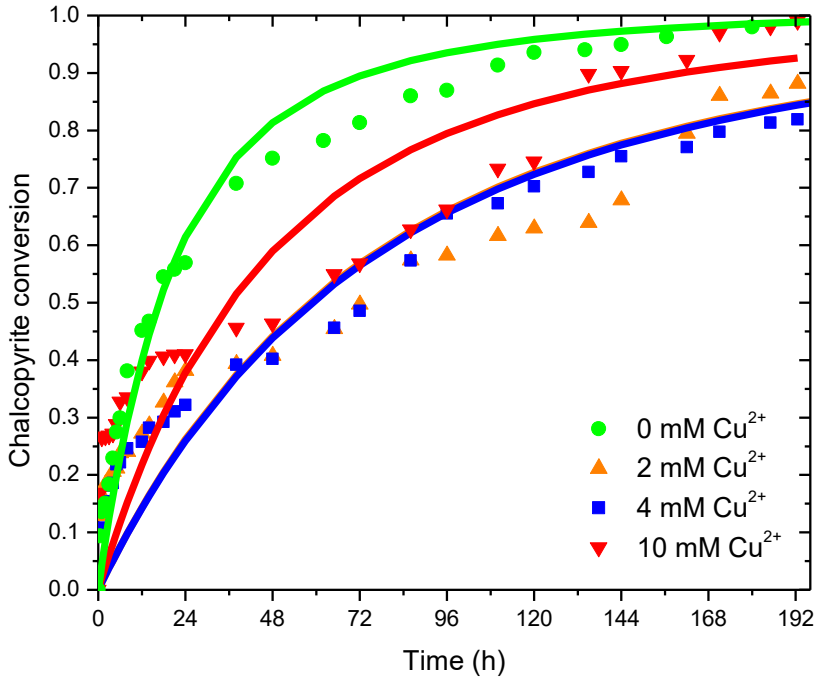

Figure 49. Model fitting for chalcopyrite conversion at different initial cupric concentrations.

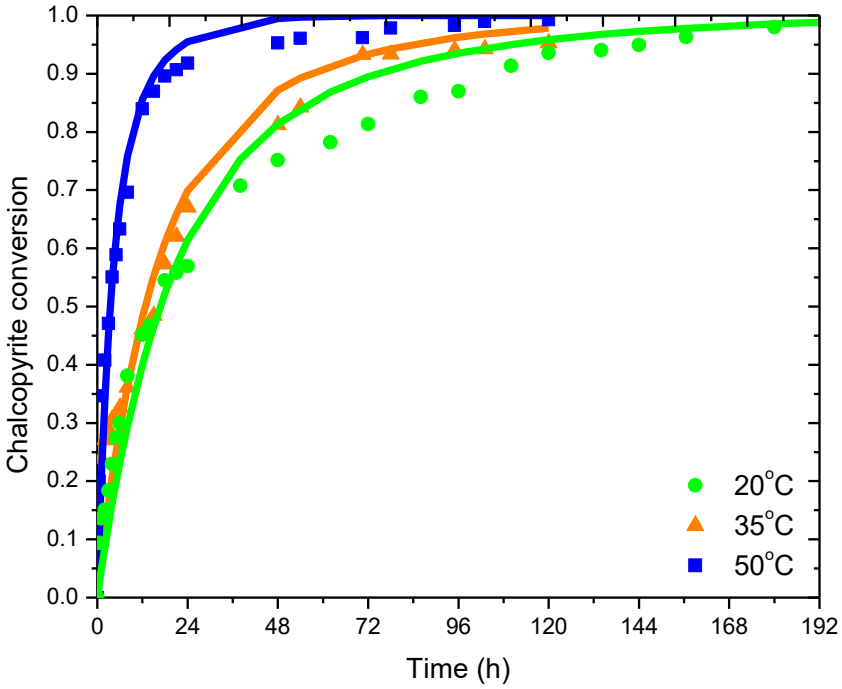

Figure 50. Model fitting for chalcopyrite conversion at different temperatures.

Table 4. Summary of fitted shrinking rates and $\sum(Pi - O_i)^2$. Baseline: 20ºC, 2 mM TU, 40 mM Fe^{3+}, 0 mM Cu^{2+}, and pH 1.8.

	Variable	**Shrinking rate (µm/h)**	**$\sum(Pi - O_i)^2$**
	Baseline	0.273	0.08
Ferric concentration	20 mM Fe^{3+}	0.091	0.14
	80 mM Fe^{3+}	0.176	0.074
	120 mM Fe^{3+}	0.171	0.11
Catalyst concentration	0.5 mM TU	0.027	0.10
	1 mM TU	0.054	0.13
pH	pH 0.8	0.037	0.16
	pH 1.2	0.055	0.12
	pH 1.5	0.156	0.11
Cupric concentration	2 mM Cu^{2+}	0.079	0.16
	4 mM Cu^{2+}	0.078	0.21
	10 mM Cu^{2+}	0.127	0.25
Temperature	35 C	0.359	0.12
	50 C	1.321	0.05

As observed from the Figures 47 – 50 and the results presented in Table 4, under specific experimental conditions the resulting model fail to yield a perfect fit. Moreover, from Figure 48 and Figure 49 it may be concluded that the shrinking sphere model (represented by the lines) deviates from the conversion data, most markedly in the presence of increasing copper concentration and the decrease in pH. This deviation could be attributed to the difficulty of keeping the TU concentration constant throughout the duration of the test. Unfortunately, a detailed study on the nature of these catalyst's interactions with both the proton and cupric ions is beyond the scope of this work.

4.9.5 Chemical reactions

Based on the results of this work, the following overall reactions are proposed to describe the leaching of chalcopyrite in acidic sulfate media in the presence of a catalyst. First, the oxidation of chalcopyrite may be written thus:

$$CuFeS_2 + 4\ Fe^{3+} \rightarrow Cu^{2+} + 5\ Fe^{2+} + 2\ S^0 \qquad \text{Eq. 34}$$

Simultaneously on the surface of the chalcopyrite the following reaction is occurring:

$$TU + Fe^{3+} \rightarrow \tfrac{1}{2}\ FDS^{2+} + Fe^{2+} \qquad \text{Eq. 35}$$

According to the literature, in the presence of an oxidizing agent FDS decompose rapidly in aqueous solution at acidic pH, into TU, cyanamide and colloidal sulfur (Arifoglu et al., 1992). As chalcopyrite leaches, Cu(II) in solution is reduced whilst the catalyst is oxidized to FDS, as shown in the following expression:

$$TU + Cu^{2+} \rightarrow \tfrac{1}{2}\ FDS^{2+} + Cu^{+} \qquad \text{Eq. 36}$$

The remaining TU forms a complex with the Cu(I) ion (Krewska et al., 1980). Is noteworthy to mention that the determination of the complexes and the study of the conditions that influence the complexation are beyond the scope of this work.

4.9.6 Reaction kinetics

As described in the previous section, the dominant parameters for the dissolution of chalcopyrite in acidic ferric sulfate media are: ferric, sulfuric acid, TU, copper and temperature. In this section, the effect of TU concentration, temperature, pH, and copper concentration, on the reaction rates are presented and discussed. The standard conditions for the leaching experiments were 20ºC, 40 mM Fe^{3+}, 2 mM TU, pH 1.8 and 2 g of synthetic chalcopyrite in two liters of solution.

Effect of thiourea concentration

A plot of ln shrinkage rate vs. ln [TU], shown in Figure 51, yields a straight line with a slope of 1.7, which represents the reaction order with respect to the catalyst concentration in solution. This finding is consistent with the results obtained from the leaching test, that showed a high dependence of dissolution rates on the TU concentration present in solution.

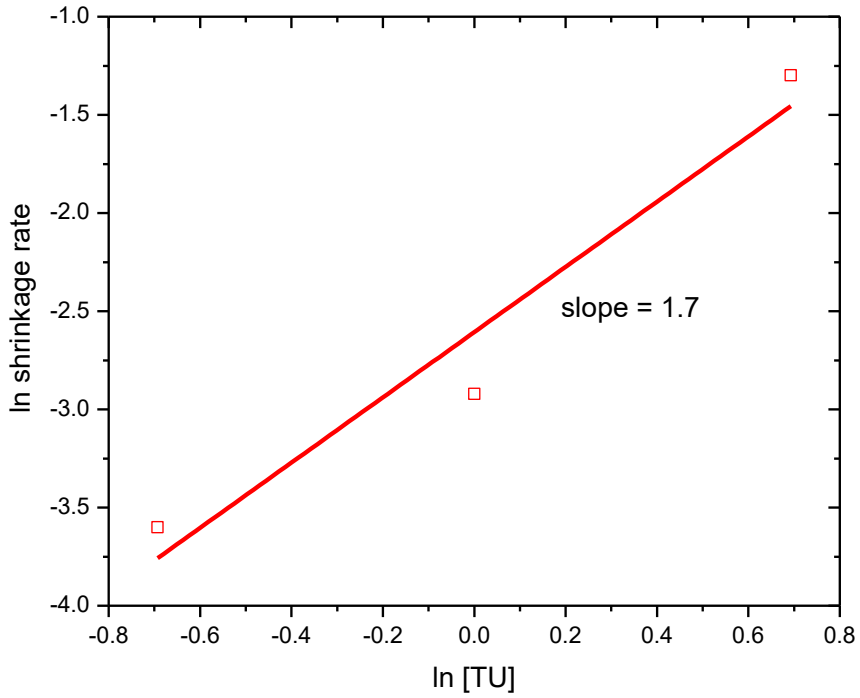

Figure 51. Log-log plot for determining reaction order with respect to thiourea concentration.

Effect of temperature

Based on previous results of temperature dependence and assuming chemical reaction as the rate-controlling step, the experimental data were analyzed using the shrinking sphere model.

Plotting the natural logarithm of the shrinkage rate versus the inverse absolute temperature, 1/T, gives an Arrhenius plot, the slope of which represents -E/R, where E is the apparent Arrhenius activation energy for chalcopyrite, and R is the ideal gas constant. As shown in Figure 52, the apparent Arrhenius activation energy by this method was calculated as 40.87 kJ/mol (9.77 kcal/mol). Confirming that the process is controlled by chemical reaction. This activation energy, is in agreement with the values, 38–63 kJ/mol, reported by Dutrizac (1978) for the leaching of synthetic chalcopyrite in ferric sulfate media.

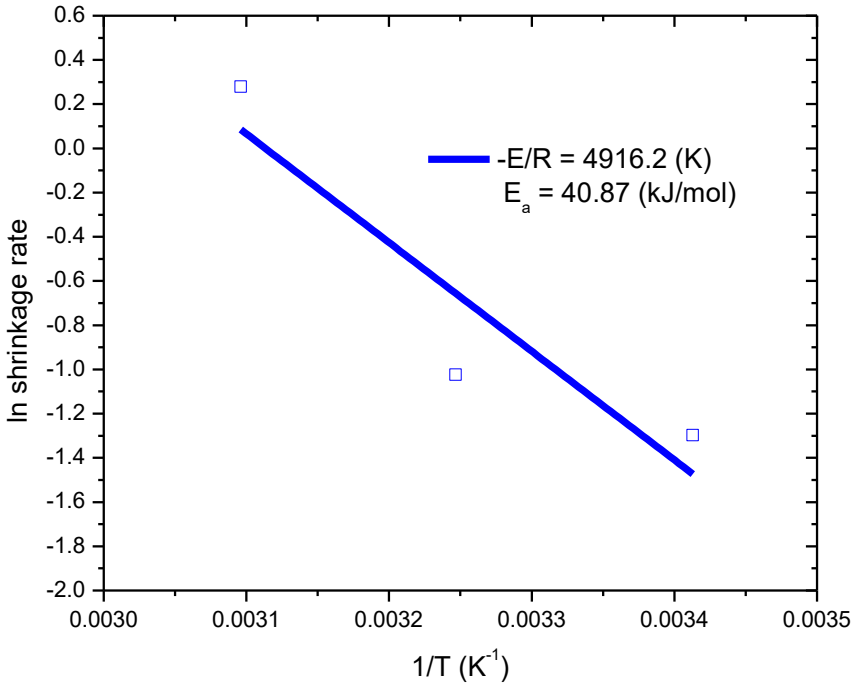

Figure 52. Arrhenius plot for leaching of chalcopyrite using thiourea as catalyst.

Effect of pH

A plot of ln shrinkage rate vs. ln [H^+], shown in Figure 53 yields a straight line with a slope of -0.91, which represents the reaction order with respect to the proton concentration in solution. As expected, this value shows that increasing the proton concentration in solution represents a hindrance for the dissolution of the chalcopyrite. Thus, considering the high dependency of the chalcopyrite dissolution with the concentration of the catalyst, it can be assumed, that this negative value is due to the interaction of the proton with TU, affecting the stability of the latter in solution. Besides, according to the literature, the oxidation rate of FDS, to further decomposition products, is also affected by a decrease in the pH (Hu et al., 2002).

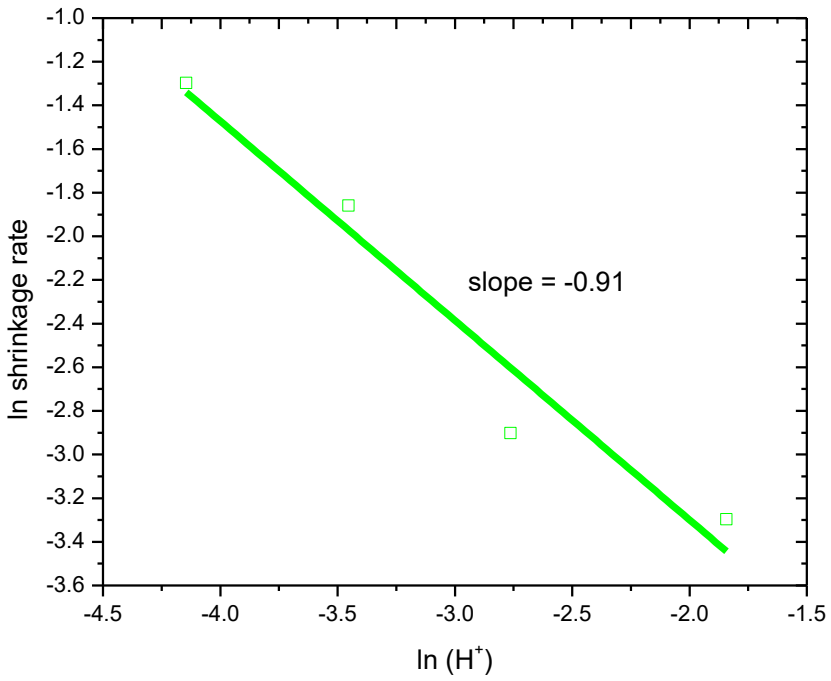

Figure 53. Log-log plot for determining reaction order with respect to pH.

Effect of copper concentration

A plot of ln shrinkage rate vs. ln [Cu^{2+}], shown in Figure 54, yields a straight line with a slope of 0.31, which represents the reaction order with respect to the cupric concentration in solution. This value shows that the dissolution of chalcopyrite is not hindered by the presence of cupric in solution. This is in agreement with the results obtained from the leaching test in the presence of TU.

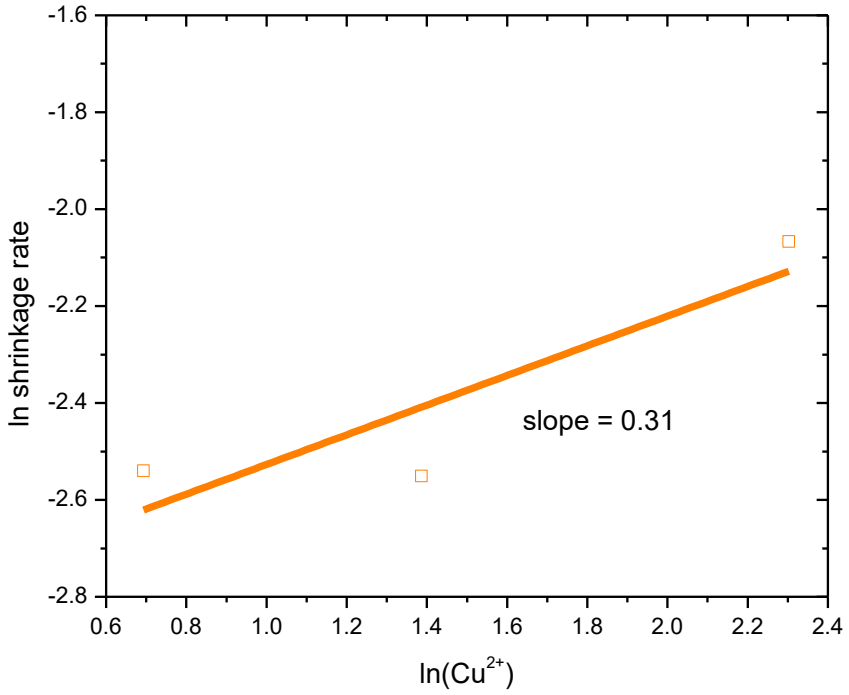

Figure 54. Log-log plot for determining reaction order with respect to cupric concentration.

4.9.7 Reaction mechanism

The dissolution kinetics of sulfides minerals such as chalcopyrite can often be described with the concepts of electrode kinetics. The Butler-Volmer equation is the key concept of electrode kinetics. In this equation, electrochemical half-cell reactions occurring simultaneously are considered and studied as separate processes. The kinetics of each process are modeled using the Butler-Volmer equation, Eq. 37. This equation relates the current density at a solid-solution interface to the established overpotential.

$$j = j_o \left[\exp\left(\frac{\alpha FE}{RT}\right) - \exp\left(\frac{-(1-\alpha)FE}{RT}\right) \right] \quad \text{Eq. 37}$$

where j is the net current density, j_0 is the exchange current density (i.e, current density of either half-cell reaction at the reversible potential), α is the transfer coefficient, F is the Faraday's constant (96,485 J/mole$^-$), R is the universal gas constant (8.314 $Jmol^{-1}K^{-1}$) and T is the absolute temperature. The Butler-Volmer expression for the net anodic, i_a, and the net cathodic, i_c, are expressed as follows:

$$i_a = n_a F k_{af} \exp\left(\frac{\alpha_a FE_a}{RT}\right) - n_a F k_{ar}[C] \exp\left(\frac{-(1-\alpha_a)FE_a}{RT}\right) \quad \text{Eq. 38}$$

$$i_c = n_c F k_{cf} \exp\left(\frac{\alpha_c FE_c}{RT}\right) - n_a F k_{cr}[C] \exp\left(\frac{-(1-\alpha_c)FE_c}{RT}\right) \quad \text{Eq. 39}$$

where:

i_a, i_c: anodic and cathodic densities, respectively.

n_a, n_c: total charge transfer for anodic and cathodic reaction, respectively.

k_{af}, k_{ar}: the rate constants for forward and reverse directions for anodic reaction.

k_{cf}, k_{cr}: the rate constants for forward and reverse directions for cathodic reaction.

E_a, E_c: potentials for anodic and cathodic reactions, respectively.

α_a, α_c: charge transfer coefficients for anodic and cathodic reactions, respectively.

As mentioned in the previous section, the dissolution of chalcopyrite is described by the redox pair described as followed:

$$CuFeS_2 \rightarrow Cu^{2+} + Fe^{2+} + 2\,S^0 + 4\,e^- \qquad \text{Eq. 40}$$

$$4\,Fe^{3+} + 4\,e^- \rightarrow 4\,Fe^{2+} \qquad \text{Eq. 41}$$

Where the equations for the anodic and cathodic current densities can be written as:

$$i_{CuFeS_2} = z_a F k_a \exp\left(\frac{\alpha_a F E_a}{RT}\right) \qquad \text{Eq. 42}$$

$$i_{Fe^{3+}} = z_c F k_{cf}[Fe^{3+}] \exp\left(-(1-\alpha_c)\frac{FE_c}{RT}\right) - z_c F k_{cr}[Fe^{2+}] \exp\left(\frac{\alpha_c F E_c}{RT}\right) \qquad \text{Eq. 43}$$

Based on the results presented in the previous section, the dissolution of chalcopyrite in the presence of a catalyst presents a 1.7 order dependency with respect to the concentration of thiourea, and a -0.91 order dependency with respect to the proton activity. Hence, the anodic current density of Eq. 40 can be taken as follows:

$$i_{CuFeS_2} = z_a F k_a [TU]^{1.7}[H^+]^{-0.91} \exp\left(\frac{\alpha_a F E_a}{RT}\right) \qquad \text{Eq. 44}$$

The activation barrier is symmetrical, and values of the transfer coefficient fall generally in the range 0.4 to 0.7, with values commonly near 0.5. It is assumed that $\alpha_a = \alpha_c = \alpha = 0.5$, for purposes of simplication. At a mixed potential E_m, $E_m = E_a = E_c$, and the sum off all anodic currents, $\sum i_a$, is equal to the negative sum of all cathodic currents, $\sum i_c$, such that:

$$\sum i_a = \sum i_c \qquad \text{Eq. 45}$$

$$\sum i_a = z_a F k_a [TU]^{1.7}[H^+]^{-0.91} \exp\left(\frac{0.5 F E_a}{RT}\right) \qquad \text{Eq. 46}$$

$$\sum i_c = z_c F k_{cf}[Fe^{3+}] \exp\left(\frac{-0.5 F E_m}{RT}\right) - z_c F k_{cr}[Fe^{2+}] \exp\left(\frac{0.5 F E_m}{RT}\right) \qquad \text{Eq. 47}$$

By re-arranging the factors the expression can be written as:

$$E_m = \frac{RT}{F} \cdot \ln\left(\frac{k_{cf} z_c F[Fe^{3+}]}{k_a z_a F[TU]^{1.7}[H^+]^{-0.91} + k_{cr} z_c F[Fe^{2+}]}\right) \qquad \text{Eq.48}$$

Substitution of Eq. 48 into Eq.44 gives:

$$i_a = z_a F k_a [TU]^{1.7} [H^+]^{-0.91} \left(\frac{k_{cf} z_c F [Fe^{3+}]}{k_a z_a F [TU]^{1.7} [H^+]^{-0.91} + k_{cr} z_c F [Fe^{2+}]} \right)^{0.5} \quad \text{Eq. 49}$$

Eq. 49 can be redefined into simpler form thus:

$$j_a = \frac{i_a}{z_a F} = k \left(\frac{[Fe^{3+}]}{K + [Fe^{2+}]} \right)^{0.5} \quad \text{Eq. 50}$$

where

$$k = k_a [TU]^{1.7} [H^+]^{-0.91} \left(\frac{k_{cf}}{k_{cr}} \right)^{0.5} \qquad \text{and} \qquad K = \frac{z_a k_a}{z_c k_{cf} [TU]^{1.7} [H^+]^{-0.91}}$$

and where j_a is the rate of oxidation of chalcopyrite per unit of mineral surface area, k is the rate constant, and K is a constant which relates to the degree of irreversibility of the cathodic half-cell. Based on the types of leaching kinetics (after M.J Nicol).

Type II: $K << [Fe^{2+}]$ and $$j_a \propto \left(\frac{[Fe^{3+}]}{[Fe^{2+}]} \right)^{0.5} \quad \text{Eq.51}$$

In Type II, the exchange current density of the oxidizing couple is higher than that of the dissolution reaction by several orders of magnitude, and the leaching rate is proportional to the square root of the ratio of the concentration of the oxidized and reduced forms of the oxidant (Dixon, 2000).

On the other hand, the effect of morphology can be related to the rate of chalcopyrite oxidation as follows:

$$r = \frac{i_a A}{z_a F} = j_a = - \frac{dn}{dt} = n_0 \frac{dX}{dt} \quad \text{Eq. 52}$$

Assuming that the grains are spherical and of identical size, the leachable surface area A and the initial number of moles of chalcopyrite n_0 can be related to the initial diameter d_0 and the conversion as follows:

$$\frac{dX}{dt} = \frac{6 M}{\rho d_0} j_a (1 - X)^{2/3} \quad \text{Eq. 53}$$

where ρ is the chalcopyrite density and M is the chalcopyrite molecular mass. By integrating the expression can be written as follows:

$$1 - X = \left[1 - \frac{2M}{\rho d_0} \int_0^t j_a \, dt\right]^3 \qquad \text{Eq. 54}$$

If the anodic charge j_a is constant with time, then Eq. 54 can be simplified thus:

$$1 - X = \left[1 - \frac{2Mj_a}{\rho} \frac{t}{d_0}\right]^3 = \left[1 - \left(\frac{\partial d}{\partial t}\right) \frac{t}{d_0}\right]^3 \qquad \text{Eq. 55}$$

where $\partial d/\partial t$ is the particle shrinkage rate which is a unique function of solution potential and temperature, thus:

$$\frac{\partial d}{\partial t} = k\,(T_{ref}) \exp\left[-\frac{E_a}{R}\left(\frac{1}{T} - \frac{1}{T_{ref}}\right)\right]\left(\frac{[Fe^{3+}]}{[Fe^{2+}]}\right)^{0.5} \frac{\mu m}{h} \qquad \text{Eq. 56}$$

For a distribution of grain sizes, Eq. 55 can be combined with the cumulative size distribution function. Based on the best-fit parameters, the conversion model for chalcopyrite particles, including the TU and pH dependence, may be written as follows:

$$1 - X\,(t, d_0) = \left[1 - \frac{t}{d_0}\left(k\,(T_{ref}) \exp\left[-4916\left(\frac{1}{T} - \frac{1}{293}\right)\right]\left(\frac{[TU]^{1.7}}{[H^+]^{0.9}}\right)\left(\frac{[Fe^{3+}]}{[Fe^{2+}]}\right)^{0.5}\right)\right]^3 \qquad \text{Eq. 57}$$

Chapter 5 Conclusions

The research work presented in this thesis addresses the lack of information of the interactions of thiourea with chalcopyrite, under the leaching conditions of our system. Several tests were conducted to evaluate the stability and the behavior of TU in solutions containing increasing concentrations of copper sulfate ($CuSO_4(H_2O)_5$), sulfuric acid (H_2SO_4), different initial ferric to ferrous ratios (Fe^{3+}/Fe^{2+}), and the presence of the mineral. The results of these studies showed that the main factors that enhanced the oxidation of TU were increasing concentration of acid, and the mineral surface. The latter factor, substantially improves the knowledge of the electrochemical nature of the oxidation of TU to FDS.

The leaching kinetics of chalcopyrite dissolution in the presence of TU in acidic ferric sulfate media were measured over the temperature range from 20 to 50ºC. This study demonstrated that in the presence of TU, it is possible to achieve ~98% of copper extraction from chalcopyrite in less than 216 hours at room temperature. These results, indicate that the catalyst positively interacts with chalcopyrite in two different ways. First, TU catalyzes the dissolution of the mineral, which could be observed by the dramatic increase in the leaching rate, when compared with the test in the absence of TU. Second, the passivation behavior intrinsic of chalcopyrite is not an inhibiting factor for the leaching once TU is added to the solution.

Moreover, according to the experimental data, it is important to notice that whilst leaching rates may appear to increase with the increase of the temperature, the stability of the catalyst decays considerably, which was also observed on the results presented by Zuñiga & Ren (personal communication, 2017). Therefore, using high temperatures may not be beneficial due to non-productive loss of the catalyst.

Incidentally, in the presence of TU, the decrease in particle size had a negative effect on the leaching rate. It is concluded, that this phenomenon could have been caused by the enhancement of the rate of oxidation of TU by the surface of the mineral. Therefore, having a smaller particle size represents a hindrance for the performance of the catalyst.

The leaching characterization analysis corroborated the theory presented by Dutrizac (1978) to explain the nonlinear kinetics observed in the sulfate system at high temperatures. Both elemental mapping and XRD analysis conducted in this study, showed that the blockage or partial blockage of the chalcopyrite surface is due to the elemental sulfur reaction product and/or precipitated iron compounds. Under control conditions, the iron-hydroxy compound found were hydronium jarosite and goethite for both temperatures (35ºC and 50ºC).

In spite of the fact that in the presence of the catalyst, the formation of the iron-hydroxy layer on the surface of the particle still occurs, the layer does not present a barrier to leaching. The results from the elemental mapping analysis suggested that the passivation layer of the leaching residues of the test catalyzed test is not as compact and thick as the one observed for the residues under control conditions. Effectively, it was proven that in the presence of the catalyst the solution is allowed to flow through the porous and the presence of this layer is not an inhibiting factor for the dissolution of chalcopyrite under the conditions studied.

Moreover, the iron-hydroxy compound formed was ammonium jarosite at both temperatures. The presence of this phase can be attributed to the decomposition of the catalyst. These results, corroborated the assumption made by Zuñiga & Ren (personal communication, 2017) regarding the possible decomposition of TU at high temperatures.

Chemical reaction was determined to be the rate controlling step based on an apparent activation energy of 41 kJ/mol, which is consistent with the values, 38–63 kJ/mol, reported by Dutrizac (1978) for the leaching of synthetic chalcopyrite in ferric sulfate media.

The reaction order of chalcopyrite was found to be 1.7 and -0.9 with respect to TU and proton concentration, (H^+), respectively. A leaching model, based on mixed potential theory, an Arrhenius temperature function, and the shrinking sphere model, assuming surface chemical reaction as the rate controlling step, integrated over the measured particle size distribution of the synthetic chalcopyrite sample was developed. The expression based on the best-fit parameters may be written as follows:

$$1 - X(t, d_0) = \left[1 - \frac{t}{d_0}\left(k(T_{ref}) \exp\left[-4916\left(\frac{1}{T} - \frac{1}{293}\right)\right]\left(\frac{[TU]^{1.7}}{[H^+]^{0.9}}\right)\left(\frac{[Fe^{3+}]}{[Fe^{2+}]}\right)^{0.5}\right)\right]^3 \qquad \text{Eq. 57}$$

Chapter 6 Recommendations and Future Work

Based on the results of this research study, several recommendations can be offered for future work:

The study of the kinetics of the oxidation of thiourea and the main factors that influences its decomposition would improve the understanding of the behaviour of the catalyst in solution. Also, the possibility of a special formulation of reagents or set-parameters to stabilize the catalyst in solution as “free TU” should be addressed.

In the interest of obtaining more precise and accurate determinations of the concentration of the catalyst, an *in situ* automatic measurement should be conducted through the duration of the leaching test.

To refine the procedure of the leaching test, it is suggested that sealed tanks with automatic sampling be used to avoid any contamination of impurities, or air getting into the system. Furthermore, to minimize the analytical error, equipment for automatic dilutions for the liquid samples could also be an improvement.

Due to the fact that the technology requires the heap leaching process to be assisted by microorganisms, the kinetics of the bioleaching of chalcopyrite in acidic sulfate media in the presence of TU should be further explored.

Finally, in this study, the kinetics of the leaching of chalcopyrite in acidic sulfate media in the presence of chalcopyrite was examined at laboratory batch scale. The next step is to use these results as part of the work to develop a mathematical model for copper heap leaching process.

References

Ahonen, L., & Tuovinen, O. (1993). Redox potential-controlled bacterial leaching of chalcopyrite ores. *Proceedings of International BioHydrometallurgy Symposium I*, 571-578.

Alodan, M., & Smyrl, W. (1998). Effect of thiourea on copper dissolution and deposition. *Electrochimica Acta*, 299-309.

Antonijevic, M., & Bogdanovic, G. (2004). Investigation of the leaching of chalcopyritic-ore in acidic solutions. *Hydrometallurgy*, 245-256.

Araneda, E. (2014). Estudio cinético y morfológico del efecto de cola, tiourea y cloruro en la electrodepositacion de cobre. *PhD. Thesis*. Concepcion, Chile.

Arifoglu, M., Marmer, W., & Dudley, R. (1992). Reaction of thiourea with hydrogen peroxide: CNMR Studies of an oxidative/reductive bleaching process. *Textile Research*, 94-100.

Arslan, H., Duran, N., Borekci, G., Koray, C., & Akbay, C. (2009). Antimicrobial activity of some thiourea derivatives and their nickel and copper complexes. *Molecules*, 519-527.

Barriga, F., Palencia, I., & Carranza, F. (1987). The passivation of chalcopyrite subjected to ferric sulfate leaching and its reactivation with metal sulfides. *Hydrometallurgy*, 159-167.

Baub, E., & Schiffner, T. (1971). The influence of thiourea on the electrolytic deposition of copper in acid copper sulfate electrolytes. 114-117.

Beckstead, L., Munoz, P., Sepulveda, J., Herbst, J., Miller, J., Olson, F., & Wadsworth, M. (1976). Acid ferric sulfate leaching of attritor-ground chalcopyrite concentrates. *Extractive Metallurgy of Copper. Volume II*, pp. 611-632.

Boekema, C., Krupski, A., Varaste, M., Parvin, K., Van Til, F., Van Der Woude, F., & Sawatzky, G. (2004). Cu and Fe valence states in $CuFeS_2$. *Journal of Magnetism and Magnetic Materials*, 559-561.

Bolzan, A., Haseeb, A., Shilardi , P., Piatti , R., Salvarezza, R., & Arvia , A. (2001). Anodisation of copper in thiourea and formamidine disulfide containing acid solution. Part I. Identification of products and reaction pathway. *Journal of Electroanalytical Chemistry*, 533-542.

Bouffard, S., Rivera, B., & Dixon, D. (2006). Leaching kinetics and stoichiometry of pyrite oxidation from a pyrite-marcasite concentrate in acid ferric sulfate media. *Hydrometallurgy*, 225-238.

Bravo, P. (2006). El panorama de la hidrometalurgia. *Revista de la Mineria Chilena*, 303.

Brierley, J., & Brierley, C. (2001). Present and future commercial applications of biohydrometallurgy. *Hydrometallurgy*, 233-239.

Brininstool, M., & Wallace, G. (2014). Copper [Advance Release]. U.S Geological Survey Minerals Yearbok. 1-29.

Burdick , C., & Ellis, J. (1917). The crystal structure of chalcopyrite determined by X-Rays. *Journal of the American Chemical Society*, 2518-2525.

Carranza, F., Palencia, I., & Romero, R. (1997). Silver catalyzed IBES process: Application to a spanish copper-zinc sulphide concentrate. *Hydrometallurgy*, 29-42.

Chaiko, D., Baczek , F., Rocks , S., Walters, T., & Klepper, R. (2015). The FLSMIDTH© rapid oxidative leach (ROL) process. Part I: Mechano-Chemical process for treating chalcopyrite. *COM 2015 The Conference of Metallurgists* (pp. 1-11). Toronto: Canadian Institue of Mining, Metallurgy and Petroleum.

Chaiko, D., Rocks, S., Walters, T., Asihene, S., Eyzaguirre , C., Klepper, R., Baczek, F., & McMahon, G. (2015). The FLSMIDTH© rapid oxidative leach (ROL) proces. Part II: A new chemical activation process for chalcopyrite. *COM 2015 The Conference of Metallurgists* (pp. 1-15). Toronto: Canadian Institute of Mining, Metallurgy and Petroleum.

Cheng, C., & Lawson, F. (1987). Leaching of gold and silver from pyrite and its calcine with aqueous cyanide and thiourea. *The Australian Institute of Mining and Metallurgy*, 79-84.

Collins, M., & Kofluk, D. (1998). *Unites States Patent No. 5, 730, 776.*

Cordoba, E., Munoz , J., Blazques, M., Gonzalez, F., & Ballester, A. (2008). Leaching of chalcopyrite with ferric ion. Part IV: The role of redox potential in the presence of mesophilic and termophilic bacteria. *Hydrometallurgy 93*, 106-115.

Cordoba, E., Munoz, J., Blazquez, M., Gonzalez, F., & Ballester, A. (2008). Leaching of chalcopyrite with ferric ion. Part I: General aspects. *Hydrometallurgy*, 81-87.

Cordoba, E., Munoz, J., Blazquez, M., Gonzalez, F., & Ballester, A. (2008). Leaching of chalcopyrite with ferric ion. Part II: Effect of redox potential. *Hydrometallurgy*, 88-96.

Cordoba, E., Munoz, J., Blazquez, M., Gonzalez, F., & Ballester, A. (2009). Passivation of chalcopyrite during its chemical leaching with ferric iron at 68°C. *Minerals Engineering*, 229-235.

Corrans, I., & Angove, J. (1993). *United States Patent No. 5, 232, 491.*

Crundwell, F., Van Aswegen, A., Bryson, L., Biley , C., Craig , D., Marsicano, V., & Keartland, J. (2015). The effect of visible light on the dissolution of natural chalcopyrite ($CuFeS_2$) in sulphuric acid solutions. *Hydrometallurgy*, 119-131.

De Filippo, D., Rossi, A., Rossi , G., & Trois , P. (1988). Surface modifications in copper sulphide minerals after bioleaching. *Biohydrometallurgy*, (pp. 245-258). Warwick, England.

Dixon, D. (1995). Hydrometallurgical Reactor Design and Analysis, Chapter 6 and 7. Vancouver, Canada.

Dixon, D. (2000). Modeling of Leaching Reactors. *Short Course Presented to Placer Dome Technology Group*.

Dixon, D., & Hendrix, J. (1993). A general model for leaching of one or more solid reactants from porous ore particles. *Metallurgical Transactions*, 157-169.

Dixon, D., & Tshilombo, A. (2005). *United States Patent No. 11, 141, 043.*

Dixon, D., Mayne, D., & Baxter, K. (2008). Galvanox™ - A novel galvanically-assisted atmospheric leaching technology for copper concentrates. *Canadian Metallurgical Quaterly*, pp. 327-336.

Dreisinger, D. (2006). Copper leaching from primary sulfides: Options for biological and chemical extraction of copper. *Hydrometallurgy*, 10-20.

Dreisinger, D., Steyl, J., Sole, K., Gnoinski, J., & Dempesey, P. (2003). The Anglo American Corporation/University of British Columbia (AAC/UBC) chalcopyrite process: An integrated pilot-plan evaluation. *Hydrometallurgy of copper proceedings of the Copper 2003 conference. Book I. Volume VI*, 223-237.

Dresher, W. (2004). Producing copper nature's way: Bioleaching. *Innovations*.

Dutrizac, J. (1978). The kinetics of dissolution of chalcopyrite in ferric ion media. *Metallurgical Transactions*, 431-439.

Dutrizac, J. (1981). The dissolution of chalcopyrite in ferric sulfate and ferric chloride media. *Metallurgical Transactions*, 371-378.

Dutrizac, J. (1989). Elemental sulfur formation during the ferric sulfate leaching of chalcopyrite. *Canadian Metallurgical Quarterly*, 337-344.

Dutrizac, J., & MacDonald, R. (1974). Ferric ion as a leaching medium. *Minerals Science Engineering*, 59-100.

Dutrizac, J., MacDonald, R., & Ingraham, T. (1969). The kinetics of dissolution of synthetic chalcopyrite in aqueous acidic ferric sulfate solutions. *Metallurgical Transactions*, 955-959.

Edelbro, R., Sandstrom, A., & Paul , J. (2003). Full potential calculation on the electron bandstructures of sphalerite, pyrite and chalcopyrite. *Applied Surface Science*, 300-313.

Elsherief, A. (2002). The influence of cathodic reduction, Fe^{2+} and Cu^{2+} ions on the electrochemical dissolution of chalcopyrite in acidic solutions. *Minerals Engineering*, 215-223.

Fabricius, G., Kontturi, K., & Sundholm, G. (1996). Influence of thiourea and thiourea aging on the electrodeposition of copper from acid sulfate solutions studied by the ring-disc technique. *Journal of Applied Electrochemistry*, 1179-1183.

Fuentes, J., Lapidus-Lavine, G., & Gonzalez, I. (2008). Electrochemical characterization of solid products formed in the electro-assited reduction of chalcopyrite. *Hydrometallurgy*, 664-670.

Garrels, R., & Christ, C. (1965). Solution, Minerals and Equilibria. New York: Harper & Row.

Glen, J., Richmond, G., Arnold , S., & Mitchell, D. (2003). The Mount Gordon ferric leach process-plant upgrade to treat lower grade feed stocks. *Hydrometallurgy of copper, Proceedings of the Copper 2002 Volume VI*, 239-251.

Guikuan, Y., & Asselin, E. (2014). Kinetics of ferric ion reduction on chalcopyrite and its influence on leaching up to 150°C. *Electrochimica Acta*, 307-321.

Gupta, P. (1963). Analytical chemistry of thiocarbamides: I. Quantitative determination of thiourea. *Fresenius' Zeitschrift für analytische Chemie*, 412-431.

Habashi, F. (1978). *Chalcopyrite its chemistry and metallurgy.* New York: McGraw-Hill .

Habashi, F., & Bauer , E. (1966). Aqueous oxidation of elemental sulfur. *Industrial and Engineering Chemistry Fundamentals 5*, 469-471.

Hackl, R. (1995). The leaching and passivation of chalcopyrite in acid sulfate media. *PhD Thesis*. Vancouver, Canada.

Hackl, R., Dreisinger, D., Peters, E., & King, J. (1995). Passivation of chalcopyrite during oxidative leaching in sulfate media. *Hydrometallurgy*, 25-48.

Hall, S., & Stewart, J. (1973). The crystal structure refinement of Chalcopyrite, $CuFeS_2$. *Acta Crystallographica*, 579-585.

Hirato, T., Majima, H., & Awakura, Y. (1987). The leaching of chalcopyrite with ferric sulfate. *Metallurgical Transactions*, 695-705.

Hiroyoshi, N., Arai, M., Miki , H., Hirajima, T., & Tsunekawa, M. (2002). A new reaction model for the catalytic effect of silver ions on chalcopyrite leaching in sulfuric acid solutions. *Hydrometallurgy*, 257-262.

Hiroyoshi, N., Hirota, M., Hirajima, T., & Tsunekawa, M. (1997). A case of ferrous sulfate addition enhancing chalcopyrite leaching. *Hydrometallurgy*, 37-45.

Hiroyoshi, N., Miki, H., Hirajima, J., & Tsunekawa, M. (2001). Enhancement of chalcopyrite leaching by ferrous ions in acidic ferric sulfate solutions. *Hydrometallurgy*, 185-197.

Hiroyoshi, N., Miki, H., Hirajima, T., & Tsunekawa, M. (2000). A model for ferrous-promoted chalcopyrite leaching. *Hydrometallurgy*, 31-38.

Hourn , M., & Halbe, D. (1999). The NENATECH process: Results on Frieda river copper gold concentrates. *Proceedings of the International Conference of Randol Copper Hydrometallurgy*, 97-102.

Hu, Y., Feng, J., Li, Y., Sun, Y., Xu, L., Zhao, Y., & Gao, Q. (2002). Kinetic study on hydrolysis and oxidation of formamidine disulfide in acidic solutions. *Science Chemistry*, 235-241.

Javet, P., & Hintermann, H. (1969). Aspects of the behavior of the thiourea in a cupric solution. *Electrochemistry*, 527-532.

Javet, P., Ibl, N., & Hintermann, H. (1967). Study of the kinetic consumption of and nivelant additive, the thiourea, during the electrolytic deposition. *Electrochimica Acta*, 781-794.

Jones, D., & Peters, E. (1976). The leaching of chalcopyrite with ferric sulfate and ferric chloride. *Extractive Metallurgy of Copper. Volume II*, pp. 633-653.

King, J., & Dreisinger, D. (1995). Autoclaving of copper concentrates. *Proceedings of Copper 95 International Conference*, 511-534.

King, J., Dreisinger, D., & Knight, D. (1993). The total pressure oxidation of copper concentrates. In *Metallurgy of copper, nickel and cobalt: Fundamentals aspects* (pp. 735-756). Warrendale, PA, USA: The Minerals, Metals and Materials Society of AIME.

Kordosky, G. (2002). Copper recovery using leach/solvent/extraction/electrowinning technology: Forty years of innovation, 2.2 million tonnes of copper annually. *The Journal of South African Institute of Mining and Metallurgy*, 445-450.

Krewska, S., Podsiadly, H., & Pajdowski, L. (1980). Studies on the reaction of copper(II) with thiourea: Equilibrium and stability constants in Cu(II)-thiourea-$HClO_4$ redox system. *Journal of Inorganic and Nuclear Chemistry*, 89-94.

Krzewska, S., Podsiadly, H., & Pajdowski, L. (1980). Studies on the reaction of copper (II) with thiourea: The modification of Bjerrum's method. The determination of equilibrium in simultaneous redox and complexation reactions. *Journal of Inorganic and Nuclear Chemistry*, 87-88.

Levenspiel, O. (1972). Chemical Reaction Engineering. In *Chemical Reaction Engineering* (pp. 357-408). New York: John Wiley & Sons.

Li, J., & Miller, J. (2007). Reaction kinetics of gold dissolution in acid thiourea solution using ferric sulfate as oxidant. *Hydrometallurgy 89*, 279-288.

Li, J., Kawashima, N., Chandra, A., & Gerson, A. (2013). A review of the structure and fundamental mechanism and kinetics of the leaching of chalcopyrite. *Advances in Colloid and Interface Science*, 1-32.

Li, J., Kawashima, N., Kaplun, K., Absolon, V., & Gerson , A. (2010). Chalcopyrite leaching: The rate controlling factors. *Geochemica and Cosmochemica Act 74*, 2881-2893.

Lowe, D. (1970). The kinetics of the dissolution reaction of copper and copper-iron sulfide minerals using ferric sulfate solutions. *PhD. Thesis*. Tucson, USA.

Majima, H., Awakura, Y., Hirato, T., & Tanaka, T. (1985). The leaching of chalcopyrite in ferric chloride and ferric sulfate solutions. *Canadian Metallurgical Quarterly*, 283-291.

Mallikarjunar, R., Venkatachalam, S., & Reddy, R. (1984). Electrochemical dissolution of chalcopyrite concentrate. *Journal of Electrochemical Society*.

McMillan, R., MacKinnon, D., & Dutrizac, J. (1982). Anodic dissolution of n-type and p-type chacopyrite. *Journal of Applied Electrochemistry*, 743-757.

Mikhlin, Y., Tomashevich, Y., Asanov, I., Okotrub, A., Varnek, V., & Vyalikh, D. (2004). Spectroscopy and electrochemical characterization of the surface layers of chalcopyrite ($CuFeS_2$) reacted in acidic solutions. *Applied Surface Science*, 395-409.

Miller, P. (1999). Bioleaching of copper concentrates. *The copper concentrate treatment. Short course*, (pp. 9-13). Phoenix.

Munoz, J., Dreisinger , D., Cooper, W., & Young , S. (2007). Silver-catalyzed bioleaching of low-grade copper ores. Part I: Shake flasks tests. *Hydrometallurgy*, 3-18.

Munoz, P., Miller , J., & Wadsworth, M. (1979). Reaction mechanism for the acid ferric sulfate leaching of chalcopyrite. *Metallurgical Transactions*, 149-158.

Nakazawa, H., Fujisawa, H., & Sato, H. (1998). Effect of activated carbon on the bioleaching of chalcopyrite concentrates. *International Journal of Mineral Processing*, 87-94.

Nazari, G. (2011). Enhancing the kinetics of pyrite catalyzed leaching of chalcopyrite. *PhD. Thesis*. Vancouver, Canada.

Orgul, S., & Atalay, U. (2002). Reaction chemistry of gold leaching in thiourea solution for a Turkish gold ore. *Hydrometallurgy*, 71-77.

Pang, J., & Chander, S. (1992). Electrochemical characterization of chalcopyrite solution interface. *Mineral and Metal Process*, 131-136.

Parker, A., Klauber , C., Kougianos, A., Watling, H., & Van Bronswijk, W. (2003). An X-ray photoelectron spectroscopy study of the mechanism of oxidative dissolution of chalcopyrite. *Hydrometallurgy*, 265-276.

Peacey, J., Guo, X., & Robles, E. (2003). Copper hydrometallurgy-current status preliminary economics, future direction and positioning versus smelting. *Hydrometallurgy of copper proceedings of the Copper 2003 conference. Volume VI (Book I)*, 205-221.

Peters, E. (1986). Leaching of sulfides. *The Society for Mining, Metallurgy and Exploration, Inc., of AIME*, 445-462. Littleton, CO, USA.

Peters, E. (1991). The mathematical modeling of leaching systems. *Journal of Metals*, 20-26.

Peters, E. (1992). Hydrometallurgical process innovation. *Hydrometallurgy*, 431-459.

Petersen, J., & Dixon, D. (2006). Competitive bioleaching of pyrite and chalcopyrite. *Hydrometallurgy 83*, 40-49.

Pinches, A., Myburgh, P., & Merwe, C. (2001). *United States Patent No. 6, 277, 341.*

Plaskin, I., & Kozhukeva, M. (1960). The solubility of gold and silver in thiourea. *Dokl. Akad. Nauk SSSR*, 671-674.

Potts, A. (2001). Profitable Bugs. *Mining Magazine*, pp. 128-134.

Ramachandran, V., Lakshmanan, V., & Kondos, P. (2007). Hydrometallurgy of copper sulfide concentrate: An update. *The John Dutrizac International Symposium on Copper Hydrometallurgy, Book I Volume IV*, 101-128.

Ren, Z. (2016, April). Patent Disclosure. Vancouver, Canada.

Rivadeneira, J. (2006). *Mining innovation in Latin American Report.* Retrieved from http://www.mininginnovation.cl/content.htm

Rivera, B. (2010). Electrochemical and leaching studies of enargite and chalcopyrite. *PhD Thesis*. Vancouver, Canada.

Romero, R., Mazuelos, A., Palencia, I., & Carranza , F. (2003). Copper recovery from chalcopyrite concentrates by the BRISA Process. *Hydrometallurgy*, 205-215.

Sahu, S., Sahoo, P., Patel, S., & Mishra, B. (2011). Oxidation of thiourea and substituded thiourea: A review. *Journal of Sulfur Chemistry*, 171-197.

Solis-Macial, O., & Lapidus, G. (2013). Improvement of chalcopyrite dissolution in acidic media using polar organic solvents. *Hydrometallurgy 131-132*, 120-126.

Staden, P. (1998). The Mintek/Bactech copper bioleach process. *Copper Hydrometallurgy Forum*, (p. Alta 1998). Brisbane.

Stanczyk, M. (1963). Oxidation leaching of copper sulfides in acidic pulps at elevated temperatures and pressures. *U.S Bureau of Mines reports of Investigations RI6193,19*.

Stott, M., Watling, H., Franzmann, P., & Sutton, D. (2000). The role of iron-hydroxy precipitates in the passivation of chalcopyrite during bioleaching. *Minerals Engineering Volume 13*, 1117-1121.

Toby, B. (2006). R factors in Rietveld analysis: How good is good enough? *Power Diffraction*, 67-70.

Tributsch, H., & Bennett, J. (1981). Semiconductor electrochemical aspects of bacterial leaching. Part I: Oxidation of metal sulphides with large energy gaps. *Journal of Chemical Technology and Biotechnology*, 565-577.

Tshilombo, A., & Dixon, D. (2003). Kinetic study of chalcopyrite passivation during electrochemical and chemical leaching. In G. K. F.M Doyle, *Eletrochemistry in Mineral and Metal Processing VI* (pp. 108-119). The Electrochemical Society. Inc.

Tunley, T. (1999). *United States Patent No. 5, 919, 674.*

Velazquez, L. (2009). Kinetics of the dissolution of chalcopyrite in chloride media. *PhD. Thesis*. Australia.

Vilcaez, J., Yamada, R., & Inoue, C. (2008). Effect of pH reduction and ferric ion addition on the leaching of chalcopyrite at thermophilic temperatures. *Hydrometallurgy*, 62-71.

Vizsolyi, A., Veltman, H., Warren, I., & Mackiw, V. (1967). Copper and elemental sulfur from chalcopyrite by pressure leaching. *Journal of Metals 19*, 52-59.

Ying, H., JiaMin, F., YanWei, L., YanYan, S., Li, X., YueMin, Z., & QingYu, G. (2012). Kinetic study on hydrolysis and oxidation of formamidine disulfide in acidic solutions. *Chemistry*, 235-241.

Zheng, Z. (2001). Fundamental studies of the anodic behaviour of thiourea in copper electrorefining. *PhD. Thesis*. Vancouver, Canada.

Appendix A XRD patterns

In this section, the X-ray patterns of the synthetic chalcopyrite samples used for the entire matrix of experiments of this study are presented. In each of the following figures, the experimental pattern obtained for the chalcopyrite, prepared by hydrothermal synthesis and considered as the head ore, is compared with the pattern of a pure chalcopyrite sample in the database provided by the International Center for Diffraction Data (ICDD) incorporated in the software Match 3. The following figures show the XRD patterns for all the conditions tested.

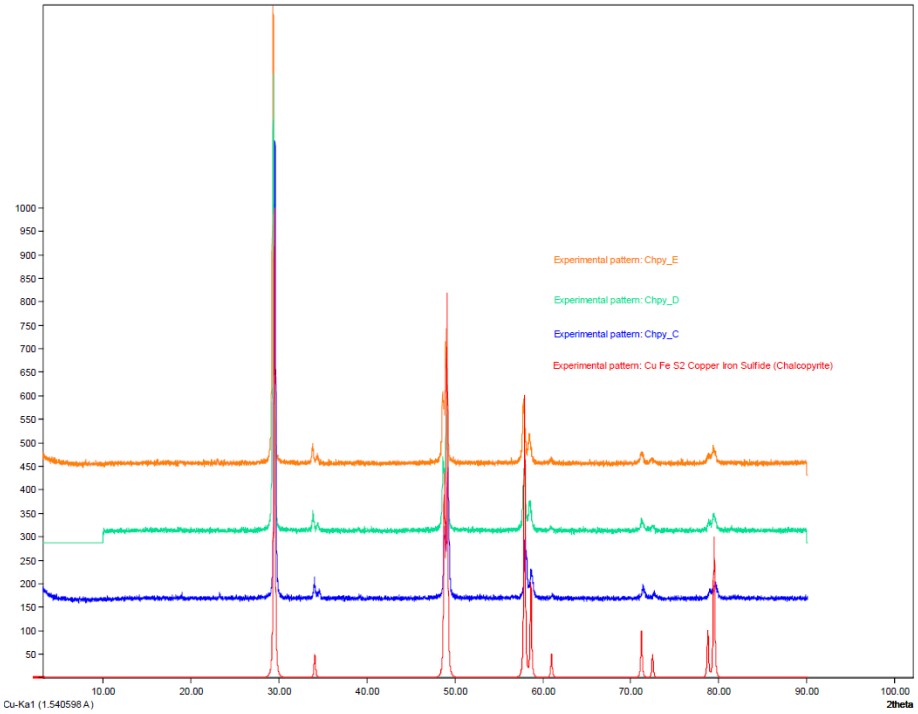

Figure A - 1. XRD pattern of synthetic chalcopyrite sample used at different initial ferric sulfate concentrations, with 0 mM TU, pH 1.8, and 20ºC.

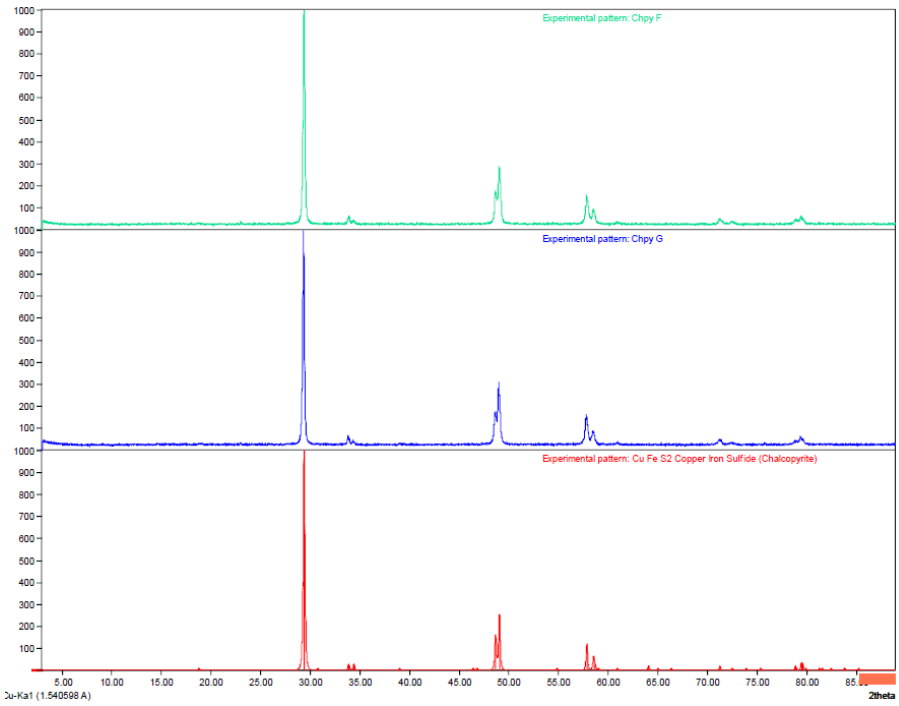

Figure A - 2. XRD pattern of synthetic chalcopyrite sample used at different initial cupric sulfate concentrations, with 40 mM Fe^{3+}, 0 mM TU, pH 1.8, and 20ºC.

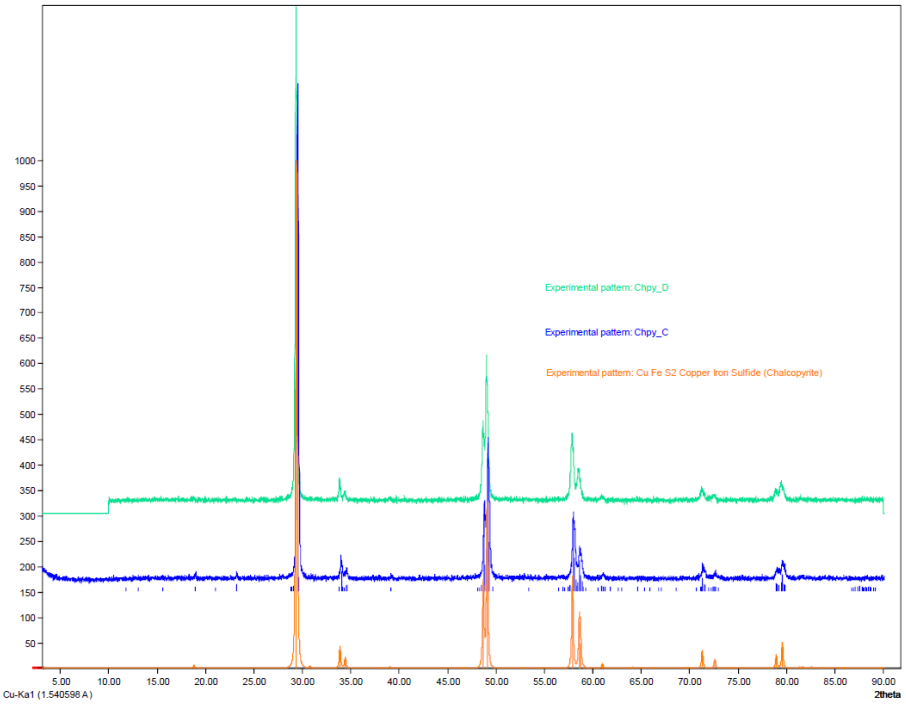

Figure A - 3. XRD pattern of synthetic chalcopyrite samples used at different pH, with 40 mM Fe^{3+}, 0 mM TU, and 20ºC.

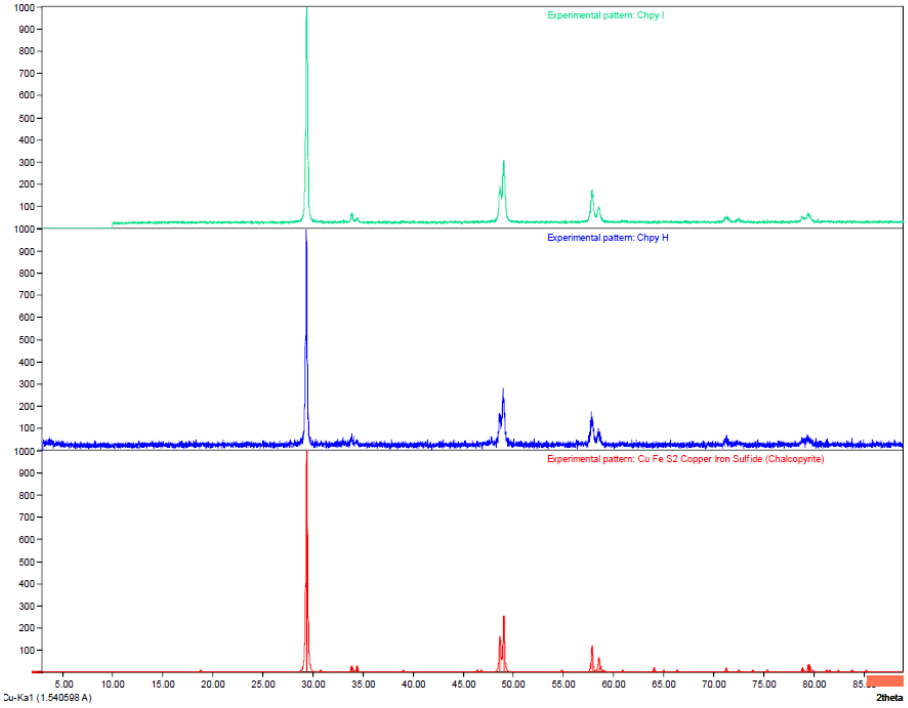

Figure A - 4. XRD pattern of synthetic chalcopyrite samples used at 35ºC and 50ºC, with 40 mM Fe^{3+}, 0 mM TU, and pH 1.8.

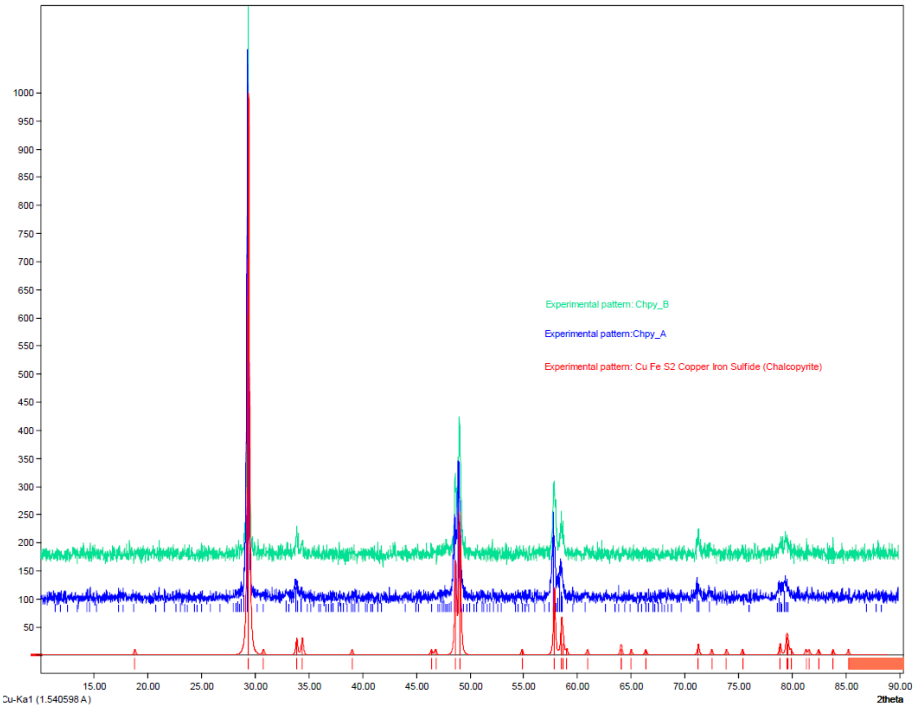

Figure A - 5. XRD pattern of synthetic chalcopyrite samples used at different initial ferric sulfate concentrations, with 2 mM TU, pH 1.8, and 20ºC.

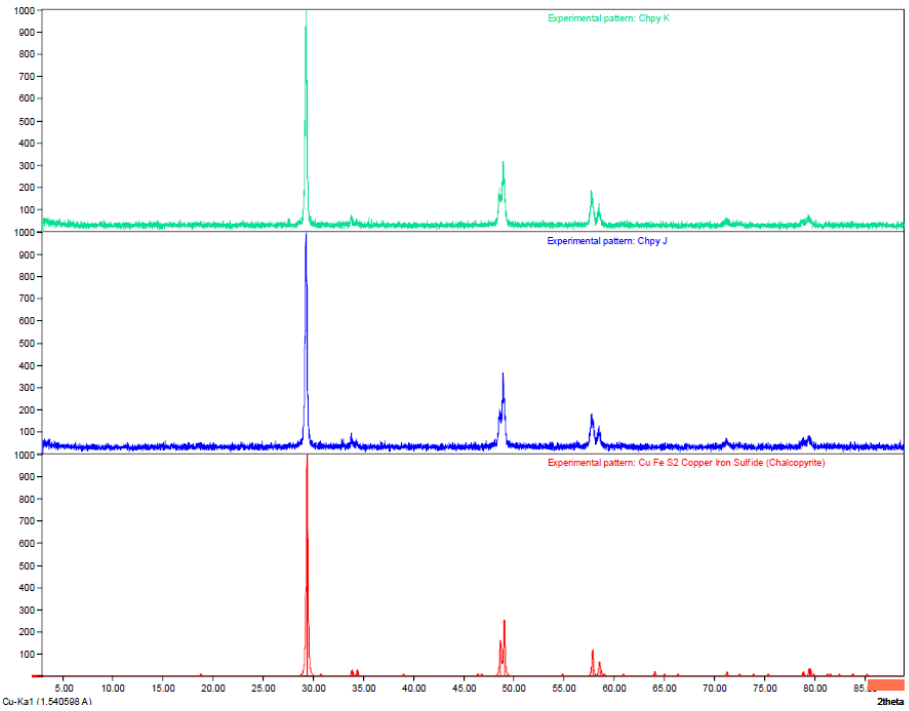

Figure A - 6. XRD pattern of synthetic chalcopyrite samples used at different initial cupric sulfate concentrations, with 40 mM Fe^{3+}, 2 mM TU, pH 1.8, and 20ºC.

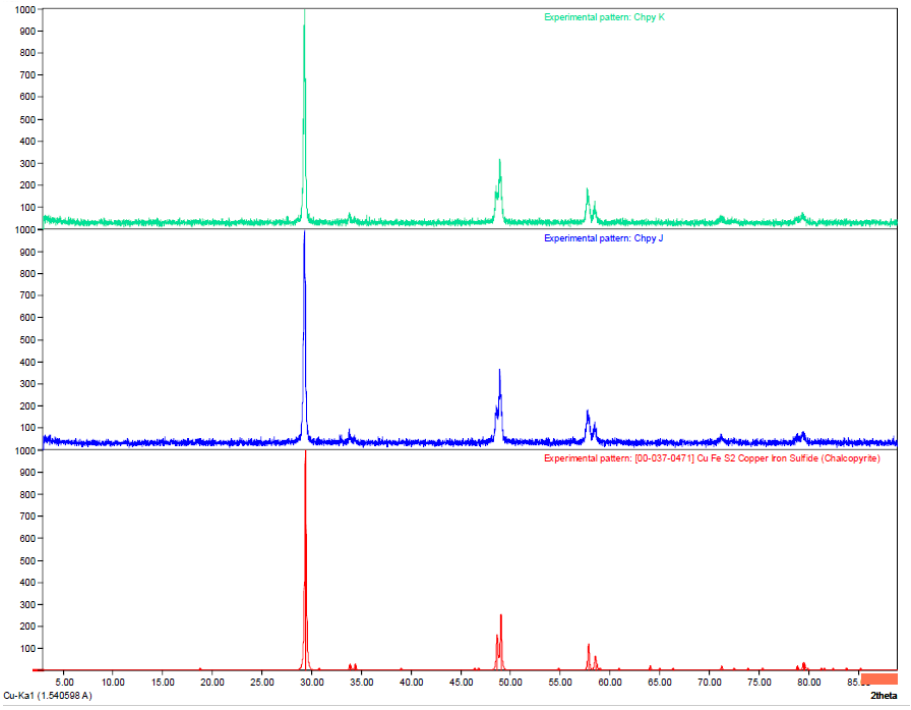

Figure A - 7. XRD pattern of synthetic chalcopyrite samples used at different initial pH, with 40 mM Fe^{3+}, 2 mM TU, and 20ºC.

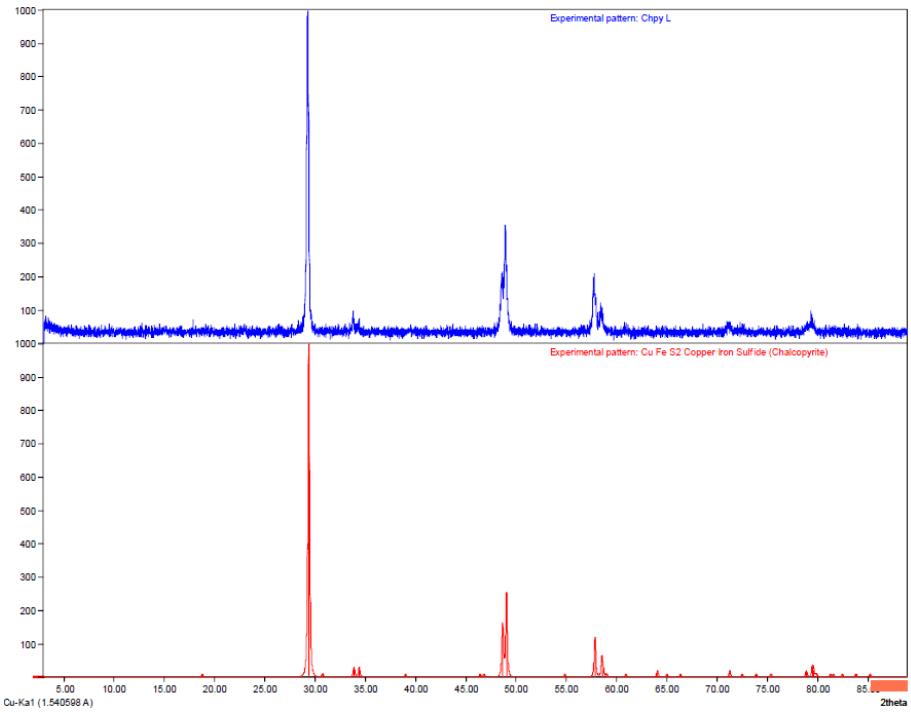

Figure A - 8. XRD pattern of synthetic chalcopyrite samples used at 35ºC and 50ºC, with 2 mM TU, 40 mM Fe^{3+}, and pH 1.8.

Appendix B Oxidation-reduction potential measurements from leaching reactors test

This section presents the ORP measurements for the entire set of experimental tests carried out in this study. The following figures show all the conditions tested in this study.

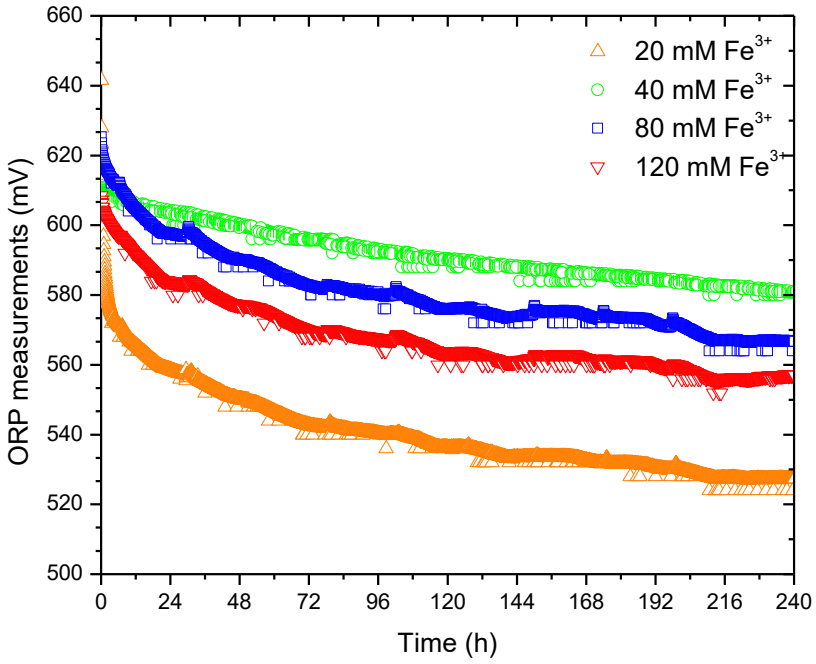

Figure B - 1. ORP values at different initial ferric sulfate concentrations, with 0 mM TU, pH 1.8, and 20ºC.

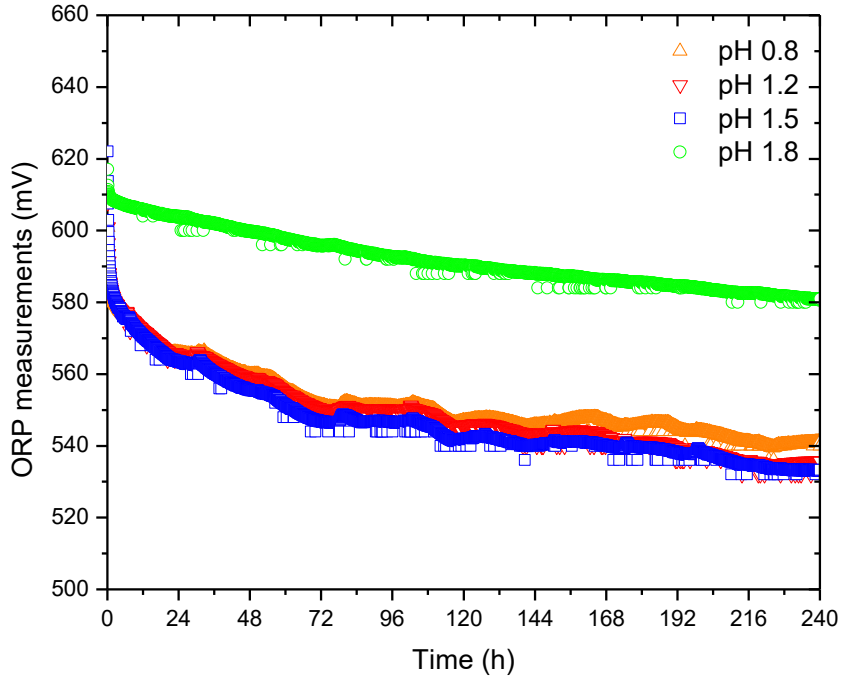

Figure B - 2. ORP values at different pH, with 40 mM Fe^{3+}, 0 mM TU, and 20ºC.

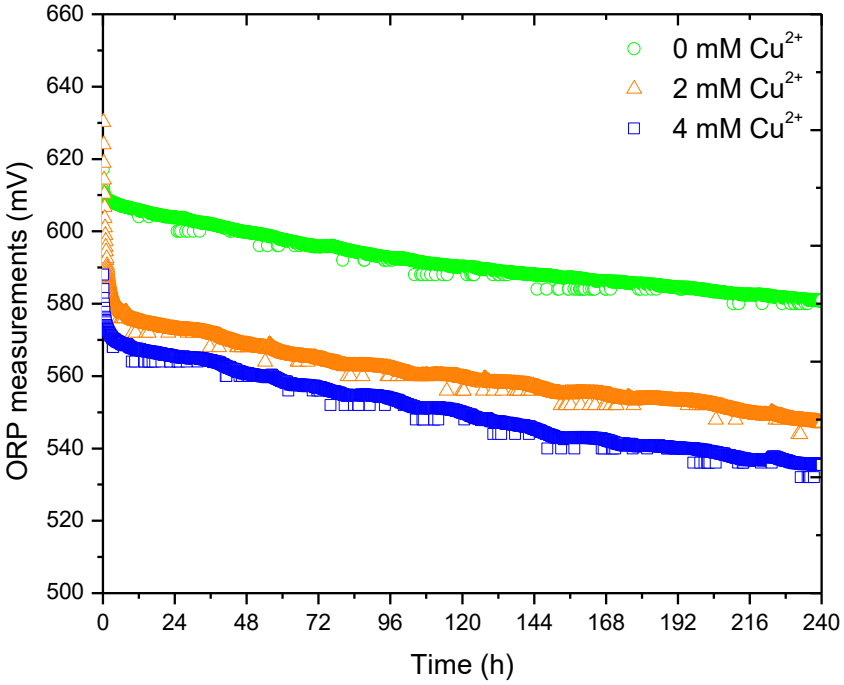

Figure B - 3. ORP values at different initial cupric sulfate concentrations, with 40 mM Fe^{3+}, 0 mM TU, pH 1.8, and 20ºC.

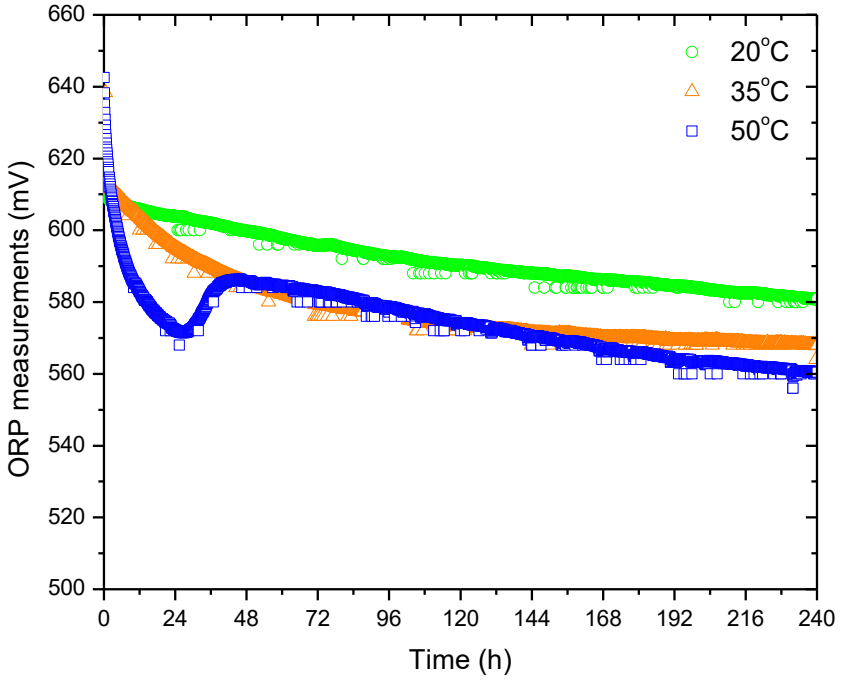

Figure B - 4. ORP values at different temperatures, with 40 mM Fe^{3+}, 0 mM TU, pH 1.2, and 20ºC.

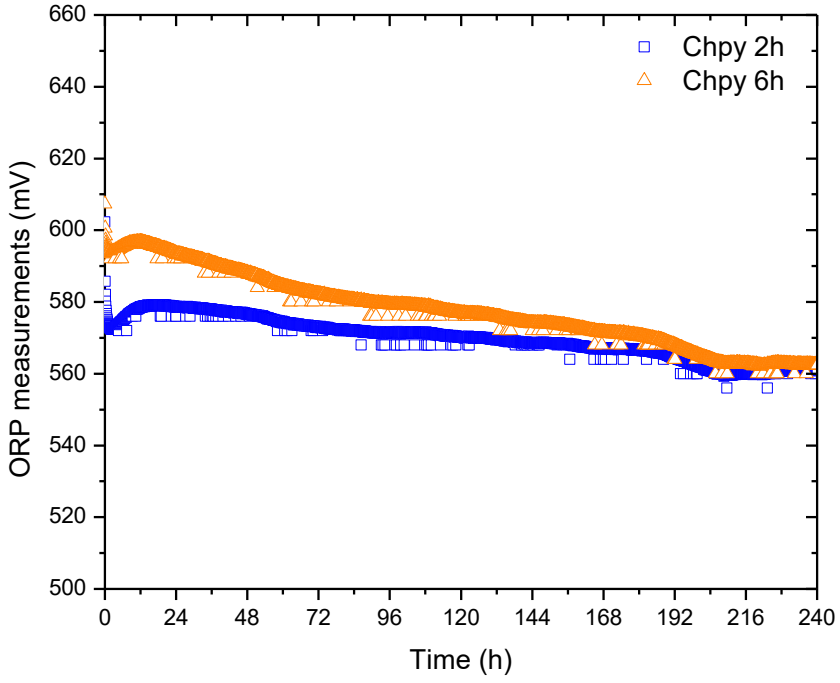

Figure B - 5. ORP values at different PSD, with 40 mM Fe^{3+}, pH 1.8, 0 mM TU, and 20ºC.

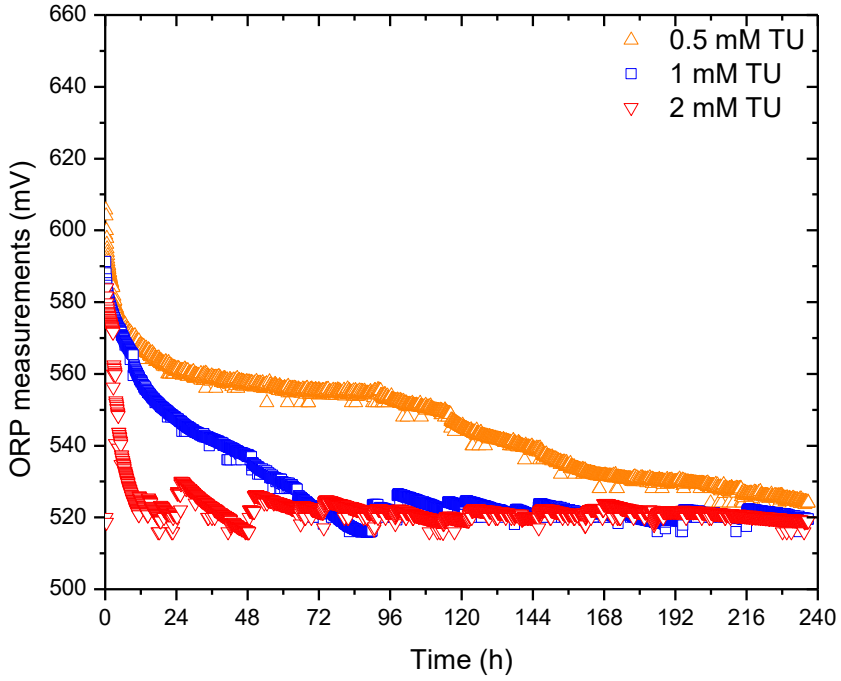

Figure B - 6. ORP values at different initial TU concentrations, with 40 mM Fe^{3+}, pH 1.8, and 20ºC.

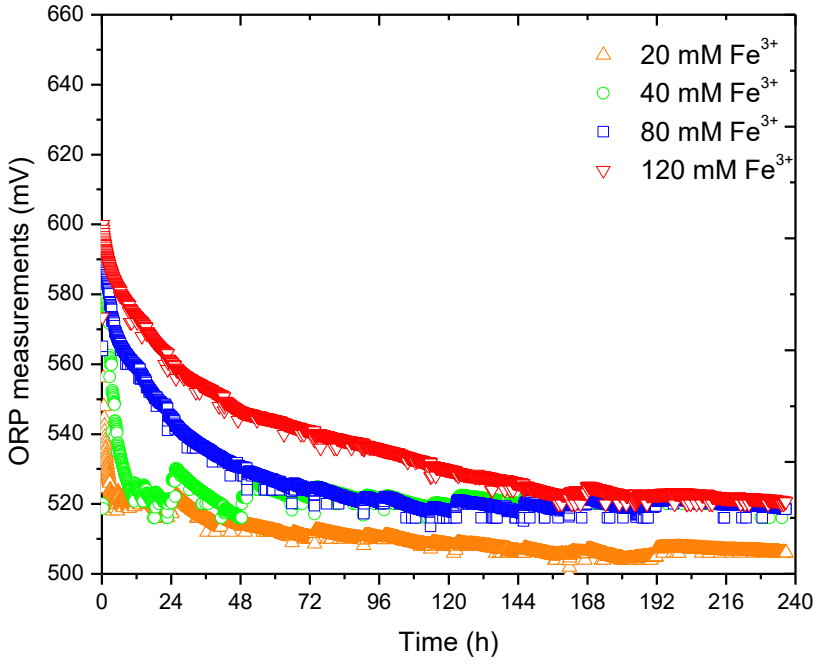

Figure B - 7. ORP values at different initial ferric sulfate concentrations, with 2 mM TU, pH 1.8, and 20ºC.

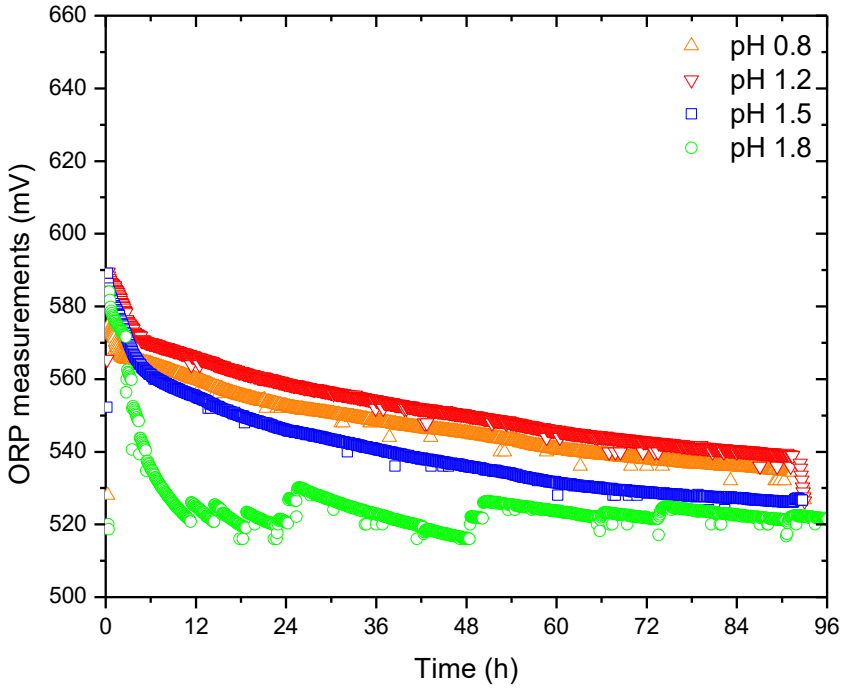

Figure B - 8. ORP values at different initial pH, with 40 mM Fe^{3+}, 2 mM TU, and 20ºC.

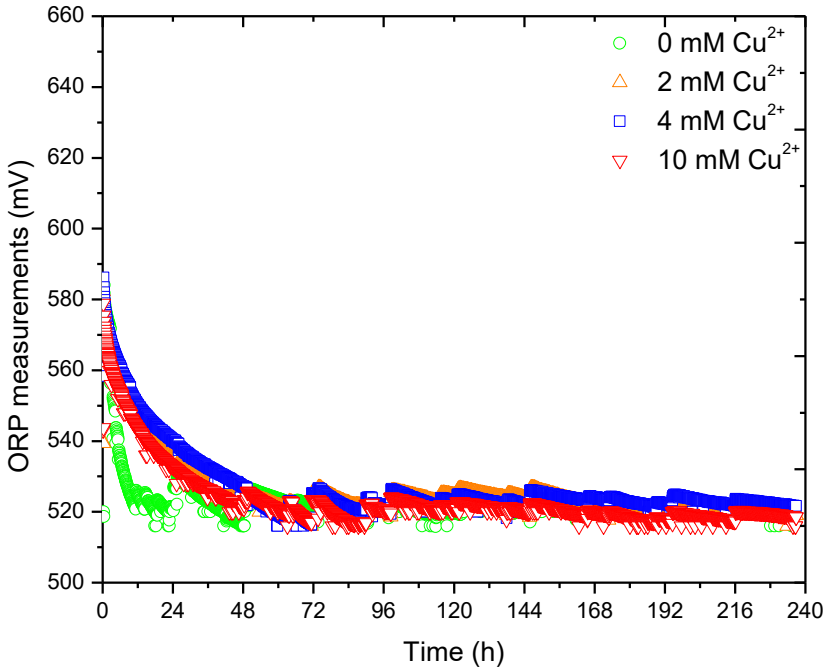

Figure B - 9. ORP values at different initial cupric sulfate concentrations, with 40 mM Fe^{3+}, 2 mM TU, pH 1.8, and 20ºC.

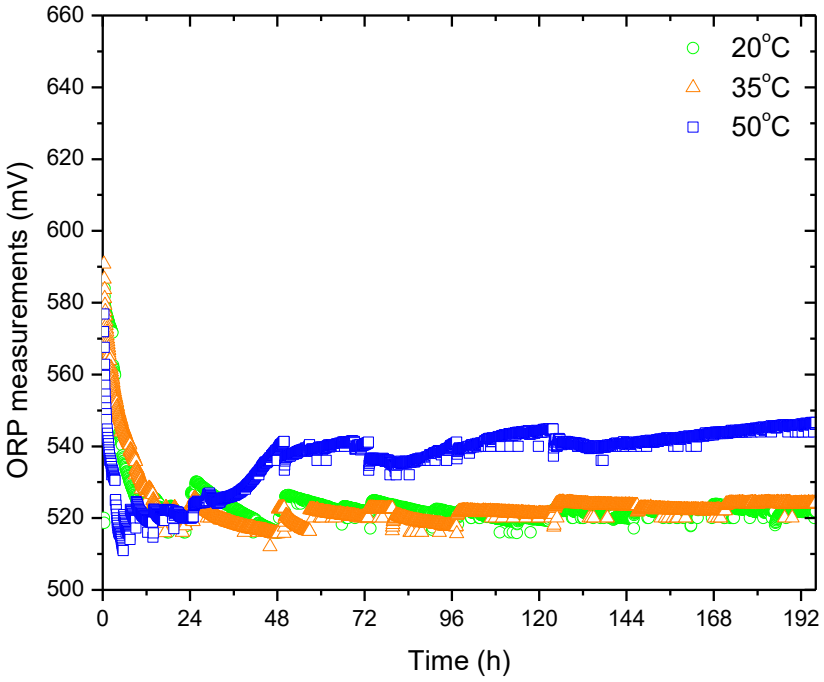

Figure B - 10. ORP values at different temperatures, with 40 mM Fe^{3+}, 2 mM TU, and pH 1.2.

Appendix C Free thiourea measurements from leaching reactors test

Measurements of the free TU concentrations for each one of the reactors conducted in the presence of the catalyst are presented in the following section.

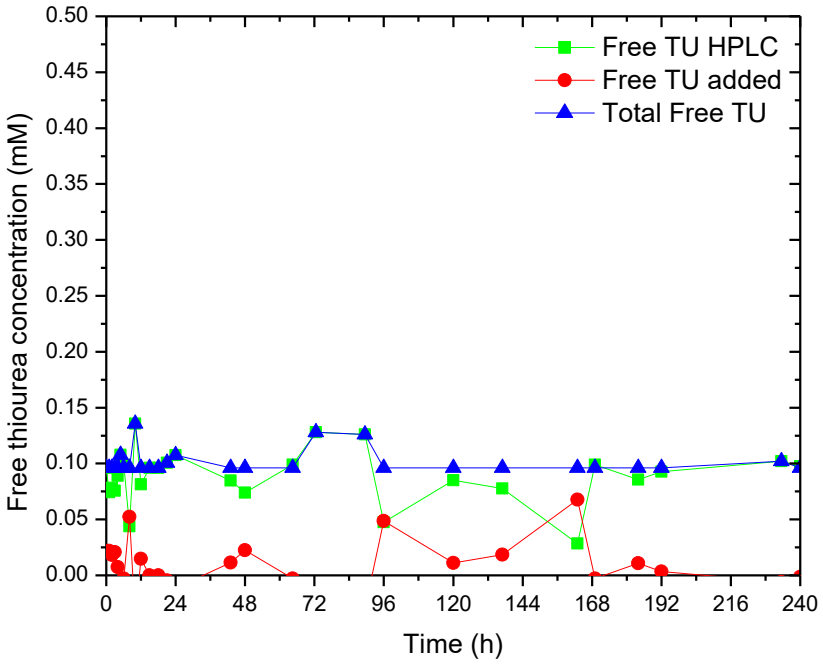

Figure C - 1. Free thiourea concentrations at initial 0.5 mM TU, with 40 mM Fe^{3+}, pH 1.8, and 20ºC.

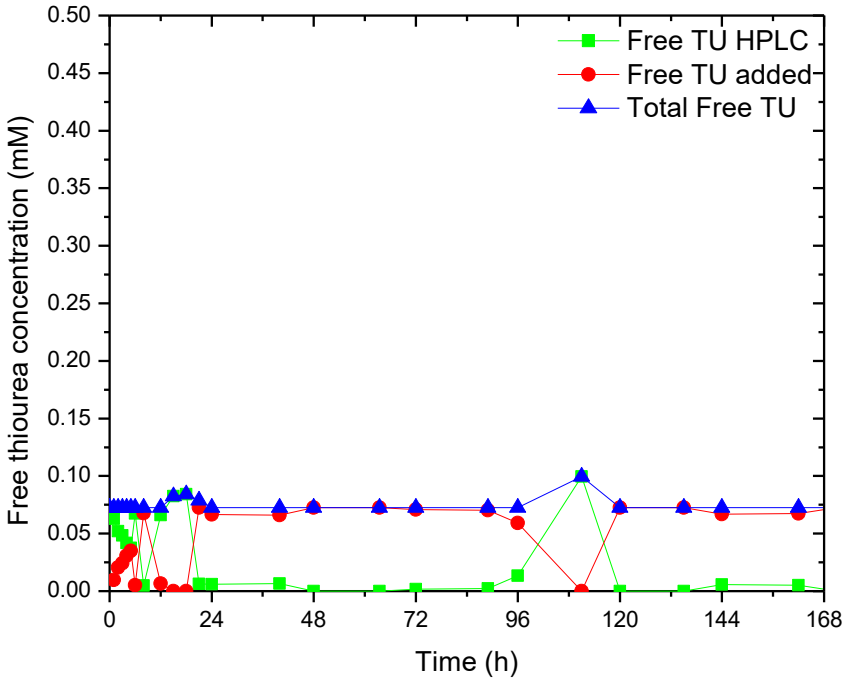

Figure C - 2. Free thiourea concentrations at initial 1 mM TU, with 40 mM Fe^{3+}, pH 1.8, and 20ºC.

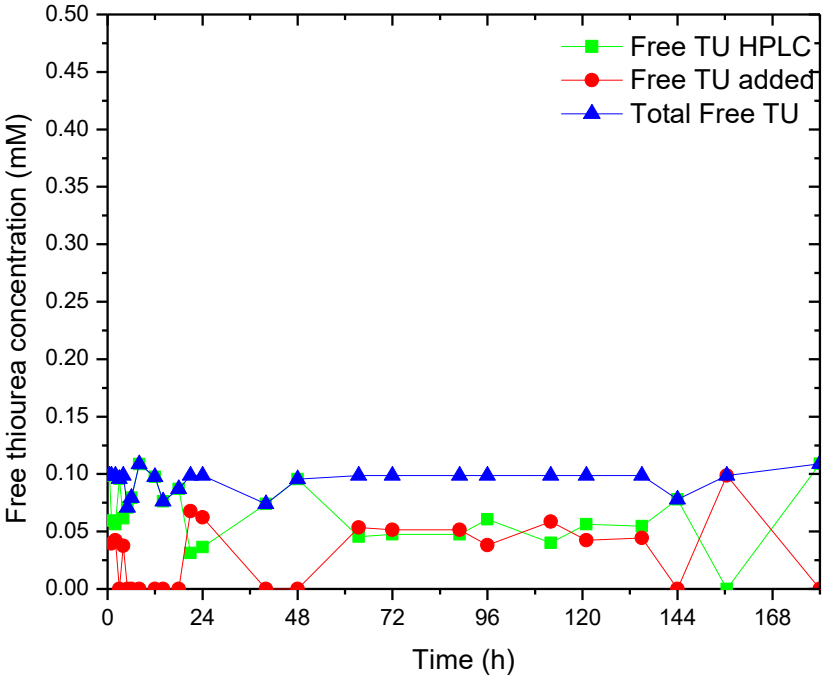

Figure C - 3. Free thiourea concentrations at 20 mM Fe^{3+}, with pH 1.8 and 20ºC.

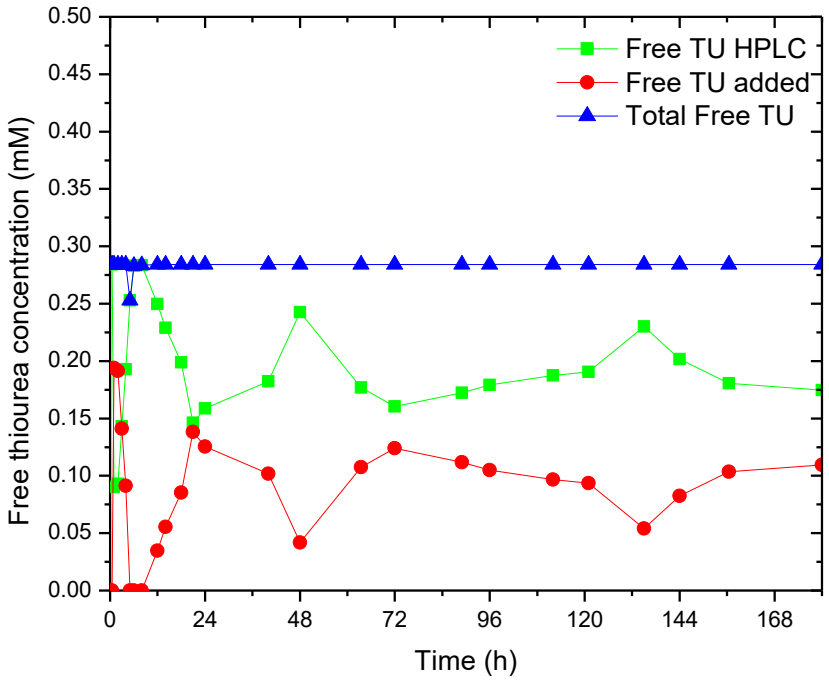

Figure C - 4. Free thiourea concentrations at 40 mM Fe^{3+}, with pH 1.8 and 20ºC.

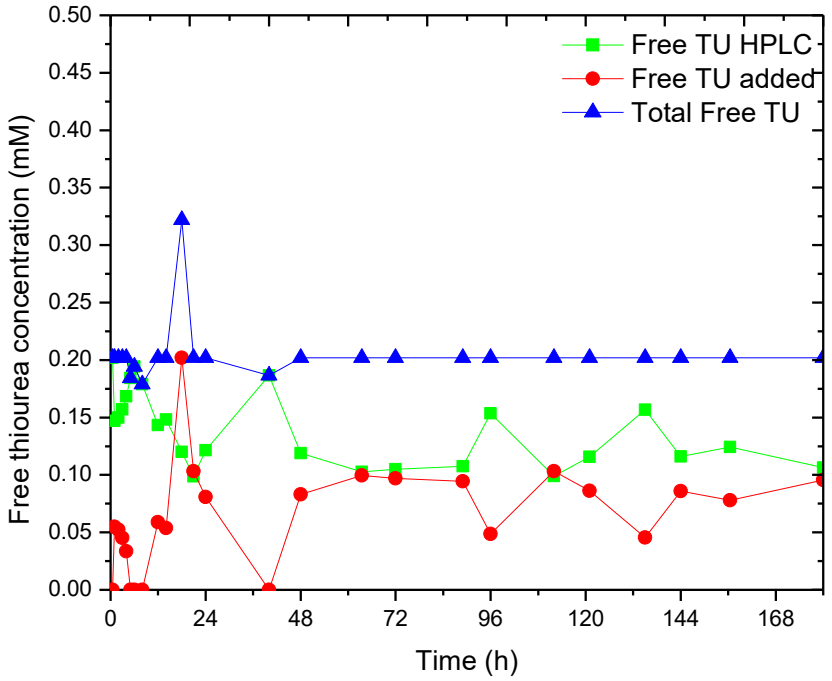

Figure C - 5. Free thiourea concentrations at 80 mM Fe^{3+}, with pH 1.8 and 20ºC.

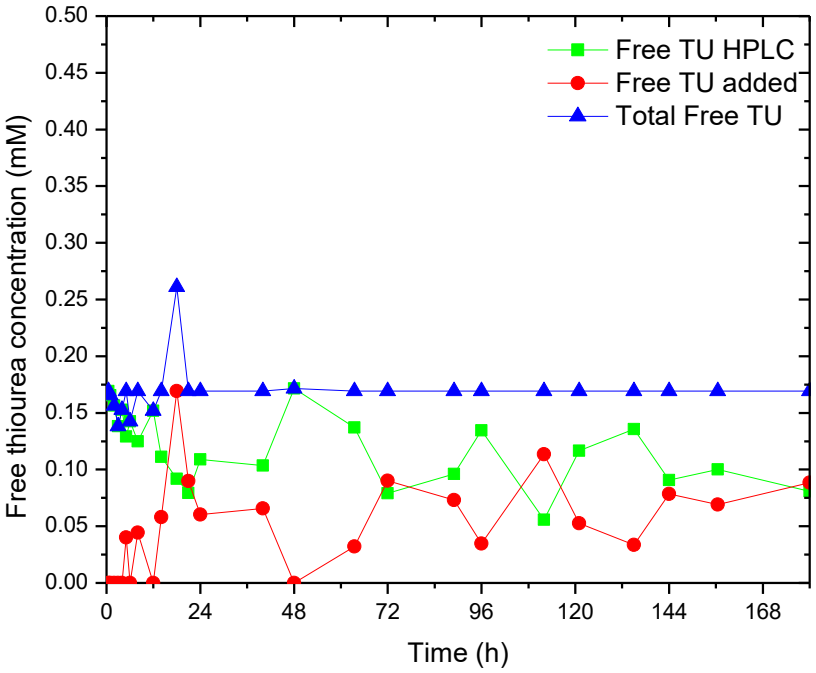

Figure C - 6. Free thiourea concentrations at 120 mM Fe^{3+}, with pH 1.8 and 20ºC.

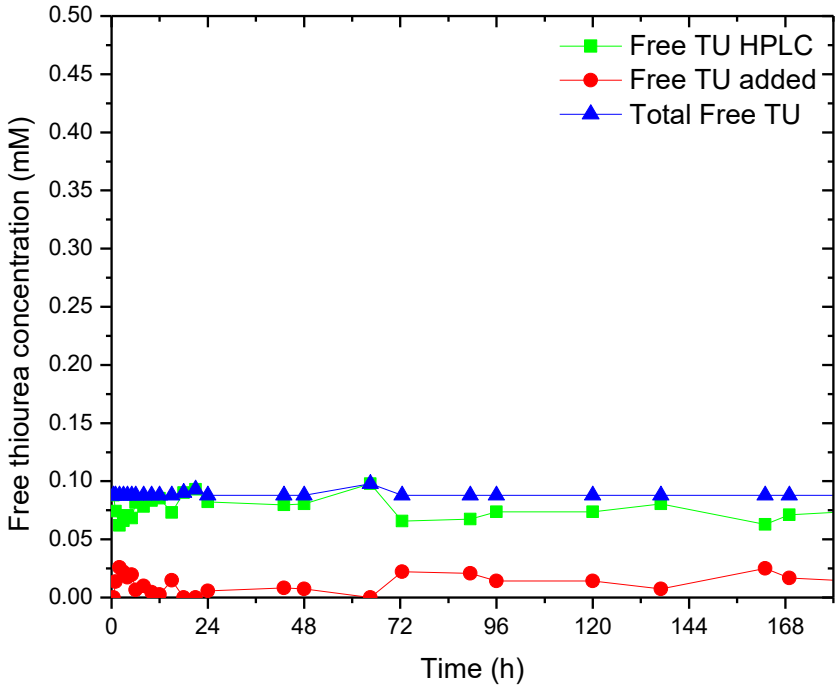

Figure C - 7. Free thiourea concentrations at pH 0.8, with 40 mM Fe^{3+} and 20ºC.

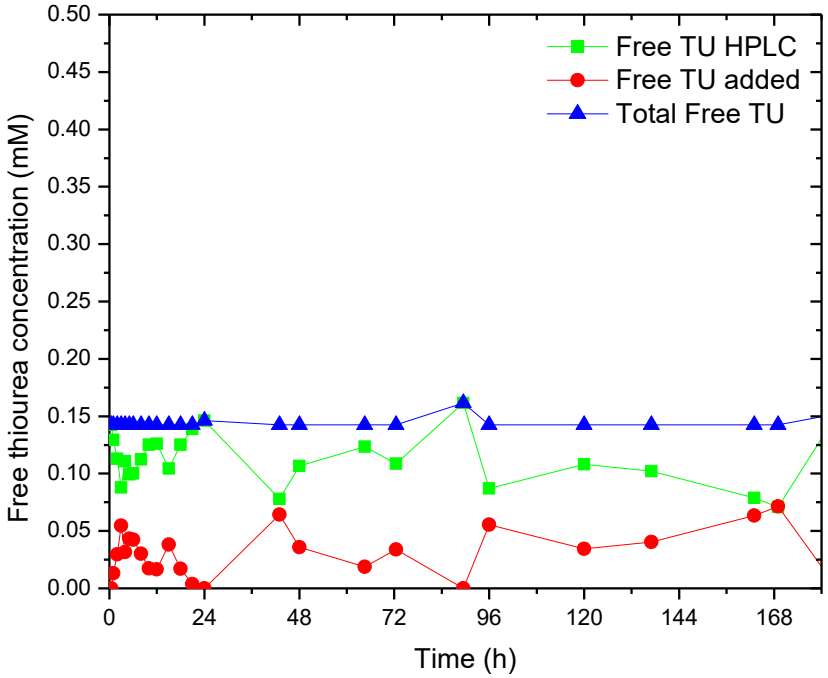

Figure C - 8. Free thiourea concentrations at pH 1.2, with 40 mM Fe^{3+} and 20ºC.

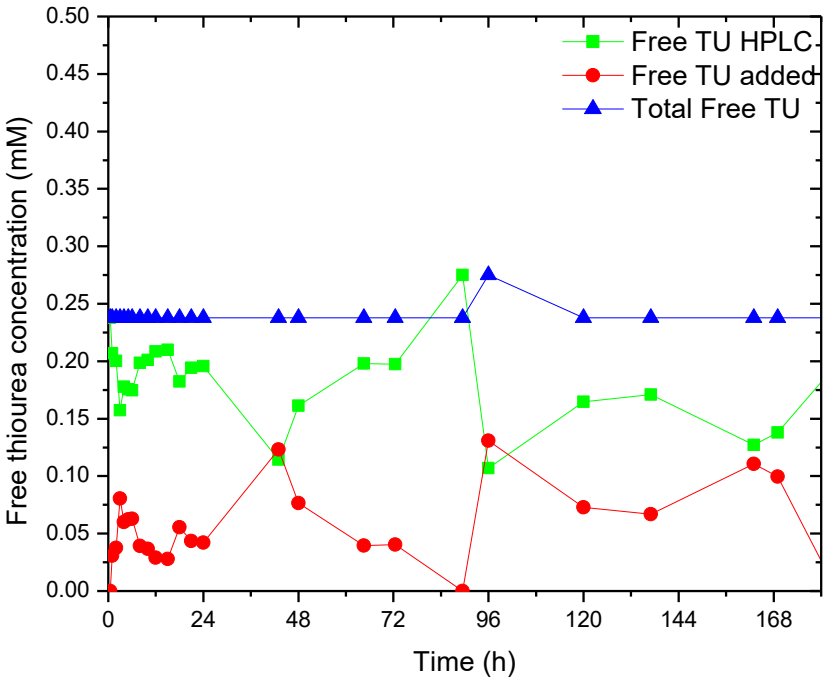

Figure C - 9. Free thiourea concentrations at pH 1.5, with 40 mM Fe^{3+} and 20ºC.

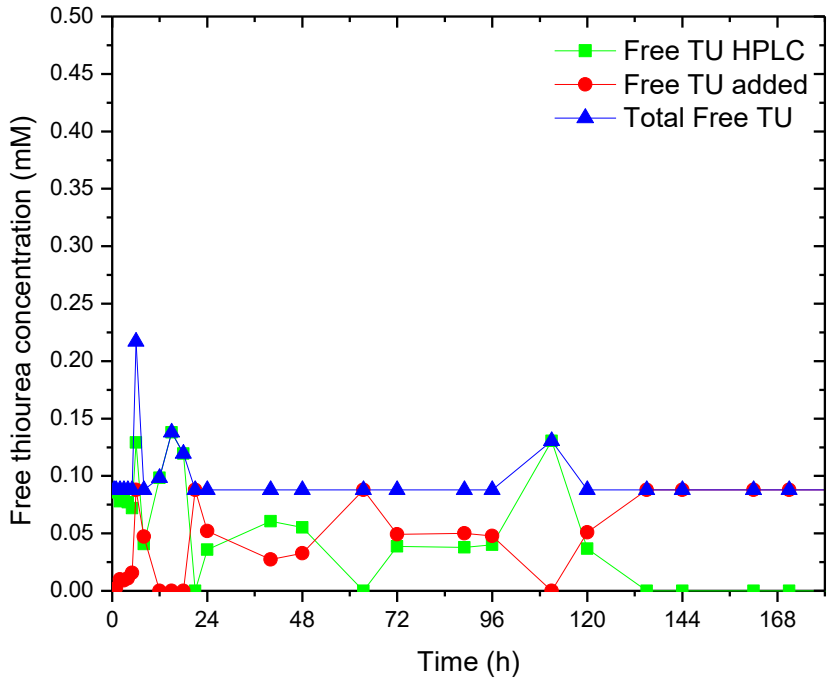

Figure C - 10. Free thiourea concentrations at 2 mM Cu^{2+}, with 40 mM Fe^{3+}, pH 1.8, and 20ºC.

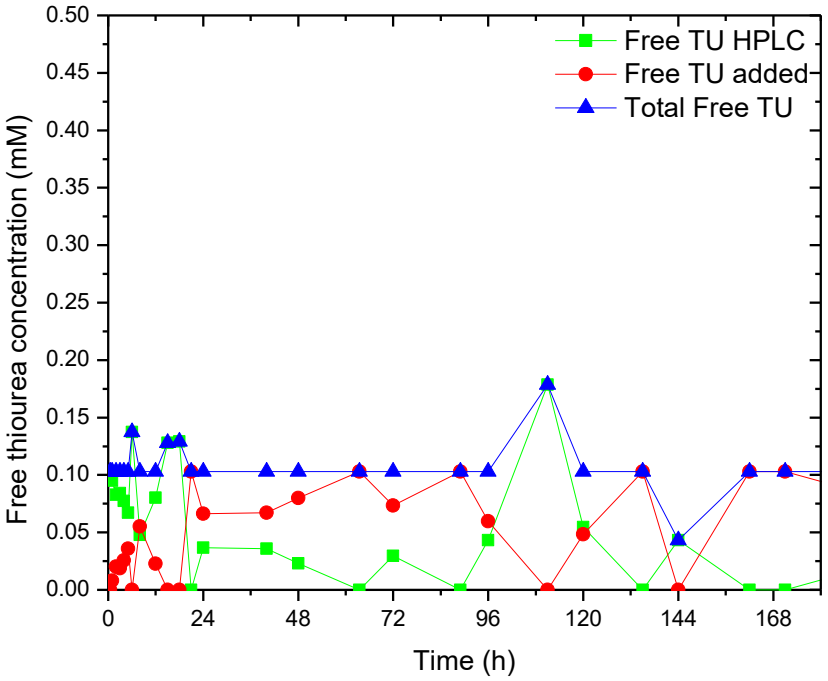

Figure C - 11. Free thiourea concentrations at 4 mM Cu^{2+}, with 40 mM Fe^{3+}, pH 1.8, and 20ºC.

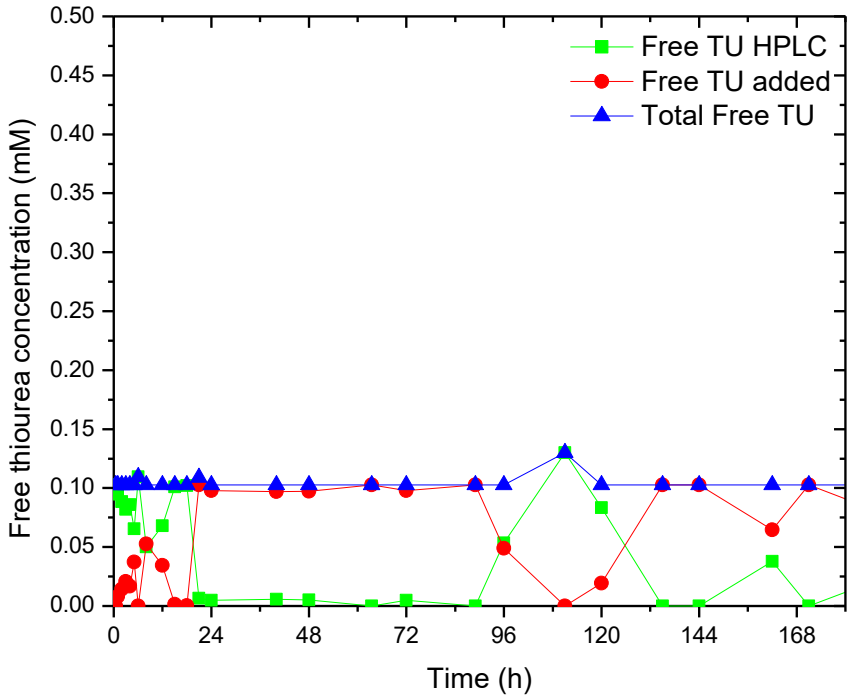

Figure C - 12. Free thiourea concentrations at 10 mM Cu^{2+}, with 40 mM Fe^{3+}, pH 1.8, and 20ºC.

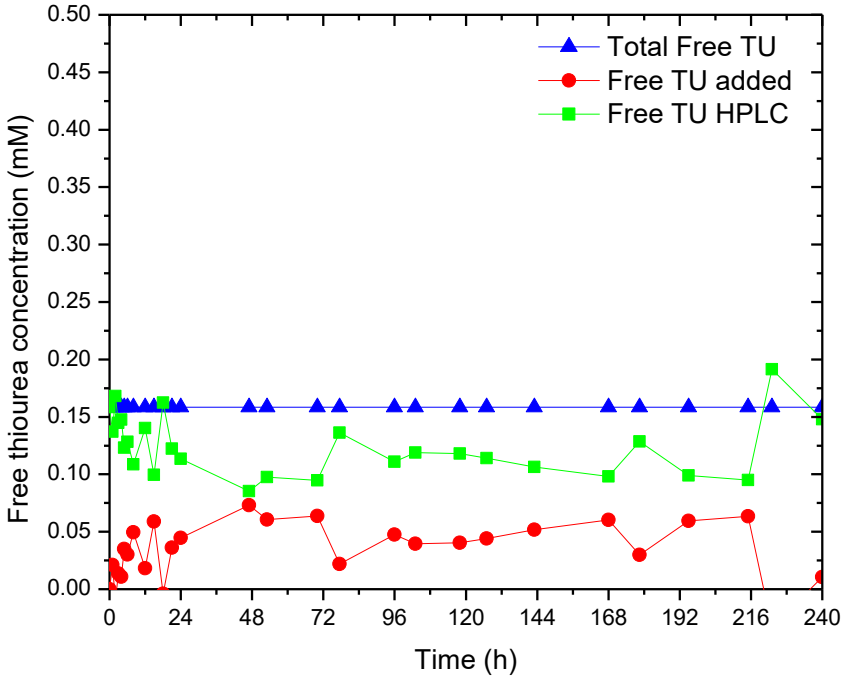

Figure C - 13. Free thiourea concentrations at P_{80} = 18.61 µm, with 40 mM Fe^{3+}, pH 1.8, and 20ºC.

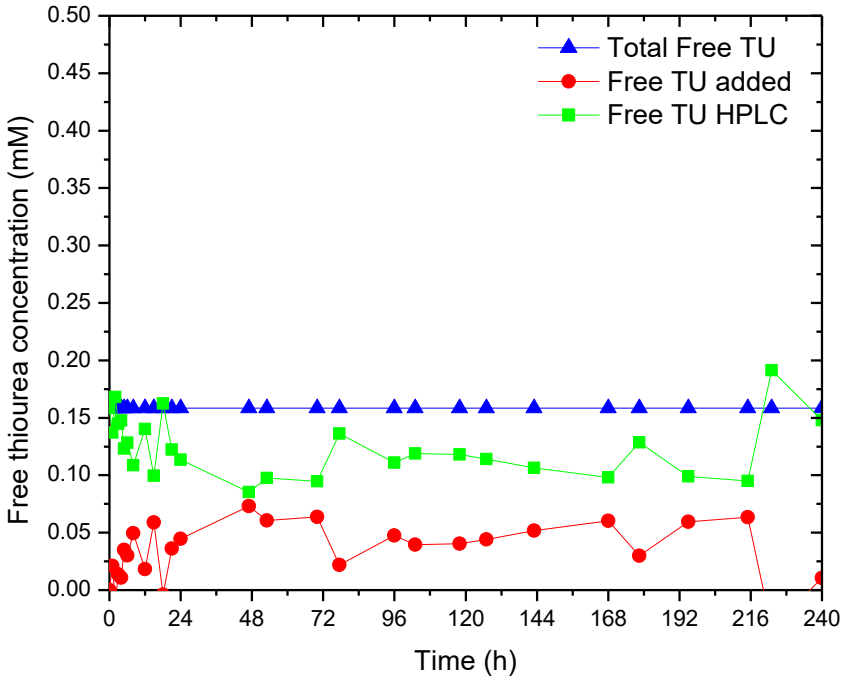

Figure C - 14. Free thiourea concentrations at P_{80} = 19.23 µm, with 40 mM Fe^{3+}, pH 1.8, and 20ºC.

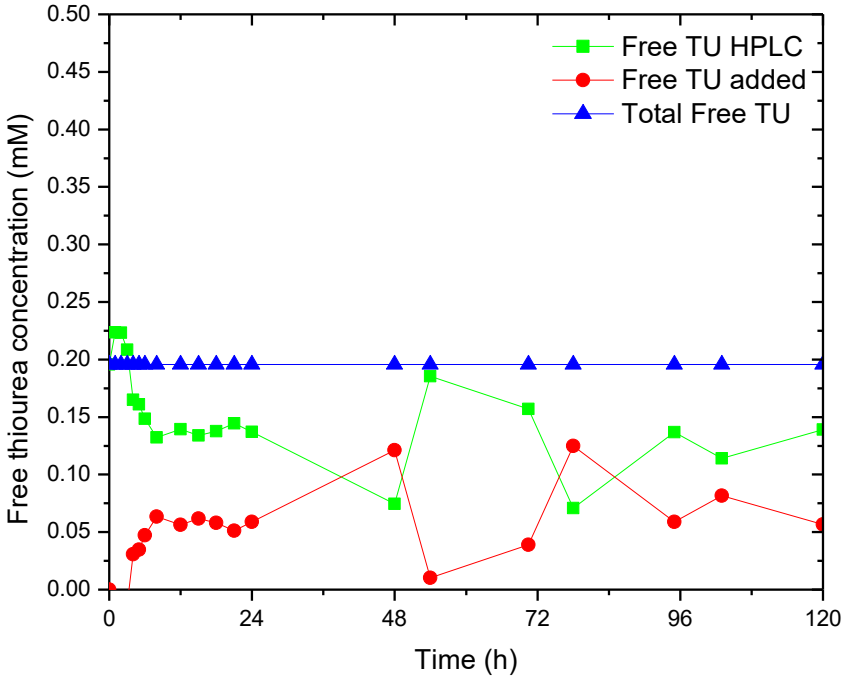

Figure C - 15. Free thiourea concentrations at 35ºC, with 40 mM Fe^{3+} and pH 1.2.

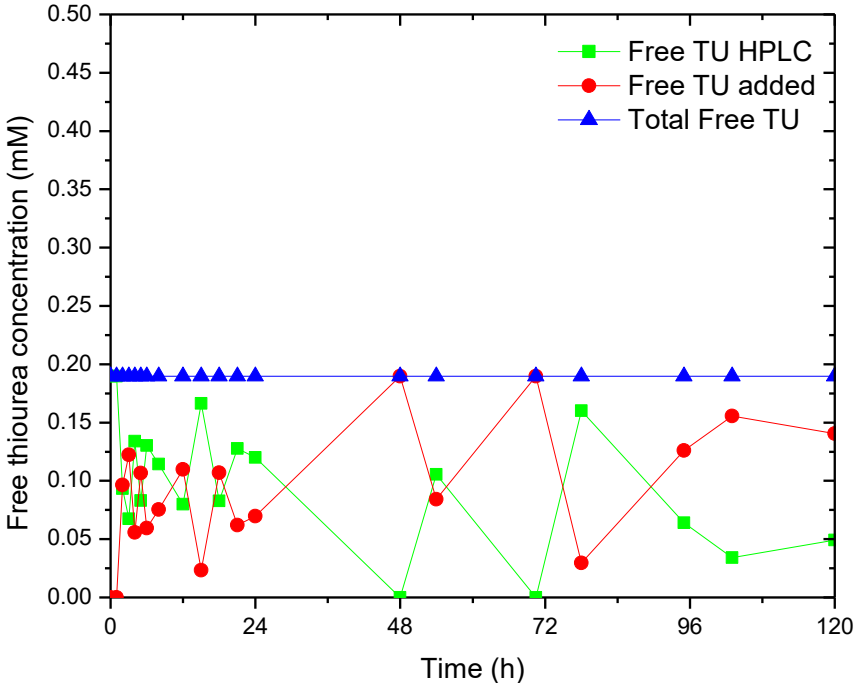

Figure C - 16. Free thiourea concentrations at 50ºC, with 40 mM Fe^{3+} and pH 1.2.